LABORATORI NAZIONALI DI FRASCATI
SIS – Pubblicazioni

LNF–95/051 (P)
28 Settembre 1995

WIZARD Collaboration

Papers presented at the XXIV International Cosmic Ray Conference August 28 – September 8, Rome 1995

CONTENTS

Rome 1995 XXIV ICRC HE 4.2.4, Vol. 1

Measurement of the Cosmic Ray Muon Spectrum and Charge Ratio in the Atmosphere from Ground Level to Balloon Altitudes

G. Basini[1], R. Bellotti[2], F. Bongiorno[1], M.T. Brunetti[3], F. Cafagna[2], M. Circella[2], A. Codino[3], G. De Cataldo[2], C. N. De Marzo[2], M. P. De Pascale[4], N. Finetti[7], N. Giglietto[2], R.L. Golden[5], C. Grimani[3], M. Hof[6], F. Massimo Brancaccio[7], M. Menichelli[3], J.W. Mitchell[8], A. Morselli[4], J. F. Ormes[8], P. Papini[7], S. Piccardi[7], P. Picozza[4], M. Ricci[1], I. Salvatori[3], M. Simon[6], P. Spillantini[7], P. Spinelli[2], S.A. Stephens[9], S.J. Stochaj[5] and R.E. Streittmatter[8]

[1] *INFN - Laboratori Nazionali di Frascati, Frascati, Italy.* [2] *Università di Bari and INFN, Bari, Italy.* [3] *Università di Perugia and INFN, Perugia, Italy.* [4] *Università di Roma "Tor Vergata" and INFN, Rome, Italy.* [5] *Particle Astrophysics Lab, New Mexico State University, Las Cruces, New Mexico, USA.* [6] *Universität Siegen, Fachbereich Physik, Siegen, Germany.* [7] *Università di Firenze and INFN, Florence, Italy.* [8] *NASA - Goddard Space Flight Center, Greenbelt, Maryland, USA.* [9] *Tata Institute of Fundamental Research, Bombay, India.*

Abstract

A measurement of the cosmic ray muon flux in the atmosphere has been carried out from the data collected by the MASS2 (Matter Antimatter Spectrometer System) apparatus during the ascent of the 1991 flight. The experiment was performed on September 23, 1991 from Fort Sumner, New Mexico (USA) at a geomagnetic cutoff of about 4.5 GV/c. The negative muon spectrum has been determined in different depth ranges in the momentum interval 0.33–40 GeV/c with higher statistics and better background rejection than reported before. Taking advantage of the high geomagnetic cutoff and of the high performances of the instrument, the positive muon spectrum has also been determined and the altitude dependence of the muon charge ratio has been investigated in the 0.33–1.5 GeV/c momentum range.

1 Introduction

In the past, only a few measurements of high altitude muons were available, prior to the results on the negative component reported by the WIZARD/MASS collaboration at the 23rd ICRC [1, *and references therein*]. Those measurements were unprecedented as to the particle identification capabilities of the instrument and to the wide ranges in energy and atmospheric depth investigated. Moreover, a renewed interest in such measurements has appeared

with the increasing evidence of the Atmospheric Neutrino Anomaly [2, *and references therein*]. A muon calibration of the atmospheric neutrino calculations can decrease the uncertainty associated with neutrino production and therefore contribute to the interpretation of the phenomenon. A measurement of the cosmic-ray muon spectrum and charge ratio in the atmosphere is reported here. The data analyzed in this work were collected with an improved version of the MASS apparatus during the ascent of the 1991 flight. The negative muon spectra have been measured in various depth ranges with higher statistics and in different conditions of geomagnetic cutoff and solar modulation than in the previous experiment. In addition, the altitude dependence of the muon charge ratio has been investigated. Some preliminary results are shown here. The complete set of results will be available at the Conference.

2 Experimental Setup

For a description of the MASS2 apparatus, the reader is referred to [3]. The main improvements with respect to the 1989 configuration were: an increased geometric factor, an increase of the MDR from 120 to 200 GV/c, a higher track reconstruction efficiency and a higher detection efficiency for the calorimeter. As a consequence, it was possible to get higher statistics and improved particle identification capabilites at the same time.

3 Data Analysis

3.1 Event Selection

The data sample analyzed in this work contained more than 220,000 triggers gathered over a period of 8,960 seconds. The events were first required to meet a set of reliability requirements for the reconstructed tracks, as described in [3]. In addition, consistency was required between the track reconstruction and the information from the other detectors. The TOF measurement was used to reject the few upward going particles.

Negative muon selection. The negative muon candidates were selected by means of the dE/dx signals from the scintillators and the hit pattern in the calorimeter. In particular, the average signal from the top scintillators and the signal from the bottom paddle were required to be between 0.7 and 1.8 I_o, I_o being the mean pulse height in the scintillator for a minimum ionizing singly charged particle. Muons were also required to show a clear single track in the calorimeter, with no evidence of interaction; for this purpose, a number of hits between 2 and 14 for one view and 2 and 10 from the other was required, with not more than one plane giving multiple hits.

Positive muon selection. In addition to the above requirements, a test of the β measurement from the TOF system was introduced for positive

muon selection at low energy, namely $1/\beta \leq 1.15$ and $1/\beta \leq 1.07$ in the momentum ranges 0.65-1.25 GeV/c and 1.25-1.5 GeV/c, respectively. No further discrimination was needed below 0.65 GeV/c.

3.2 Efficiencies and Background Rejection

The exposure time as well as the altitude-dependent dead-time fraction was considered in the calculation of the absolute fluxes. The geometric factor of the apparatus was evaluated by means of two independent calculations. Detailed checks were performed on the energy-dependence of the track reconstruction efficiency of the spectrometer. A trigger efficiency of 0.82±0.01 was introduced. The selection efficiencies of the scintillators and the calorimeter were determined to be 0.86±0.01 and 0.89±0.01, respectively. Finally, a β-selection efficiency of 0.916±0.005 was introduced for positive muons in the range 1.25–1.5 GeV/c. The Cherenkov detector was used to reject the low energy electrons and positrons misidentified in the calorimeter: particles with a Cherenkov signal larger than the equivalent of 3 photoelectrons were removed from the muon sample. Assuming an efficiency of 96% for this selection of particles well above the Cherenkov threshold, the residual contamination in the muon sample is expected to be comparable to the number of muons lost because of the test. Contamination should be well below 1% of the surviving events even at the lowest energies. A conservative upper limit of 1% was set on the residual proton background in the positive muon sample in the range 1.25–1.5 GeV/c. The proton background at lower momenta as well as the contamination by heavier particles is negligible. Pion contaminations of the order of a few percent cannot be excluded at this point of the analysis, more accurate estimates are in progress.

4 Results and Conclusion

A sample of 4,976 negative muons and 3,120 positive muons were finally selected in the momentum ranges 0.33-40 GeV/c and 0.33–1.5 GeV/c, respectively. They were distributed between 886 and 5 g/cm^2 in atmospheric depth. Despite the great deal of cross-checks performed to support the event selection and the efficiency estimates, the results shown here are still preliminary for the following two reasons: 1) the ascent curve of the payload was determined from the measurements taken with the payload sensors and may be inaccurate up to the level of 5–10%; 2) some global quantities related to the absolute normalization are under current investigation. An upper limit on the flux uncertainty of 20% can be set at this time. The spectral distribution of muons of either charge was determined in different depth intervals. Results for the negative component are reported in Figure 1, where the MASS measurements

are also shown. The muon charge ratio is shown in Figure 2, in the momentum bins indicated. The data are plotted at the average payload depths in different depth intervals. The current evidence is that there is no significant variation of the ratio with changing altitude, while the mean value increases with increasing momentum in the 0.33–1.5 GeV/c interval.

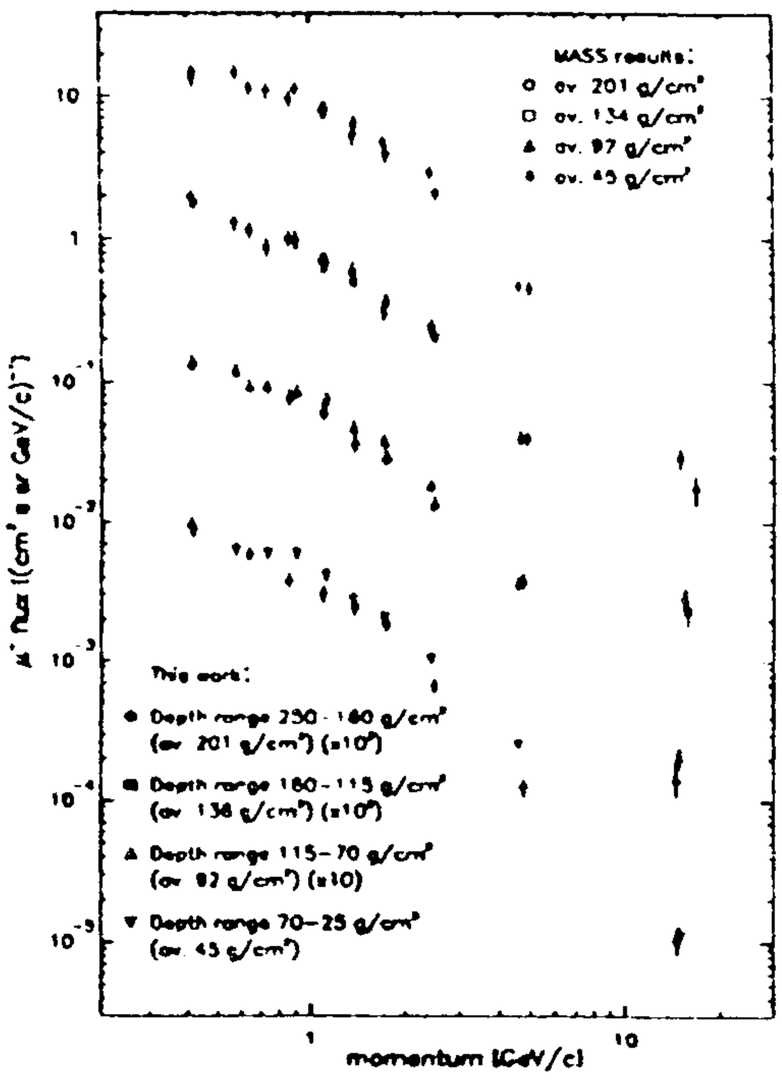

Figure 1: *Negative muon momentum spectra at various average depths in the atmosphere. The MASS results are from [1].*

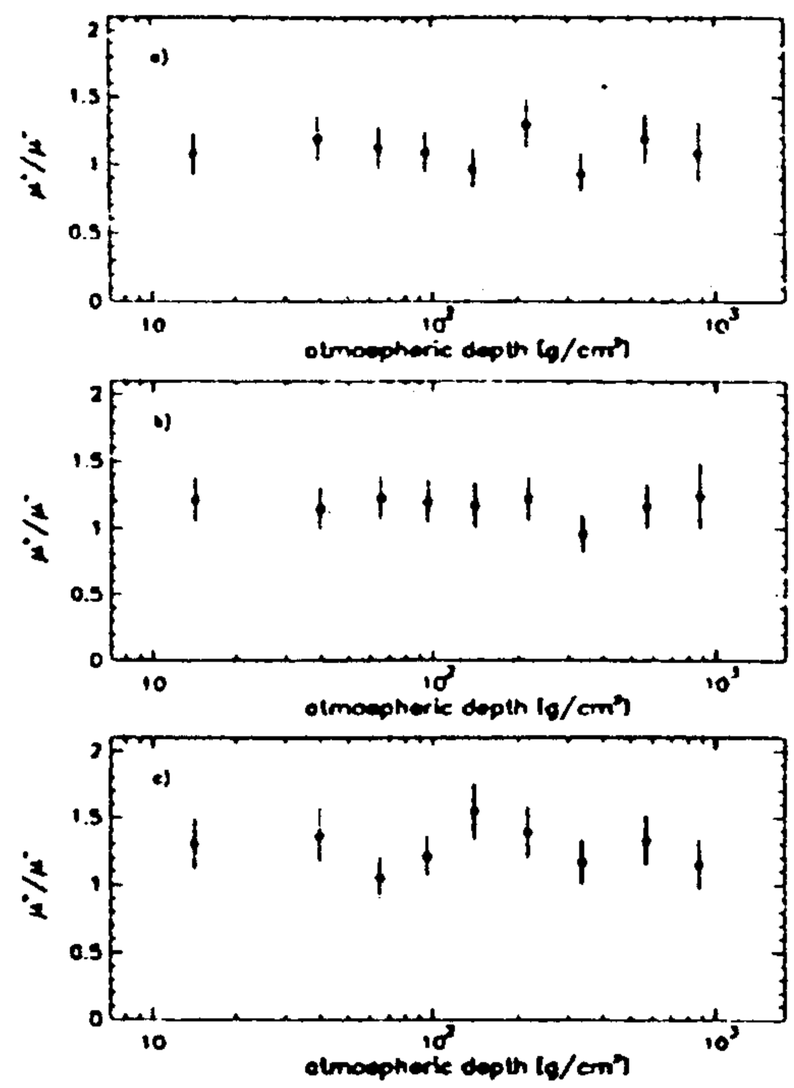

Figure 2: *Altitude dependence of the muon charge ratio in the momentum bins: a) 0.33–0.65 GeV/c; b) 0.65–1 GeV/c; c) 1–1.5 GeV/c.*

Acknowledgments. This work was supported by NASA, grant NAG-110, the National Scientific Balloon Facility, USA, the Istituto Nazionale di Fisica Nucleare and the Agenzia Spaziale Italiana, Italy, DARA and DFG, Germany.

References

[1] Circella, M., et al., Proc. of the 23rd ICRC, Calgary **4** (1993) 503. See also Bellotti, R., et al., LNGS 95/02, submitted to J. Geophys. Res.

[2] Perkins, D. H., Astropart. Phys. **2** (1994) 249.

[3] Basini, G., et al., *Measurement of electron and positron energy differential fluxes with MASS2 apparatus*, presented at this conference.

Rome 1995 XXIV ICRC OG 7.1.1, Vol 3

Measurement of Electron and Positron Energy Differential Fluxes with MASS2 Apparatus.

G. Basini[1], R. Bellotti[2], F. Bongiorno[1], M.T. Brunetti[3], F. Cafagna[2], M. Circella[2], A. Codino[3], G. De Cataldo[2], C. N. De Marzo[2], M. P. De Pascale[4], N. Finetti[7], N. Giglietto[2], R.L. Golden[5], C. Grimani[3], M. Hof[6], F. Massimo Brancaccio[7], M. Menichelli[3], J.W. Mitchell[8], A. Morselli[4], J. F. Ormes[8], P. Papini[7], S. Piccardi[7], P. Picozza[4], M. Ricci[1], I. Salvatori[3], M. Simon[6], P. Spillantini[7], P. Spinelli[2], A.S. Stephens[9], S.J. Stochaj[5] and R.E. Streittmatter[8]

[1] *INFN - Laboratori Nazionali di Frascati, Frascati, Italy.* [2] *Università di Bari and INFN, Bari, Italy.* [3] *Università di Perugia and INFN, Perugia, Italy.* [4] *Università di Roma "Tor Vergata" and INFN, Rome, Italy.* [5] *Particle Astrophysics Lab, New Mexico State University, Las Cruces, New Mexico, USA.* [6] *Universität Siegen, Fachbereich Physik, Siegen, Germany.* [7] *Università di Firenze and INFN, Florence, Italy.* [8] *NASA - Goddard Space Flight Center, Greenbelt, Maryland, USA.* [9] *Tata Institute of Fundamental Research, Bombay, India.*

Abstract

The Matter Antimatter Spectrometer System (MASS2) apparatus is a balloon-borne instrument. This experiment was flown for 9.8 hours on September 23, 1991 from Fort Sumner, New Mexico, USA, the geomagnetic cut-off of the launch site being about 4.5 GV/c. Differential fluxes of electrons and positrons have been measured at an average depth of residual atmosphere of about 5.8 gr cm^{-2}. These fluxes have been studied in the range 2–50 GeV and 2–15 GeV respectively. Preliminary results will be presented and compared with previous experiments.

1 Introduction

The determination of the electron and positron energy spectra is of primary importance in studying the cosmic ray confinement and propagation processes in the Galaxy. The use of a magnet spectrometer makes it possible to directly determine the charge of the particles, allowing a clear separation for the two components. Extracting the positrons signal is difficult due to the large proton flux.

2 The MASS2 Apparatus

This apparatus is the evolution of the one used in the original MASS flight in 1989. It consists of a tracking system, a time of flight (TOF), a Cherenkov detector and a streamer tube imaging calorimeter. The tracking system is composed of a superconducting magnet and 8 multiwire proportional chambers (MWPC) stacked with two 10-plane drift chambers. The superconducting magnet produces a field varying from 10 to 40 kG over the volume of the detectors. A total of 8 MWPC and 12 DC positions along the maximum magnet bending direction (X view) with 4 MWPC and 8 DC along the orthogonal axis (Y view) were digitized giving a maximum detectable rigidity (MDR) greater than 200 GV [2]. The TOF consists of two planes of two layers of plastic scintillator. A coincidence between the planes gives the acquisition trigger. The Cherenkov counter is filled with Freon 12 having a threshold Lorentz factor of $\gamma_{th} \simeq 23$. The photoelectrons are collected by a spherical mirror and focused on 4 photomultipliers (PMT). The calorimeter is made with 40 layers of 64 brass streamer tubes each, piled up along orthogonal views. It has a total depth of 7.33 radiation and 0.75 nuclear interaction lengths.

3 Selection Criteria and Data Analysis

To select reliable momentum reconstruction, we required at least 11 position measurements in the x-view and 6 in the y-view. Also, a $\chi^2 \leq 8$ on both views and a $\sigma \leq 0.03 GV^{-1}$ were used to define a good reconstructed deflection from a least–square fitting procedure. For e^+ analysis we required a deflection at more than 5 σ from zero. The TOF system was used to reject upward going particles. We also required a signal, on each plane, lower than $2.5 I_0$, I_0 being the pulse height for a minimum ionizing singly charged particle. Consistency between the position reconstructed into the TOF from both tracking and timing signal were used. The signals of the Cherenkov and the calorimeter hit pattern were used to select both electrons and positrons. The former were identified requiring the sum of the PMTs equivalent to at least 4 photoelectrons, the latter requiring at least 6 photoelectrons (the average number of photoelectrons from an $e^{\pm}$ is approximately 10). In the calorimeter, e^- induced electromagnetic showers were identified by selecting events showing more than 4 planes containing a cluster of hits inside 2.5 Molière radii. In selecting e^+ attention must be paid in eliminating hadronic initiated shower. To assure a high proton rejection power for the positron measurement, we required that both views of the calorimeter show a cluster on at least 7 planes and that the starting point of the shower be in the first 5 planes.

To calculate absolute flux, correct estimates of the selection criteria efficiencies and the acceptance are needed. Using more stringent selection criteria

for one instrument, within a restricted energy range, it is possible to select a set of low background particles of a given family and calculate the requested efficiency. To calculate the geometrical factor we used a Monte Carlo program that tracks a simulated particle through the instrument. The geometrical factor is $\simeq 190$ cm^2 sr for particles crossing the whole calorimeter with E $\geq$5 GeV. We found a spectrometer efficiency of 0.95 for $E \geq 2GeV$. The requirement of a completely recorded event in the calorimeter was satisfied by 82% of the events and 74.4% of the events passed the consistency check on the TOF. The TOF and Cherenkov pulse height selections are 91% and 94% efficient. The calorimeter selection efficiency for e^- is 0.98 and 0.625 for e^+. A Monte Carlo simulation was used to double check the last two efficiencies.

4 Conclusion

The preliminary electron flux at top of the atmosphere is shown in Figure 3. Using the calculation by Stephens [3], the atmospheric background was evaluated at the average float altitude. After background subtraction the flux was corrected to the top of the atmosphere by scaling them by a factor $f_{Atm} = \gamma^{h/ln2}$, were h is the residual atmosphere depth in radiation lengths, following [4]. The electron flux follows a power law: $J(E) = 111 * E^{-2.89\pm0.12}$ (m^{2}sr sec GeV)$^{-1}$, in the energy range 5–50 GeV. The e^+ flux was evaluated using the same procedure and the charge ratio, $e^+/(e^+ + e^-)$, was found to be $R = 0.103 \pm 0.043$ in the 6–13 GeV energy range.

Acknowledgments
This work was supported by NASA, grant NAG-110, the National Scientific Balloon Facility, USA, the Istituto Nazionale di Fisica Nucleare and the Agenzia Spaziale Italiana, Italy, DARA and DFG, Germany.

References

[1] Golden R.L. et al. Ap.J. Lett. **24** (1984) 75 , Nishimura J. et al. Ap.J. **238** (1980) 394 , Tang K.K. Ap.J. **278** (1984) 881 , Buffington A. et al. Ap.J. **199** (1975) 669 , Golden R.L. et al. Astr. Ap. **188** (1987) 145 , Golden R.L. et al. Ap.J. **436** (1994) 769

[2] Golden R.L. et al. N.I.M. **A306** (1991) 366, Hof M. et al. 23th ICRC Calgary **OG, V.2** (1993) 544, Menn W. et al. 23th ICRC Calgary **OG-2** (1993) 548

[3] Stephens S.A. 17th ICRC Paris **SH** (1981) 282

[4] Schmidt P.J. J.G.R. **77** (1972) 3295

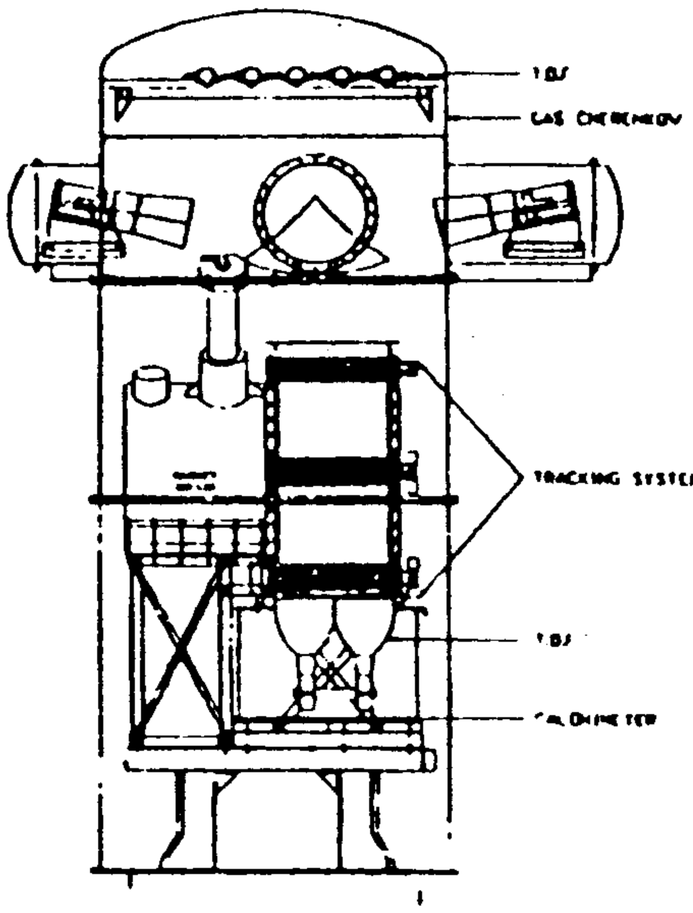

Figure 1: *MASS2 for 1991 flight.*

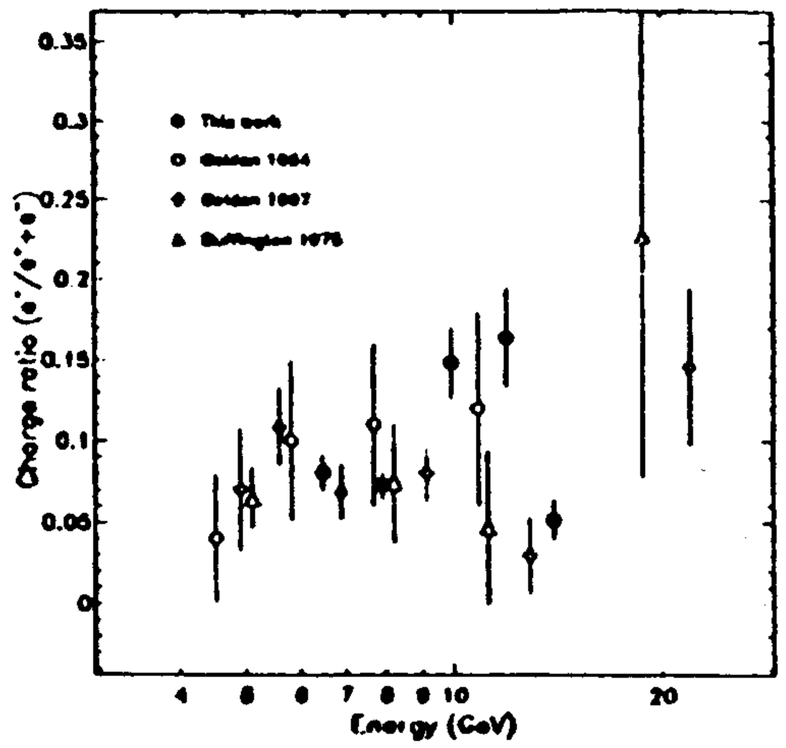

Figure 2: *Charge ratio, $e^+/(e^+ + e^-)$, compared with [1].*

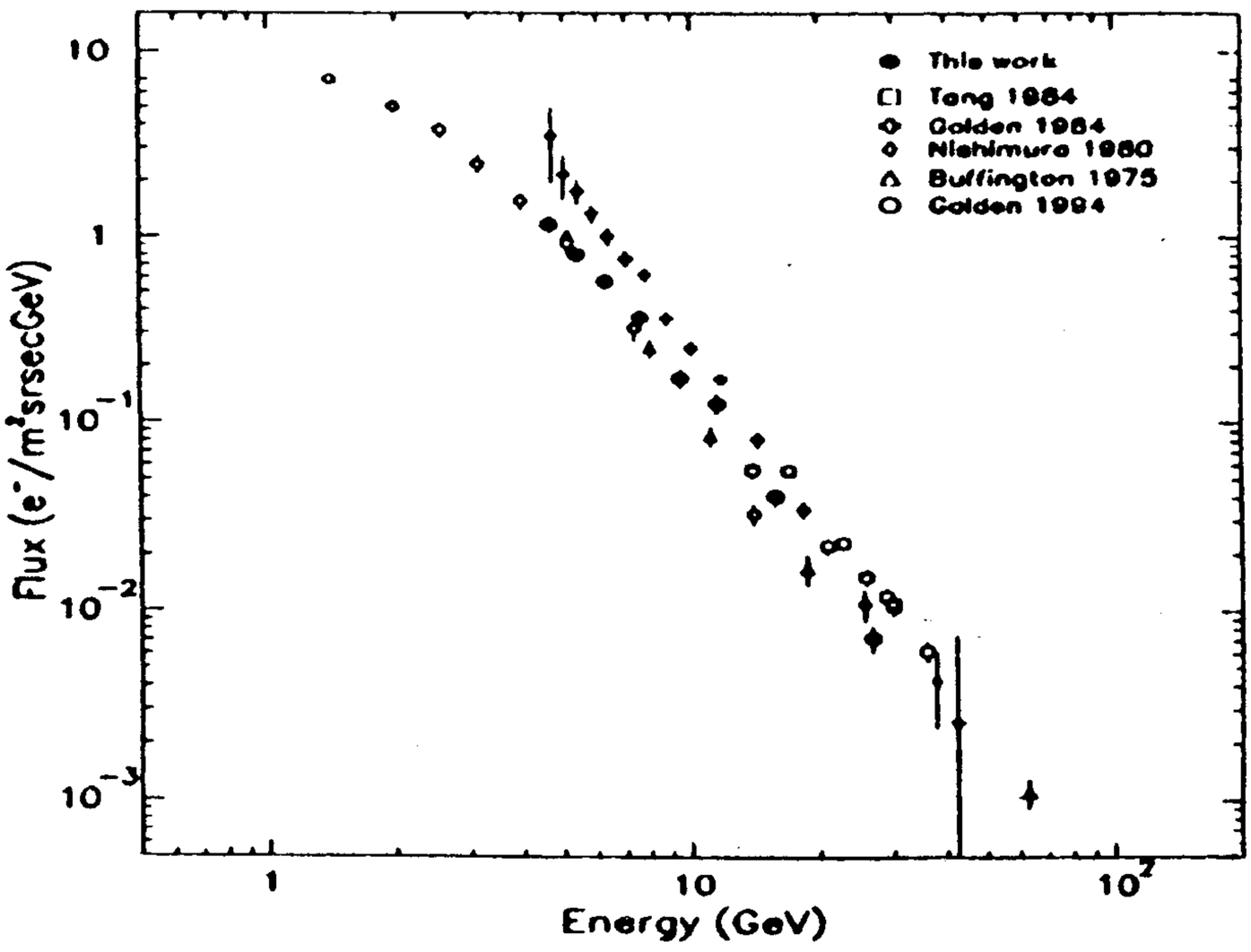

Figure 3: *e^- flux at the top of the atmosphere compared with [1].*

Rome 1995 XXIV ICRC OG 7.1.3, Vol. 3

Observations Of Cosmic Ray Positrons During The 1993 Flight Of The NMSU/WiZard-TS93 Balloon-borne Apparatus

F. Aversa[10], G. Barbiellini[10], G. Basini[6], R. Bellotti[4], V. Bidoli[9], M. Bocciolini[5], M. Boezio[10], F.M. Brancaccio[6], U. Bravar[10], F. Bronzini[8], M.T. Brunetti[7], A. F. Cafagna[4], M Candusso[9], M. Casolino[9], M. Castellano[4], F. Celletti[5], M. Circella[4], A. Codino[7], Colavita[10], G. De Cataldo[4], C. De Marzo[4], M.P. De Pascale[9], N. Finetti[5], F. Fratnik[10], N. Giglietto[4], R.L. Golden[1], M. Grandi[5], C. Grimani[7], M. Hof[11], B. Marangelli[4], G. Mazzenga[6], M. Menichelli[7], W. Menn[11], M. Miozza[7], J.W. Mitchell[3], A. Morselli[9], J.F. Ormes[3], P. Papini[5], A. Perego[5], S. Piccardi[5], P. Picozza[9], A. Rainò[4], M. Ricci[6], P. Schiavon[10], M. Simon[11], R. Sparvoli[9], P. Spillantini[5], P. Spinelli[4], S.A. Stephens[2], S.J. Stochaj[1], R.E. Streitmatter[3], A. Vacchi[10], N. Zampa[10]

[1] *New Mexico State University, Las Cruces, USA*
[2] *Tata Institute of Fundamental Research, Bombay, India*
[3] *N.A.S.A. Goddard Space Flight Center, Greenbelt, USA*
[4] *Dipartimento di Fisica and Sezione I.N.F.N. dell'Università di Bari, Italy*
[5] *Dipartimento di Fisica and Sezione I.N.F.N. dell'Università di Firenze*
[6] *I.N.F.N. Laboratori Nazionali, Frascati, Italy*
[7] *Dipartimento di Fisica and Sezione I.N.F.N. dell'Università di Perugia*
[8] *Dipartimento di Fisica and Sezione I.N.F.N. dell'Università "La Sapienza", Roma, Italy*
[9] *Dipartimento di Fisica and Sezione I.N.F.N. dell'Università di "Tor Vergata", Roma, Italy*
[10] *Dipartimento di Fisica and Sezione I.N.F.N. dell'Università di Trieste*
[11] *Siegen University, Siegen, Germany*

Abstract

As part of a series of experiments to search for antimatter in the primary cosmic rays, the NMSU balloon-borne apparatus was configured for a flight dedicated to the search of positrons. Two completely new instruments were added to the magnetic spectrometer: a Transition Radiation Detector (TRD) and a Silicon-Tungsten tracking calorimeter.

The function of these two instruments complemented one another and the combined action provided a proton rejection factor better than 5×10^5. We report here the results from the analysis on the complete set of data. All the presented spectra are at the level of the spectrometer.

1 Description of the Flight

For the description of the NMSU balloon facility we refer to ref. [1]. The apparatus was launched from Fort Sumner, New Mexico on 8 August 1993 and floated at a mean altitude of 36 km for 25 hours. During this time about 750,000 events having a single charged track in the spectrometer were selected. The balloon drifted west during the flight and the resulting mean geomagnetic cutoff was of 4.5 GV/c.

Table 1: *Efficiency and contamination for each detector in the rigidity range 4 - 50 GV/c.*

	Efficiency e^-	Contamination p	Contamination α
TRD	$(69 \pm 2) \times 10^{-2}$	$(1.30 \pm 0.04) \times 10^{-2}$	$(30.4 \pm 0.3) \times 10^{-2}$
Scint.	$(95.5 \pm 0.8) \times 10^{-2}$	$(98.30 \pm 0.04) \times 10^{-2}$	$(0.11 \pm 0.06) \times 10^{-2}$
Calo.	$(79 \pm 2) \times 10^{-2}$	$(0.34 \pm 0.02) \times 10^{-2}$	$(0.79 \pm 0.07) \times 10^{-2}$
Tot.	$(52 \pm 2) \times 10^{-2}$	$(4.3 \pm 0.3) \times 10^{-5}$	$(2.6 \pm 1.5) \times 10^{-6}$

2 Data Analysis

The performances of the spectrometer and of the individual detectors have been evaluated using electron and proton data collected during the flight [2]. A sample of electrons, obtained by applying strict cuts for electrons with the calorimeter, was used to determine the overall efficiency for the TRD. In a similar manner, the efficiency of the calorimeter was determined using an electron sample selected with the TRD. Both the performances of these instruments have been previously studied at particle accelerator beams; the results are reported in ref. [3].

2.1 Electron Spectrum

In order to obtain the e^- spectrum, we have established selection criteria for the time of flight system, for the TRD and for the tracking calorimeter. These criteria were chosen to have a high detection efficiency for electrons while maximazing the rejection power of the apparatus for protons. Table 1 reports the experimentally evaluated efficiency and contamination of the chosen selection criteria in the rigidity range 4 - 50 GV/c.

The dE/dX information from the TOF scintillators has been used to contribute to the identification of α particles. For the study of the negative side of the particle spectrum we have used only the calorimeter since its high electron efficiency and hadron rejection power are adequate to identify the e^- component. In Figure 1 we see the resulting e^- spectrum selected using calorimeter cuts only. The portion below about 5 GeV shows the effect of the geomagnetic cutoff. A power law fit to this curve in the range 6 - 50 GeV is in (see continuous line) good agreement with a spectral index of 3.3. We observe a total of 980 electrons during the flight, 315 of which are in the range 6 - 50 GeV.

2.2 The Positron Spectrum

To obtain the energy distribution of the e^+ candidates, the same cuts used to identify e^- , along with the TRD cuts, have been used on the positively charged particles. Figure 2 shows the resulting e^+ spectrum. To compare this plot with Figure 1 the values have been divided by the TRD efficiency.

2.3 $e^+ / (e^+ + e^-)$ Ratio

We have evaluated the surviving proton background by using the raw spectrum (after tracking cuts) of the particles with charge equal to +1 . That was done by evaluating

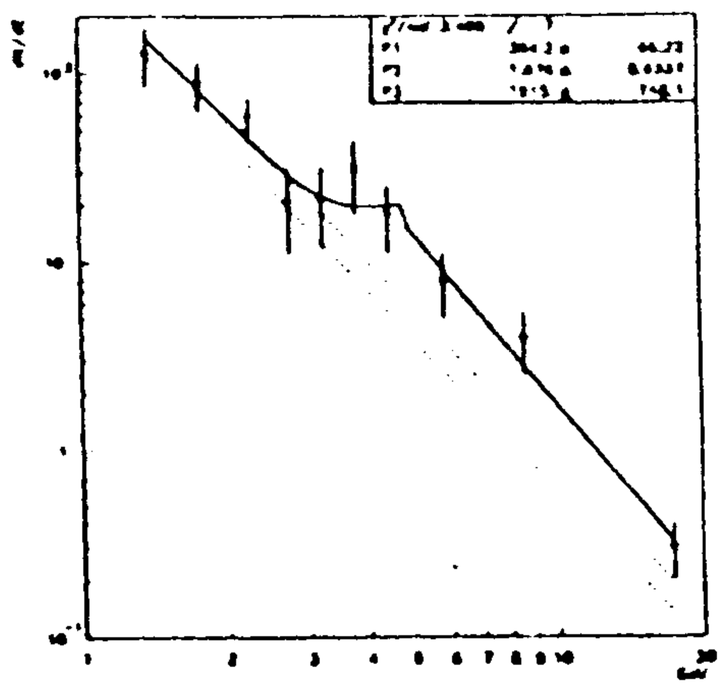

Figure 1: *Global e^- spectrum. The continuous line is a power law fit of the primary e^- spectrum.*

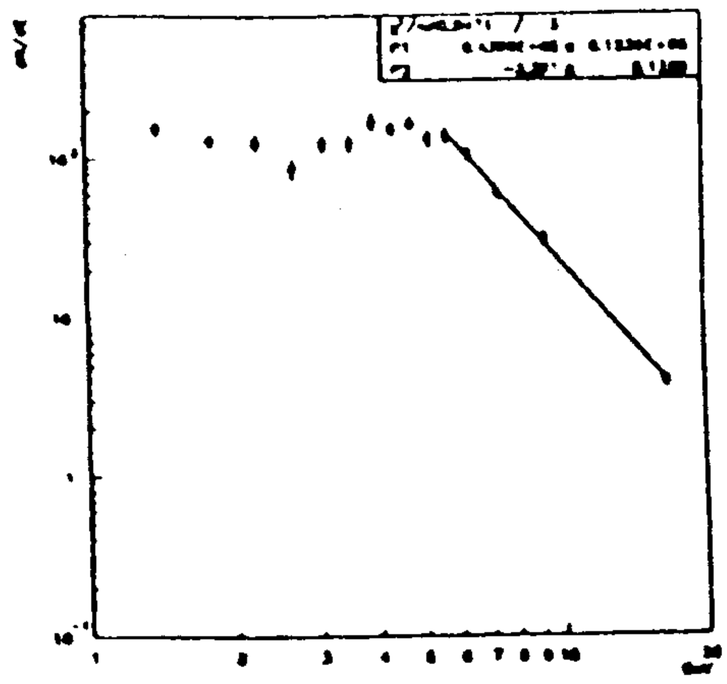

Figure 2: *Global e^+ spectrum. The continuous line is a fit of the primary plus secondary spectra. The dotted lines are the ± 1 standard deviation from the mean value of the atmospheric background spectrum.*

contamination left by each detector using the separation power of the remaining detectors (see Table 1). The overall contamination is the product of the contaminations left by each detector. Using this and the raw proton spectrum we have determined the proton background for each energy bin.
We have evaluated the positron atmopsheric background using a first order Monte Carlo simulation. We have simulated the e^- spectrum at the level of the spectrometer starting with a primary electron spectrum with a spectral index of 3.3. This spectrum was then propagated through the atmosphere and material in the apparatus down to the top of the spectrometer. We have assumed that the primary e^- spectrum at energies below the maximum of the distribution has a slope identical to that of the protons in the same region. The simulated spectrum includes corrections for bremsstrahlung losses, and assumes that the e^- and e^+ atmospheric backgrounds are generated by the process of pair production of the primary γ-rays which follow a $E^{-2.7}$ power law. Using this spectrum we have been able to reproduce (continous line in Figure 1) the experimental spectrum . That is for energies greater than 4.8 GeV:

$$P1 \cdot E^{-2.7} + P3 \cdot E^{-3.14} \tag{1}$$

and a function $f_2(E)$ [1] for lower energies. From the spectrum reported in Figure 2 and using Formula 1 and $f_2(E)$, the weight of the distribution of secondary e^+ was found to be:

$$364.2 \cdot E^{-2.7} \tag{2}$$

In conclusion, we find that the experimental positron atmopsheric background comes from Equation 2 evaluated for each energy bin and multiplied by the TRD efficiency (Table 1). The dotted lines in Figure 2 are the ± 1 standard deviation from the mean value of this background. The results and the measured $\frac{e^+}{e^+ + e^-}$ ratio from this analysis are reported in Table 2 and compared with previous results in Figure 3. The mean value of $\frac{e^+}{e^+ + e^-}$ ratio is: $(7.3 \pm 1.6) \times 10^{-2}$ at the center of gravity of the positron energy equal to 8.11 GeV.

---

[1] $f_2(E) = P1 \cdot E^{-2.7} + P2 \cdot (E^{0.8} + 3.5 \cdot e^{\frac{(E-4.8)^2}{2 \cdot 0.9^2}})$

Table 2: *Experimental results.*

Energy bin	e^-	e^+	P back.	e^+ atm. back.	$e^+ / (e^+ + e^-)$
$4 \div 5$	111	13	1.3 ± 0.1	4.4 ± 0.9	0.064 ± 0.031
$5 \div 7$	164	17	2.2 ± 0.2	4.3 ± 0.8	0.062 ± 0.024
$7 \div 11$	98	13	2.0 ± 0.1	2.7 ± 0.5	0.080 ± 0.032
$11 \div 50$	56	11	2.0 ± 0.1	2.6 ± 0.5	0.107 ± 0.053

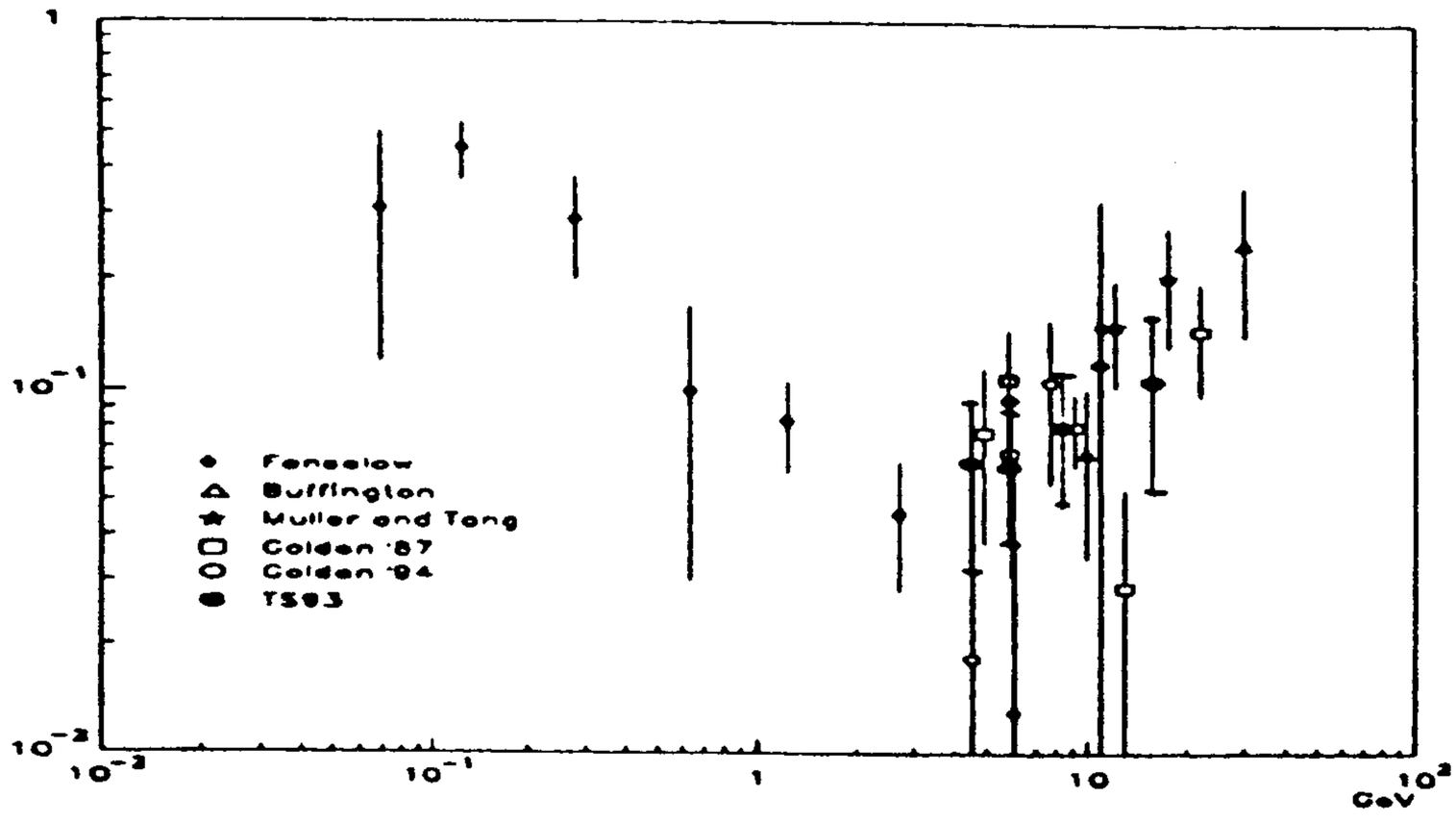

Figure 1: *Experimental $e^+ / (e^+ + e^-)$ (ref.[4]).*

Aknowledgments. This work was supported by NASA Grant NAG-110, the National Scientific Ballon Facility, The Istituto Nazionale di Fisica Nucleare and the Agenzia Spaziale Italiana.

References

[1] R.L. Golden et al., Nucl. Instr. and Meth. **A306** (1991) 366.
M. Hof et al., Nucl. Instr. and Meth. **A345** (1994) 561-569.

[2] F. Aversa et al., Nucl. Instr. and Meth. **A360** (1995) 17.

[3] R. Bellotti et al., Proc. XXIII Int. Cosmic Ray Conf., Calgary (1993) Vol.2 p. 512;
E. Barbarito et al., Nucl. Instr. and Meth. **A313** (1992) 295;
R. Bellotti et al., Nucl. Instr. and Meth. **A323** (1992) 295;
M. Bocciolini et al., Nucl. Instr. and Meth. **A333** (1993) 560;
M. Bocciolini et al., Nucl. Phys. **32** (1993) 77;
F. Aversa et al., Nucl. Instr. and Meth. **A334** (1993) 589.

[4] R.L. Golden et al., accepted by Ap. J.;
J.L. Fanselow et al., Ap. J. 158 (1969) 771;
A. Buffington et al., Ap. J. 199 (1975) 669;
R.L. Golden et al., (1987) Astr. Ap. 188 (1987) 145;
D. Muller and K.K. Tang, Ap. J. 312 (1987) 183.

Rome 1995 XXIV ICRC OG 7.3.1, Vol. 3

Cosmic Ray Antiproton Measurements in the 4-19 GeV Energy Range using the NMSU/WiZard-Matter Antimatter Superconducting Spectrometer 2 (MASS2)

M Hof [1], R.L.Golden[2], S.J Stochaj[2], G.Basini[5], F.Bongiorno[5], F Massimo Brancaccio[6], M.T.Brunetti[7], A.Codino[7], C.Grimani[7], M.Menichelli[7], J.W.Mitchell[9], A Morselli[8], J.F.Ormes[9], P.Papini[6], M.P.de Pascale[8], C.Pfeifer[1], S.Piccardi[6], P.Picozza[8], M.Ricci[5], I.Salvatori[7], M.Simon[1], S.Spillantini[6], S.A.Stephens[3], R.E.Streitmatter[9], W.R.Webber[4]

[1]Universität Siegen, Fachbereich Physik, 57068 Siegen, Germany. [2]Particle Astrophysics Lab, New Mexico State University, Las Cruces, USA. [3]Tata Institute of Fundamental Research, Bombay, India. [4]Department of Astronomy, New Mexico State University, Las Cruces, USA. [5]INFN, Laboratori Nazionali di Frascati, Italy. [6]Università di Firenze and INFN, Firenze, Italy [7]Università di Perugia and INFN, Perugia, Italy. [8]Università di Roma II "Tor Vergata" and INFN Roma II, Roma, Italy. [9]NASA Goddard Space Flight Center, Maryland, USA.

Abstract

The $\bar{p}/p$-ratio from 4 to 19 GeV has been measured using the NMSU/WiZard balloon borne Matter Antimatter Superconducting Spectrometer (MASS2) instrument. This is the first confirmation of the cosmic ray antiproton component made in this energy range since their discovery in 1979 [1]. The MASS2 instrument is an updated version of the instrument flown in 1979. The observed $\bar{p}/p$-ratio is $1.52 \cdot 10^{-4}$.

1 Introduction

Antiprotons in the cosmic radiation were discovered in 1979 ([1],[2]). Since this time several experiments have measured or set upper limits on the antiproton component of cosmic rays. However, all of the experiments have covered a lower energy range. The MASS2 experiment provides a remeasurement of the original 1979 observation. This instrument is an improved version of the original payload. Using the MASS2 instrument it was possible to measure the antiproton flux in the 4 to 19 GeV range without the need for any instrumental background subtraction.

2 Instrument

The MASS2 instrument, as shown in Figure 1, is composed of a magnetic spectrometer, a plastic scintillator time-of-flight (ToF) system, a gas Cherenkov counter and an imaging calorimeter. The spectrometer measures the deflection, defined as the inverse of the rigidity, of the particle in the magnetic field. It consists of a superconducting magnet and a position measuring device. The superconducting magnet coil provides a magnetic field within the tracking device, which varies from 2.2 to 0.15 Tesla. The tracking device is a hybrid detector, made of multiwire proportional chambers [3] and drift chambers [4]. The hybrid system provides a maximum detectable rigidity (MDR) of 210 GV/c.

The charge of the particle and the direction that the particle traversed the instrument is measured with the ToF system. The system provides 3 independent dE/dx-measurements for charge separation and a timing resolution of 415 ps for singly charged particles.

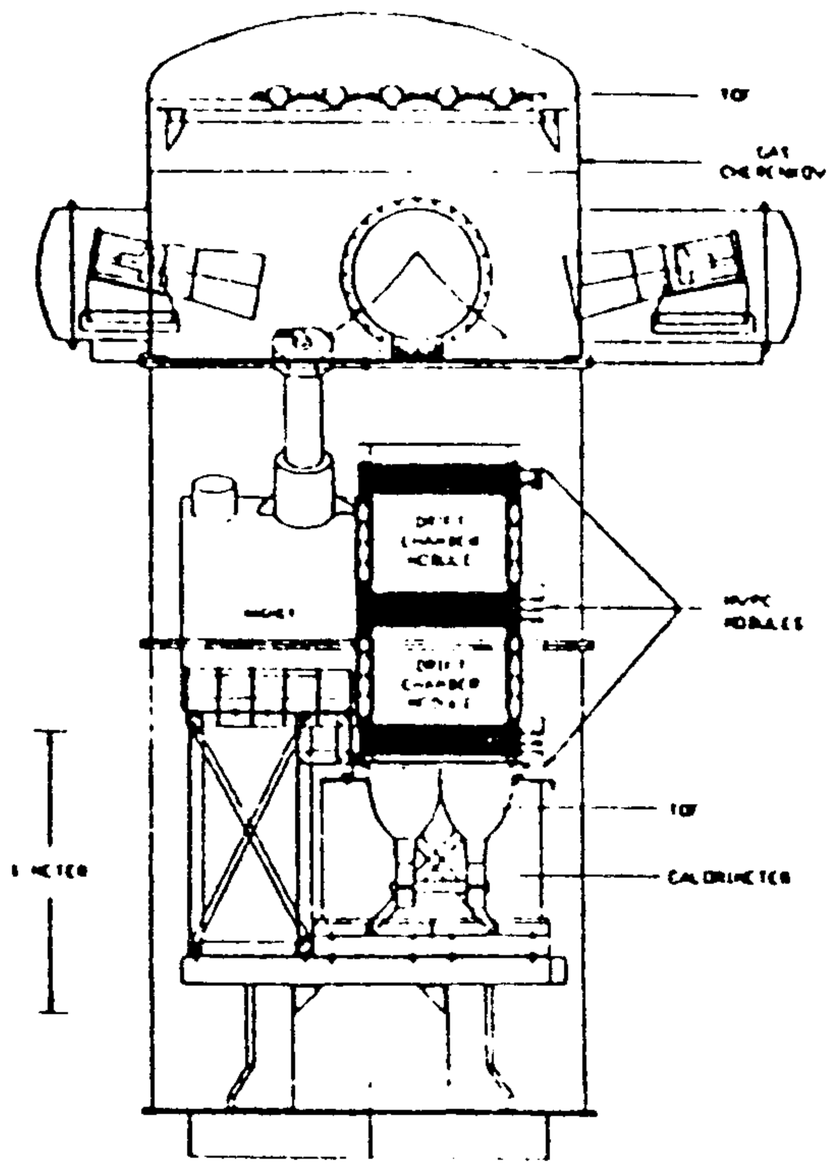

Figure 1 : The MASS2-instrument

The gas Cherenkov counter (G) is used as a threshold device to separate the light, charge one particles (muons, electrons and positrons), from the heavier protons and antiprotons. During the flight the gas volume was filled with Freon 12, which gives a Cherenkov threshold of $\gamma_{th} \approx 25$. The Cherenkov light produced is focussed by a 4 segment mirror onto 4 photo-tubes. Each segment is a piece of a spherical mirror with a radius of 40 inches.

The calorimeter is used to distinguish electrons and positrons with electromagnetic showers from non-interacting muons or hadronically interacting protons. It is an imaging streamer tube calorimeter with a depth of 7.33 radiation lengths.

The flight of the instrument took place in september 1991 from Fort Sumner, New Mexico, with a geomagnetic cutoff of about 5 GV/c. The experiment stayed at an altitude of about 36 km for 9.8 hours. The average residual atmosphere was 5.8 g/cm^2.

3 Analysis

In order to select charge one particles it was required that the 3 dE/dx-measurements, provided by the ToF scintillators, should be consistent and that each of them have a signal less than 3 times that of a minimum ionizing particle.

The main selecting device is the gas Cherenkov counter. Its threshold for muons and protons defines the lower and upper end for the observation. Negative curvature particles within this range which do not have accompanying Cherenkov light are identified as antiproton candidates. Background events may mimic an antiproton as a result of inefficiency of the Cherenkov counter, albedos traversing the instrument from the bottom to the top, positive particles spilling over to negative curvature (due to the finite spectrometer resolution or due to scattering within the instrument).

The inverse of the velocity, as derived from the ToF timing measurement, is required to be greater than 0.75 c^{-1}. This separates downward going particles from albedos by more than 35 sigma.

Electromagnetic showers are identified by their signature within a cylinder of ±3 Molière-radii and than removed from the sample.

The Cherenkov counter, being the only device which is able to suppress the muon background, plays a crucial role in the analysis. An extensive monte carlo study was carried out along with ground measurements in order to understand the behaviour of this device. This work is well described in [5]. Since the light collection of the Cherenkov counter is position dependent, only the parts of the mirror having sufficient signal were

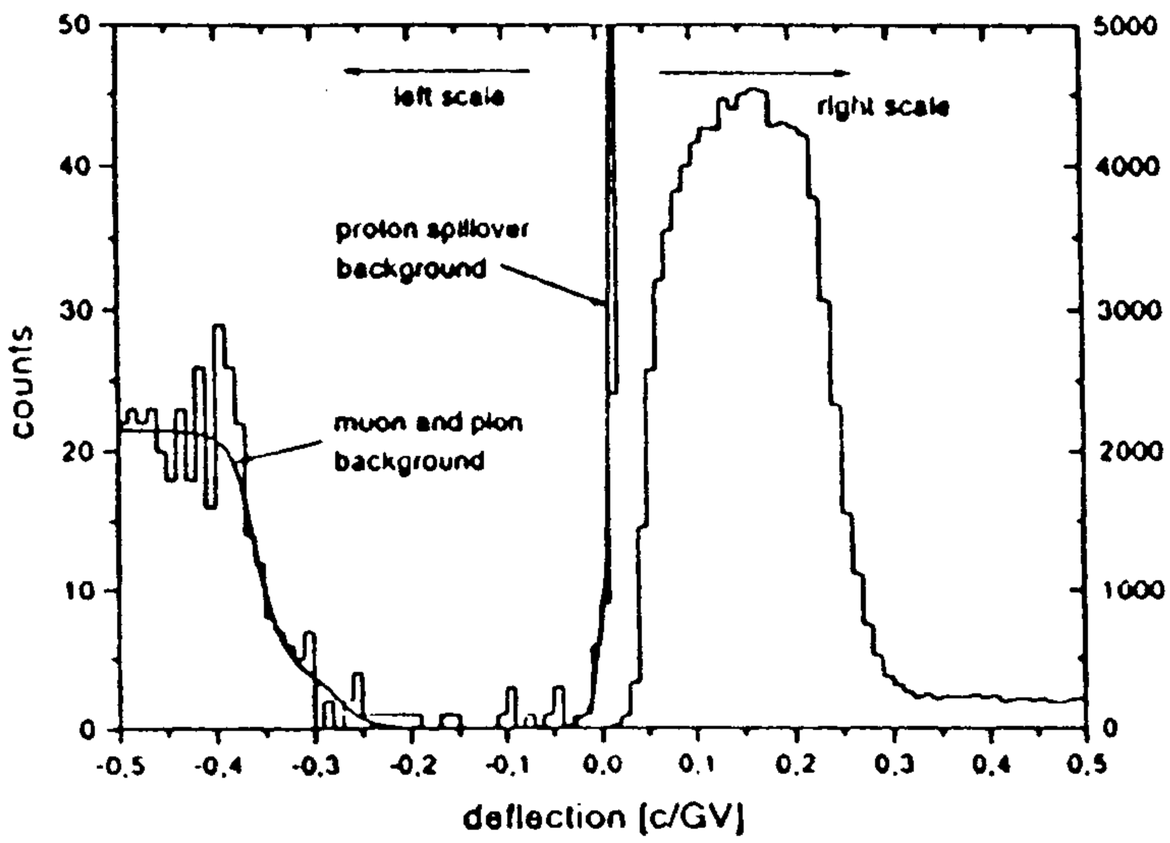

Figure 2 : Data from the flight with Z = 1, no shower, G=OFF and the tracking cuts described in the text

used. Particles intersecting the mirror close to the peak, the seams or the edges were excluded from the analysis. For the remaining parts the average signal corresponded to 18.4 photoelectrons. The inefficiency of the detector in suppressing muons in the rigidity range of 5 to 20 GV/c was found to be less than 0.2 %

For the spectrometer, we require at least 15 measurements (out of 19) in the bending X-coordinate and 8 (out of 11) in Y. The normalized χ^2-values are asked to be less than 4 and the error in the measured deflection should be less than 0.02 c/GV. In addition to this we examined the top and the bottom part of the spectrometer separately and required consistency between the fitted deflections.

Figure 2 shows the data with no Cherenkov light after applying all these cuts. In the deflection range from -0.2 to -0.05 c/GV we detected 9 antiproton candidates, while in the corresponding positive range 60286 protons were observed.

4 Corrections

To get the number of primary antiprotons, the number of particles detected as antiprotons has to be corrected for several remaining background. While the background from albedos is negligible, the smooth curve on the left side of Figure 2 shows a folding of the Cherenkov counter inefficiency, the spectrometer resolution and the muon spectrum with a contamination of 15% pions, which was estimated from [7]. Due to the finite spectrometer resolution protons are capable of spillover to negative curvature. The smooth curve on the right side of Figure 2 shows a folding of a power law proton spectrum $R^{-2.75}$, the Cherenkov counter inefficiency for protons and the spectrometer resolution. The remaining background is also negligible in the observed rigidity range. The number of atmospherically produced antiprotons is calculated by propagating an incident cosmic ray spectrum observed at the top of the atmosphere through the residual 5.8 g/cm^2 above the instrument using the known antiproton production cross sections [6]. The number of secondary antiprotons is then normalized to the number of high energy protons. This results in a background of 3.43 atmospheric antiprotons.

Antiprotons may be vetoed due to annihilation products backscattering from the calorimeter into the instrument. To examine this, we processed the raw data with no restrictions on the bottom ToF or the tracking system. No candidates showing backscatter signature were found. Nevertheless we tried to determine a correction factor. We first considered a sample of protons to see if we could properly predict the number of interacting events in the calorimeter. The observed ratio of interacting events to non-

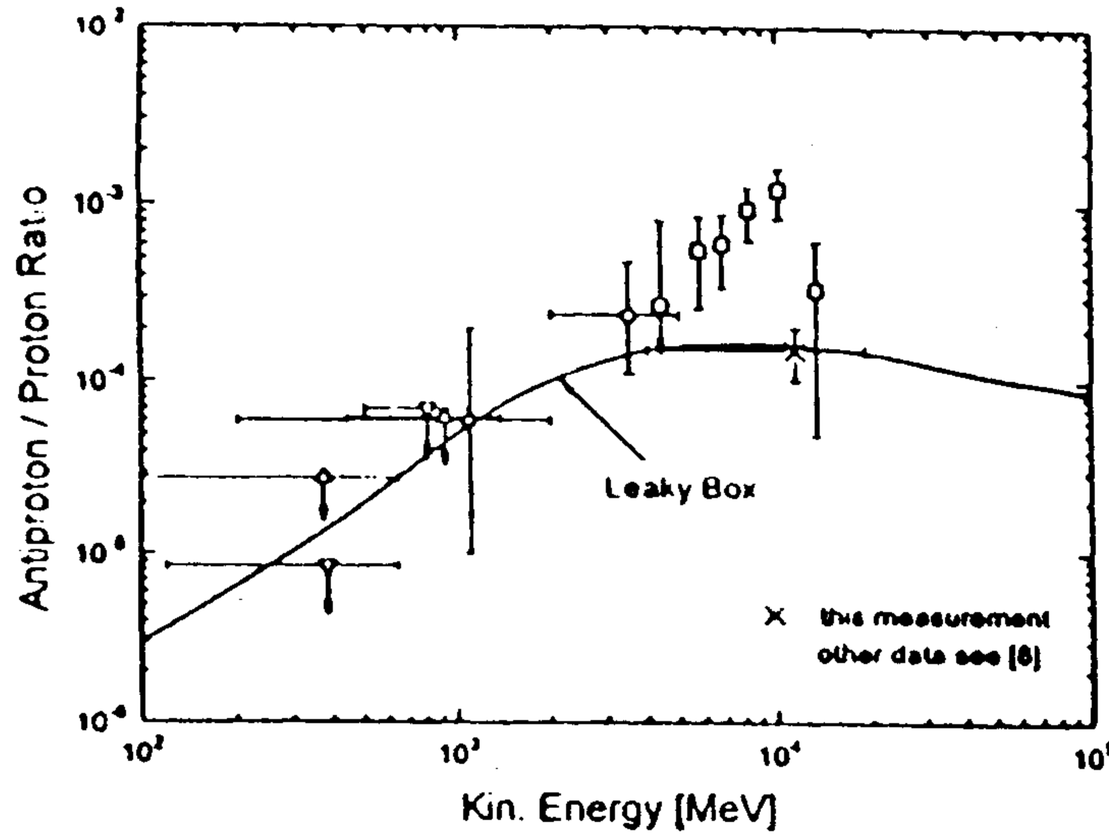

Figure 3 : Measured antiproton/proton ratio from the MASS2-experiment in comparison with other data and a calculation from Gaisser and Schaefer [8]

interacting events agreed with the predicted values to 2.5%. A similar analysis made for the antiprotons showed some difference between theory and observation. We expected 11.3 interactions, while only 7 interactions were found. This implies, as an upper limit, that 36% of the antiprotons could be self-vetoed, and hence should be corrected for.

K^- are also produced in the atmosphere above the instrument and could be interpreted as antiprotons. From [7] we estimated an upper limit for the K^- of 2% of the atmospherically produced antiprotons. Therefore this background was neglected.

Starting with the 9 observed antiprotons, we apply the self-veto correction factor and get 12.24 events. Subtracting the atmospheric antiproton background, yields 8.81 antiproton events. This gives an $\bar{p}/p$-ratio of $1.46 \cdot 10^{-4}$ at the payload or a ratio of $(1.52 \pm 0.52) \cdot 10^{-4}$ at the top of the atmosphere.

5 Conclusion

Figure 3 shows the result of this measurement together with other measurements. The $\bar{p}/p$-ratio, reported here, is lower than the previous measurement in this energy region [2] and is compatible with the predictions of a standard leaky box model.

To finally clear up the situation in this energy range one should aim for another measurement with more statistics.

Acknowledgements. This work was supported by NASA Grant NAG-110 and the National Scientific Balloon Facility on the US side, by the Instituto Nazionale di Fisica Nucleare and the Agenzia Spaziale Italiana on the Italian side and by the DARA and the DFG on the German side.

References

[1] Golden, R.L., et al., Phys. Rev. Letters 43 (1979) 1196
[2] Golden, R.L., et al., Astrophys. J. Letters 24 (1984) 75
[3] Golden, R.L., et al., Nucl. Instr. & Methods A306 (1991) 366-377
[4] Hof, M., et al., Nucl. Instr. & Methods A345 (1994) 561-569
[5] Golden, R.L., et al., to be submitted to Nucl. Instr. & Methods (1995)
[6] Stephens, S.A., Proc. 23rd Int. Cosmic Ray Conf. (Calgary), 2 (1993) 144
[7] Stephens, S.A., Proc. 17th Int. Cosmic Ray Conf. (Paris), 4 (1981) 282
[8] Gaisser, T.K., Schaefer, R.K., Astrophys. J. 394 (1992) 174

Rome 1995 XXIV ICRC OG 7.3.6, Vol. 3

$\bar{p}$ and e^+ identification capabilities of CAPRICE

G. Barbiellini[10], G. Basini[7], R. Bellotti[11], M. Bocciolini[8], M. Boezio[10], F. Massimo Brancaccio[8], U. Bravar[10], F. Cafagna[11], M. Candusso[9], P. Carlson[4], M. Casolino[9], M. Castellano[11], G. De Cataldo[11], M. Circella[11], A. Codino[6], N. Finetti[6], T. Francke[4], N. Giglietto[11], R.L. Golden[1], C. Grimani[6], M. Hof[12], B. Marangelli[11], C.N. De Marzo[11], J.W. Mitchell[3], A. Morselli[9], M.P. De Pascale[9], P. Papini[8], A. Perego[8], S. Piccardi[8], P. Picozza[9], M. Ricci[7], P. Schiavon[10], M. Simon[12], R. Sparvoli[9], P. Spillantini[8], P. Spinelli[11], S.A. Stephens[2], S.J. Stochaj[1], R.E. Streitmatter[3], M. Suffert[5], A. Vacchi[10], N. Weber[4], N. Zampa[10]

[1] Particle Astrophysics Lab, New Mexico State Univ., Las Cruces, New Mexico, USA
[2] Tata Institute of Fundamental Research, Bombay, India
[3] Goddard Space Flight center/NASA, Greenbelt, Maryland, USA
[4] Royal Institute of Technology, Stockholm, Sweden
[5] Centre de Recherches Nucléaires, Strasbourg, France
[6] Dipartimento di Fisica dell'Univ. di Perugia and INFN-Sezione di Perugia, Perugia, Italy
[7] INFN Laboratori Nazionali di Frascati, Frascati, Italy
[8] Dipartimento di Fisica dell'Univ. di Firenze and INFN-Sezione di Firenze, Florence, Italy
[9] Dipartimento di Fisica dell'Universita` di Roma II "Tor Vergata" and INFN-Sezione di Roma II "Tor Vergata", Roma, Italy
[10] Dipartimento di Fisica dell'Univ. di Trieste and INFN-Sezione di Trieste, Trieste, Italy
[11] Dipartimento di Fisica dell'Universita` di Bari and INFN-Sezione di Bari, Bari, Italy
[12] University of Siegen , Siegen, Germany

Abstract

The Cosmic AntiParticle Ring Imaging Cherenkov Experiment (CAPRICE) flew on a stratospheric balloon 8-9 August 1994 over northern Canada and collected data for more than 21 hours with less than 5 g/cm^2 of residual atmosphere. The instrument includes a solid radiator RICH detector and an electromagnetic calorimeter for particle identification in the magnetic spectrometer. Preliminary antiproton and positron identification capabilities are presented.

1 Introduction

The goal of the Cosmic AntiParticle Ring Imaging Cherenkov Experiment (CAPRICE) is to accurately measure the flux of antimatter (antiprotons and positrons) and light isotopes in the cosmic radiation and to continue the search for antinuclei. The main difficulty in these measurements is to safely identify the antiparticles in the presence of a large back-

ground. The spectrometer flew 8-9 August 1994 from Lynn Lake, Manitoba, Canada, (geomagnetic cut-off 0.1 GV/c and near solar minimum) for 27 hours, and collected data above 36 km for 21 hours. The analysis is still in an early phase but some preliminary results on the antiproton and positron identification capabilities are presented below.

The NMSU/WiZard CAPRICE balloon-borne magnet spectrometer [1] includes from top to bottom: a compact RICH detector (7 g/cm^2 material) [2-3], a time-of-flight system of scintillators (2 g/cm^2), a tracking system of drift chambers [4] and multiwire proportional chambers (<0.2 g/cm^2) with a super conducting magnet and a Si-W electromagnetic calorimeter (7 radiation length) [5-7].

2 Antiprotons

In the few GeV energy range the background for antiprotons, selecting negative particles by the bending in the magnetic field, consists mostly of e^-, π^- and μ^-. The number of K^- is small. In this preliminary analysis rather hard cuts were made on the tracking and on the RICH image. For the latter the image of the Cherenkov light (a circle with 10 cm radius for β=1 perpendicular incidence; for non-perpendicular incidence the image is a U-shaped pattern) was required to be well separated from the ionization of the primary particle. The Si-W calorimeter efficiently rejects events with an electromagnetic shower.

Interactions in or above the RICH are suppressed by requiring that only one charged particle traverses the RICH, the top scintillator and the tracking volume. Antiprotons that interact in the calorimeter are rejected in this first study since they will in some cases produce back scattered charged particle through the tracking system.

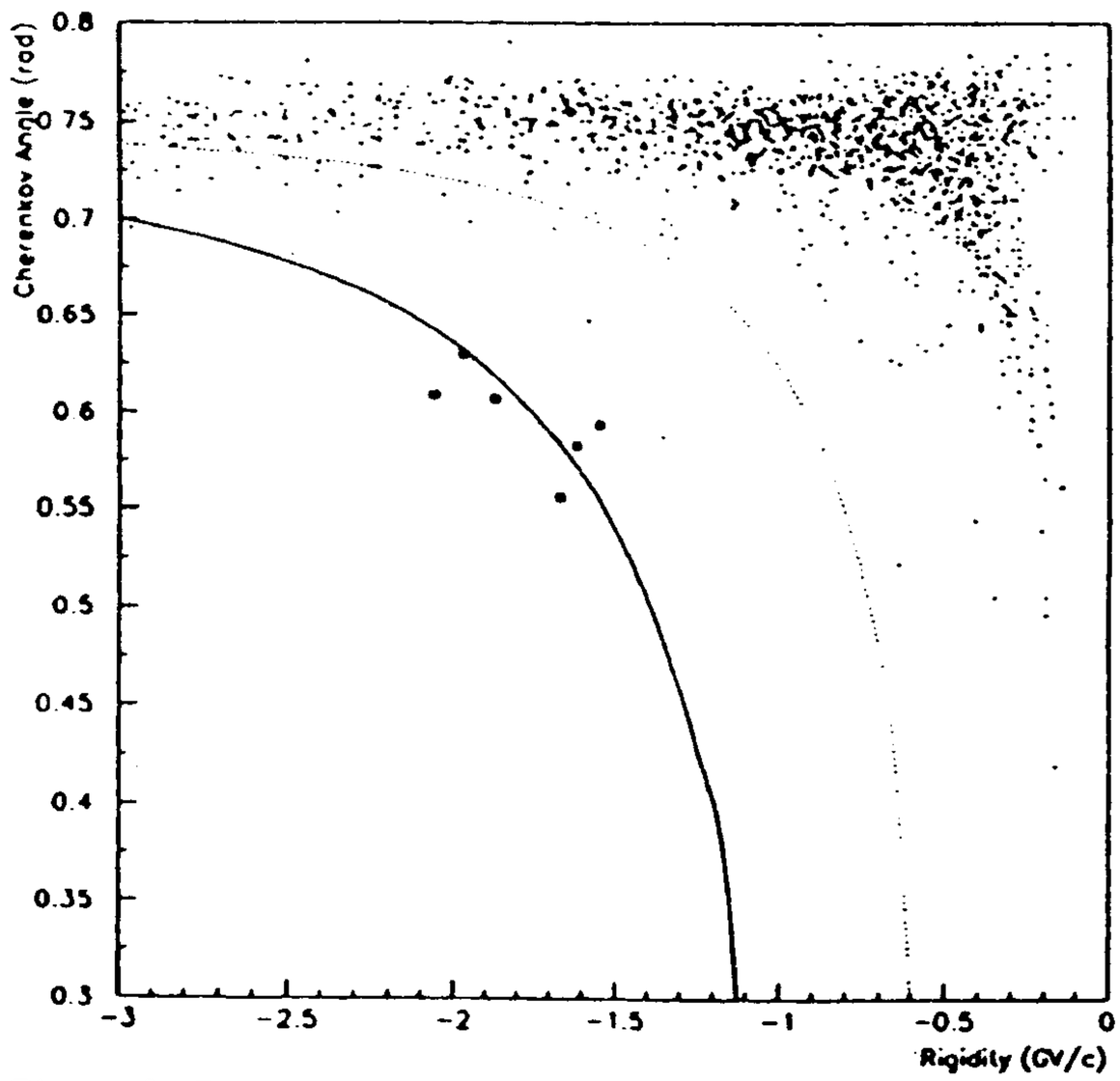

Figure 1. Cherenkov angle versus rigidity for negative particles.

Figure 1 shows the reconstructed Cherenkov angle as a function of rigidity for the negative particles after the cuts described above. The solid line indicates the expected Cherenkov angle for antiprotons and the dotted line that for kaons. For the preliminary results presented here a limited rigidity interval is selected, 1.5-2.3 GV/c (kinetic energy interval 0.8-1.5 GeV). The lower limit (1.5 GV/c) is chosen in order to safely discriminate the Cherenkov image from the ionization of the particle in the detector gas, and the upper limit (2.3 GV/c) corresponds to a separation between antiprotons and pions/muons of six standard deviations (r.m.s. is 15-18 mrad depending on incidence angle). There is a clear antiproton signal and the six antiprotons observed in this energy range are indicated with squares in the figure. In the same kinetic energy region there are 48057 protons. The energy range over which antiprotons can be identified by the spectrometer is significantly larger than described above by using the time-of-flight at lower energies and a refined combination of the RICH and the calorimeter at higher energies. The full analysis, which is in progress, will include corrections for antiprotons produced in the detector and in the atmosphere above as well as corrections for antiprotons interacting in the lower part of the spectrometer.

3 Positrons

For positrons in the few GeV energy range the dominating background is protons once positive particles have been selected by the bending in the magnetic field. In addition there are μ^+ and (less frequent) π^+ and K^+. The combination of an electromagnetic calorimeter and a RICH gives the necessary rejection power ($>\cdot 10^5$) to safely select positrons.

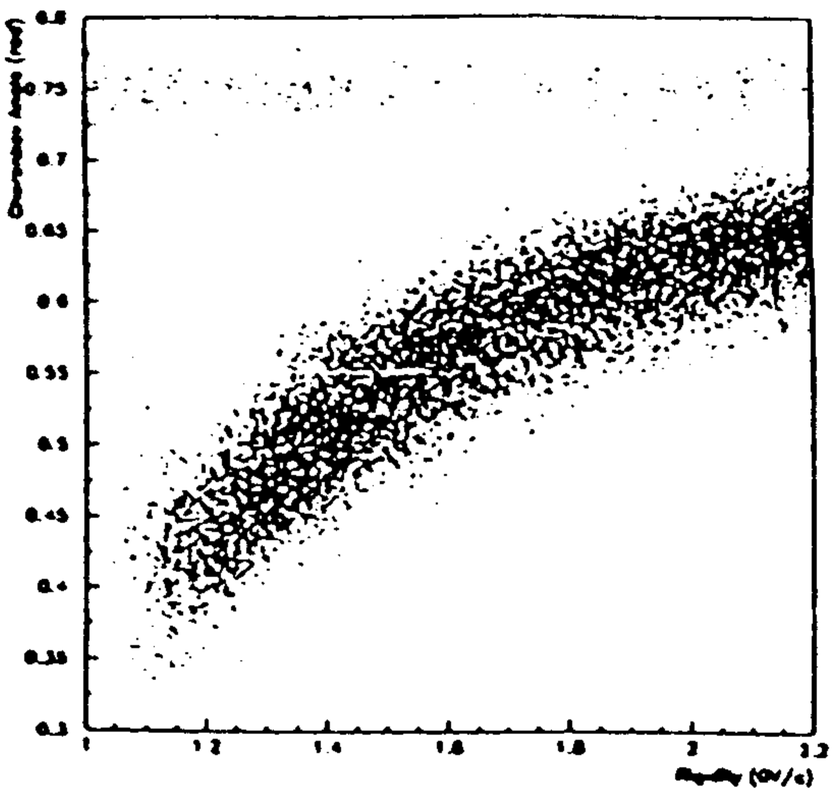

Figure 2. The Cherenkov angle versus rigidity after the RICH cuts, except the β=1 selection.

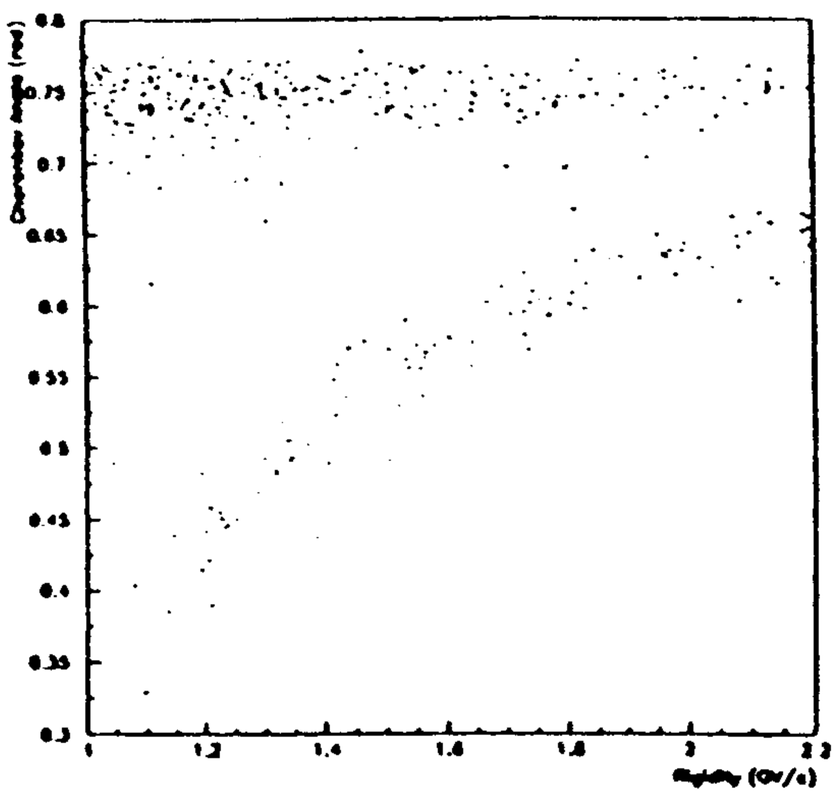

Figure 3. The Cherenkov angle versus rigidity after combining the calorimeter and the RICH cuts, but not the β=1 selection.

CAPRICE is one of the first experiments with good positron identification capabilities at kinetic energies below 3 GeV. Positrons are selected by first using the calorimeter data to reject non-electromagnetic particles on grounds of energetical and topological features of the shower. The remaining proton background is rejected by selecting only $\beta=1$ particles using the RICH. As for the antiprotons, the time-of-flight rejects albedo particles. Alphas are rejected by the RICH and the two scintillators. Figure 2 shows the Cherenkov angle versus rigidity for positively charged particles without using the calorimeter cuts but requiring a good quality of the Cherenkov image. Figure 3 shows the same events after the powerful calorimeter cuts that removes more than 99.9% of the protons. Combining the two detectors efficiently suppresses the large proton background.

Using these cuts, 1170 electron and 203 positron candidates are identified in the energy range 1-2.2 GeV where the positrons develop characteristic electromagnetic showers in the calorimeter, and where $\beta=1$ particles are well separated from the protons by the RICH. Simulations show that the cuts described above suppress all muons but leave a contamination of 0.18% pions and protons in the positron sample. Out of the 203 positron candidates this would mean that less than one is a proton or a pion. As with the antiprotons, the energy range where CAPRICE can identify positrons is significantly larger than what is described above if also the time-of-flight information and a more refined combination of the calorimeter and the RICH is included.

4 Discussion

All results presented above should be considered as preliminary since the analysis of the flight is still in an early stage, but they illustrate how the CAPRICE spectrometer can identify positrons and antiprotons.

The RICH and the calorimeter combined with the scintillators also identify light nuclei like ^{3}He and ^{4}He in the 1 GeV energy range. The combination of a RICH and an electromagnetic calorimeter constitutes a very efficient particle identifier.

Because the spectrometer can be made compact, a large solid angle can be achieved. The CAPRICE experiment will give significant results on antiproton and positron fluxes as well as of ratios of light nuclei in the few GeV energy range.

References

[1] Golden R.L., et al., Nucl. Instr. and Meth. **A306** (1991) 366.

[2] Carlson P., et al., Nucl Instr. and Meth. **A349** (1994) 577.

[3] Barbiellini G. et al., *The CAPRICE RICH detector*, this conf. proc.

[4] Hof M., et al., Nucl. Instr. and Meth. **A345** (1994) 561.

[5] Barbiellini G., et al., Nucl. Instr. and Meth. **A333** (1993) 560.

[6] Barbiellini G., et al., Nucl. Phys. C **32** (1993) 77.

[7] Barbiellini G., et al., *The WiZard/CAPRICE Silicon-Tungsten Calorimeter*, this conf. proc.

Rome 1995 XXIV ICRC OG 10.3.7, Vol. 3

The Magnetic Spectrometer PAMELA for the Study of Cosmic Antimatter in Space

O. Adriani[1], B. Alpat[2], G. Barbiellini[3], L.M. Barbier[4], S. Bartalucci[5], R. Bellotti[6], G. Basini[5], M. Bocciolini[1], M. Boezio[3], F M. Brancaccio[1], U. Bravar[3], F. Cafagna[6], M. Candusso[7], R. Cardarelli[7], P. Carlson[8], M. Casolino[7], M. Castellano[6], G. Castellini[1], M. Circella[6], E.R. Christian[4], A.J. Davis[9], G. De Cataldo[6], C.N. De Marzo[6], M.P. De Pascale[7], E. Fiandrini[2], N. Finetti[2], T. Francke[8], C. Fuglesang[8], A.M. Galper[10], F. Giannini[7], N. Giglietto[6], R.L. Golden[11], M. Hof[12], S.V. Koldashov[10], M.G. Korotkov[10], J. Krizmanic[4], M.L. Lamorte[5], M. Lanfranchi[2], P. La Riccia[2], B. Marangelli[6], L. Marino[5], R.A. Mewaldt[9], V.V. Mikhailov[10], J.W. Mitchell[4], A.A. Moiseev[10], A. Morselli[7], J.F. Ormes[4], J.V. Ozerov[10], P. Papini[1], A. Perego[1], S. Piccardi[1], P. Picozza[7], M. Ricci[5], P. Schiavon[3], S.M. Schindler[9], M. Simon[12], R. Sparvoli[7], P. Spillantini[1], P. Spinelli[6], S.J. Stochaj[11], R.E. Streitmatter[4], O. Toker[2], A. Vacchi[3], V. Vignoli[1], S.A. Voronov[10], N. Weber[8], N. Zampa[3]

[1] *Università and INFN, Firenze, Italy.* [2] *Università and INFN, Perugia, Italy.* [3] *Università and INFN, Trieste, Italy.* [4] *NASA Goddard Space Flight Center, Greenbelt, USA.* [5] *Laboratori Nazionali INFN, Frascati, Italy.* [6] *Università and INFN, Bari, Italy.* [7] *II Università and INFN, Roma, Italy.* [8] *Royal Institute of Technology, Stockholm, Sweden.* [10] *Moscow Engineering and Physics Institute, Moscow, Russia.* [11] *Particle Astrophysics Lab. New Mexico State University, Las Cruces, USA.* [12] *Universität Siegen, Fachbereich Physik, Siegen, Germany.*

Abstract

In the framework of the Russian Italian Mission (RIM) program, PAMELA is the experiment devoted to the accurate measurement of the positron and antiproton spectra from the very low energy threshold of 100 MeV up to more than 50 GeV, and to hunt antinuclei with sensitivity better than 10^{-7} in the antihelium/helium ratio. A permanent magnet equipped by microstrip silicon sensors, measures the particle momentum with MDR=400 GV/c on GF=25 cm^2 sr. An accurate ToF system, a 19 X_0 deep imaging calorimeter, an aerogel Cherenkov counter and a TRD detector complement the spectrometer in order an efficient $e^{\pm}/p^{\pm}$ separation and some light isotope identification capability. The PAMELA experiment will be carried out on a 700 km high polar orbit, on board of the Earth-Observation Meteor-3A satellite, to be launched at the end of 1988.

1 Introduction

The Russian Italian Mission (RIM) program takes advantage of the polar satellites of the series RESOURCE that the VNIIEM Institute of Moscow is regularly sending in space for the Earth surface observation. The polar orbit of these satellites guarantees the best collection rates and explorable energy ranges for the cosmic ray observation. The "downward to the Earth" attitude

of the Earth observation satellites is the proper one for the "outward form the Earth" required for observing cosmic rays. Finally the high height of their orbit (700 kg) allows a very long life of these satellites, whose attitude is mainly regulated by magnetic guidance systems. For these reasons during the 1993 our collaboration had an intense negotiation with the VNIIEM for accommodating particle telescopes on board of their satellites, concluded in November by the RIM feasibility study report [1].

The RIM program develops on three strictly interconnected stages:

– the RIM-1 experiment, by the small silicon detector telescope NINA, that besides a rich program of physics in the low energy range (tens of MeV/nucleon) will study the background fluxes and the silicon detector stability and possible degradation parameters on the RESOURCE orbit;

– the RIM-2 experiment, by the magnetic spectrometer PAMELA described in this talk, for the antimatter study in the cosmic rays;

– the preparation of the technology for a possible RIM-3 experiment, based on the imaging calorimeter GILDA, for the detection of high energy γ-rays.

The NINA telescope and the GILDA project are described in other papers presented at this conference.

2 The scientific objectives of the PAMELA experiment

The objectives of the RIM-2 experiment performed with the PAMELA telescope are the following:

– measurement of the antiproton and positron fluxes from less than 100 MeV up to more than 50 GeV;

– search for antinuclei with a sensitivity approaching 10^{-8} for the antihelium/helium ratio;

– energy spectra of the light isotopes in the few GeV/nucleon range;

– energy spectra up to several tens of GeV for the most abundant elements.

Additional objectives can be addressed, profitting of the polar orbit and of the long duration (>3 years) of the mission before and after the maximum of the 23rd solar activity cycle:

– modulation of galactic rays in heliosphere, by the study of latitude and longitude distributions of observed fluxes as a function of solar activity in a wide range of energies and particles;

– generation, distribution and acceleration of solar cosmic rays in the internal heliosphere;

– magnetosphere of the Earth in quiet and in disturbed conditions;

– stationary and disturbed fluxes of high energy particles in the Earth magnetosphere, such as protons and electrons from decay of albedo neutrons, antiprotons from albedo antineutrons, or fluxes variation connected with Earth

seismic activity and formation of typhoons;
- anomalous component of cosmic rays.

Table 1: Main parameters of the elements of the PAMELA telescope

	Volume(xyz) (cm×cm×cm)	Mass (kg)	R.O.ch (#)	Power (W)
Scintillation counters	38×34×2 + 17×15×2 + 33×30×1	24	24	40
Cherenkov	36×32×8	16	12	1
TRD	31×27×21	23	1.536	<30
Anti-coincidences	(21×6×1)×4+ (44×15×1)×8	13	20	1
Tracker	(28×24×0.8)×6	10	35.328	<90
Calorimeter	30×24×19	120	3.456	<60
Fast trigger		5		10
Electronics		5		25
Power supply		10		85
magnet	30×30×47	150		
Total	38×34×105	376	40.376	<342

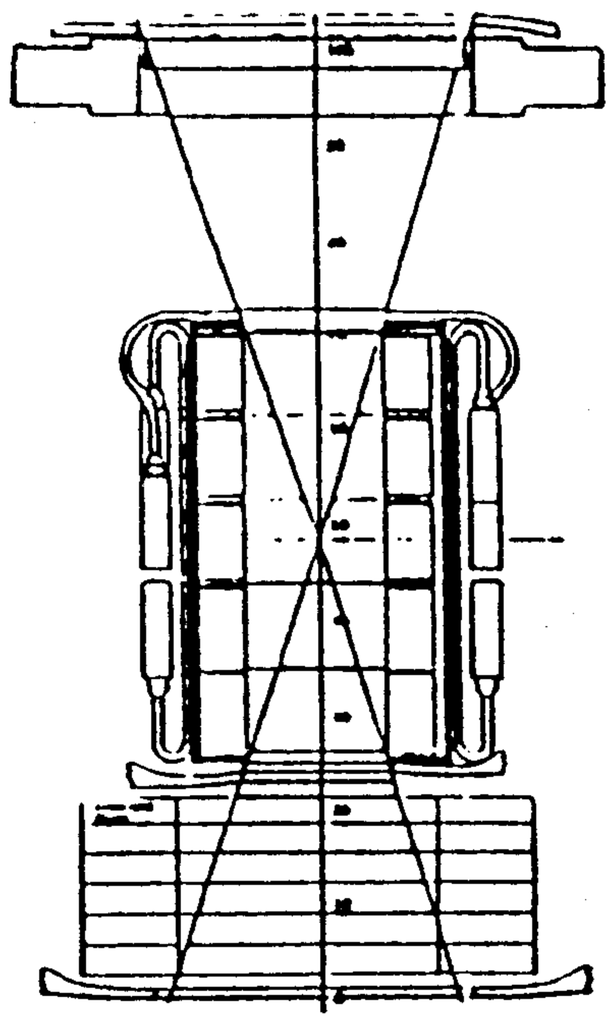

Figure 1: *The Pamela telescope*

3 The baseline design of the telescope

The experimental approach is the same of that proposed for the Wizard experiment on Astromag and used for the balloon flights of the Wizard collaboration (see the appropriate papers presented at this conference). It is based on the simultaneous measurement of the momentum of the particle in a magnetic spectrometer and of the pattern of the energy released in an imaging calorimeter. An energy release greater than that deduced from the rigidity measured in the spectrometer will be a significant signature for the annihilation identification. Furthermore the imaging capability of the calorimeter combines in the same instrument the particle identification by the pattern of its interaction inside the calorimetric volume.

Therefore the PAMELA telescope consists of:

(a) a permanent magnet equipped by a tracker based on microstrip silicon crystals for measuring the rigidity of the particle;

(b) an imaging calorimeter based on macrostrip silicon crystals for measuring the energy released by the particle and for identifying its nature by its interaction inside the calorimetric volume.

Other detectors complete the telescope:

(c) the first level trigger and the Time of Flight of the particle through the telescope are given by a system of four hodoscopes of scintillation counters;

(d) an aerogel Cherenkov counter helps the calorimeter in identifying the electrons and positrons up to 3 GeV;

protons	3×10^{8}
antiprotons	$\geq3\times10^{4}$
electrons	6×10^{6}
positrons	$\geq6\times10^{5}$
He nuclei	4×10^{7}
Be nuclei	4×10^{4}
C nuclei	4×10^{5}
antinuclei limit (90% c.l.)	7×10^{8}

Table 2: Expected rates in PAMELA in 10^8s

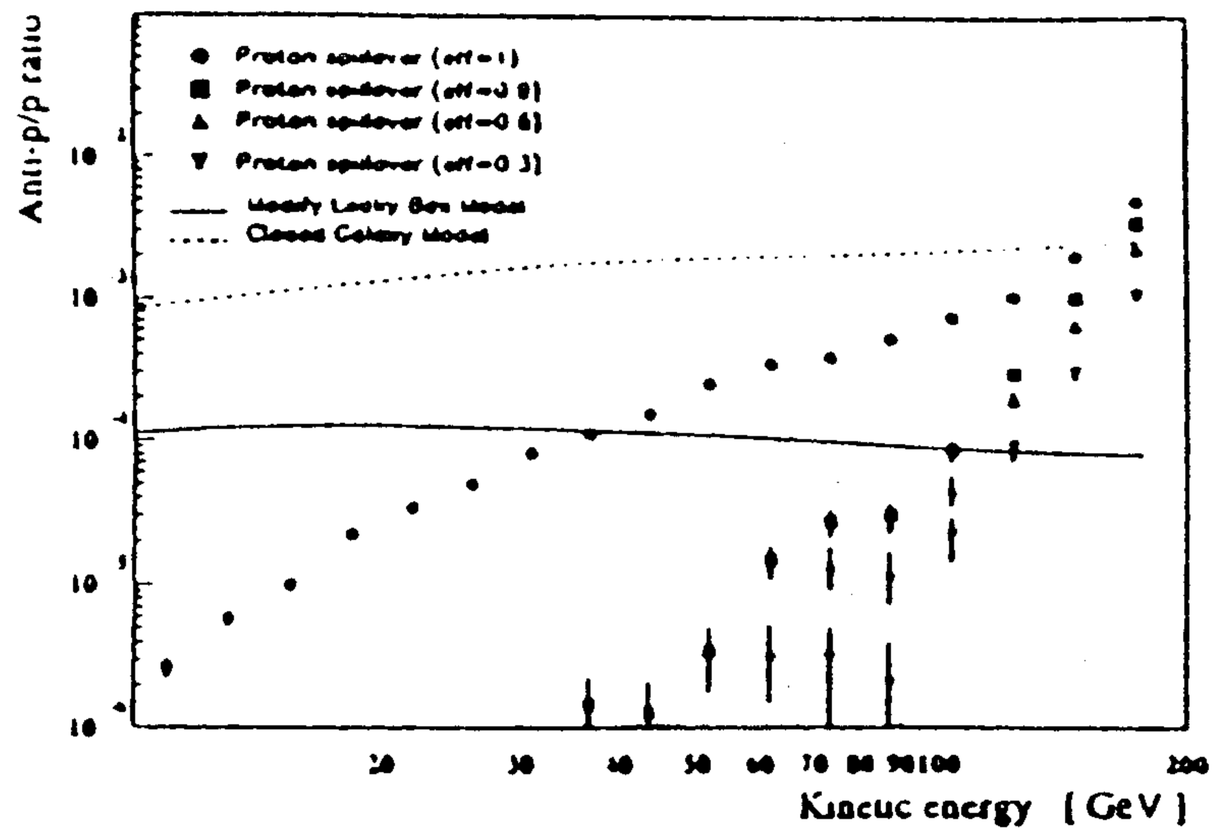

Figure 2: *Proton spillover background in the $\bar{p}/p$ measurement (cut efficincies: 1, 0.9, 0.6, 0.3)*

(e) a Transition Radiation Detector gives the same identification from 1.5 GeV up to the highest energies;

(f) several scintillation counters surround the magnet and can be put in anticoincidence for a better definition of the magnet entrance and for shielding the tracker from particle showering in the magnet;

(g) a scintillation counter on the bottom of the telescope give a fast label of the going through particles and of the not contained showers.

The telescope is closed in an Aluminium shell. The inner diameter and height of the shell are 140 cm and 105 cm. It will be mounted on the "outward from Earth" basis of the cylindrical body of the satellite. The total mass of the experiment will be 376 kg, and it will need 342 W to operate. The scheme of the telescope is reported in Fig. 1 and the volume, mass, number of channels and power consumption of each element are reported in table I.

The magnetic system is constituted by five identical permanent magnets interleaving six detection planes, each plane consisting of eight double-side microstrip silicon crystals It gives an average magnetic field of more than 3.5 kG on a 45 cm long path; the corresponding Maximum Detectable Rigidity is 385 GV/c. The Geometry Factor is 25 cm^2 sr, allowing to collect the numbers of particles and nuclei reported in Table 2. This acceptance was chosen for matching the collection of a significant rate on the most rear particles (the antiprotons) up to the highest detectable rigidity. The foreseen $\bar{p}/p$ flux ratio is compared in Fig. 2 with the spillover of protons on the antiproton side.

References

[1] "Objectives and feasibility of the Russian-Italian Mission program in Astroparticle Physics", November 1993.

Rome 1995 XXIV ICRC OG 10.3.11, Vol. 3

A Satellite Born Charged Particles Telescope for the Study of Cosmic Ray Nuclei

Barbiellini G. [1], Batischev A.G.[2], Bakaldin A.V.[2], Bidoli V.[3], Bartalucci S.[4], Bellotti R.[5], Bocciolini M. [6], Boezio M. [1], Bonvicini V.[1], Cafagna F.[5], Casolino M.[3], F. Fratnik[1], Candusso M. [3], Castellano M.[5], Circella M. [5], De Marzo C.[5], De Pascale M.P.[3], Galper A.M.[2], Koldashov S.V.[2], Korotkov M.G.[2], Mikhailov V.V.[2], Moiseev A. [2], Morselli A. [2], Murashov A.M.[2], Picozza P.[2], Ricci M. [4], Schiavon P.[1], Sparvoli R. [3], Spillantini P. [6], Spinelli P. [5], Vacchi A. [1], Voronov S.A.[2], Zampa N. [1]

1 *INFN and Dept. of Physics Univ. of Trieste*
2 *Moscow Engineering Physics Institute 31 Kashirskoe shosse Moscow 115409 Russia*
3 *INFN and Dept. of Physics Univ. of Roma Tor Vergata*
4 *INFN Laboratori Nazionali di Frascati, Italy*
5 *INFN and Dept. of Physics Univ. of Bari*
6 *INFN and Dept. of Physics Univ. of Firenze*

Abstract

The deseription of the high energy particle telescope NINA for the study of cosmic ray nuclei is presented. The instrument will be installed on board of the Resource 01 satellite and will fly on a polar orbit at 690 Km . The telescope consists on a pile of 16 detecting planes each of them is composed by two silicon strip detectors with perpendicular strips and has a total area of 60 x 60 mm^2 .The experiment goals are the study of cosmic ray protons and nuclei in the energy range 12-100 MeV/amu. It will be sensitive to the anomalous component and will also make the observation of the large solar flare events and geophysical phenomena as well. This experiment is the first step of the program RIM whose goal is the satellite study of anti particles in primary cosmic rays.

1 Introduction

In the frames of a study of the primary components of cosmic rays the INFN, Italian National Institute for Nuclear Physics and MEPI Moscow Engineering Physics Institute and VNIIEM - one of the largest Russian space companies - are developing a program of observation with satellite borne detectors. The astroparticle physics program RIM (Russian Italian Mission) [1] has as a main objective the investigation of antiparticle fluxes - antiprotons and positrons of galactic and extra galactic nature - in a wide energy range. The final experiment will use magnetic spectrometer, particles identifiers and imaging calorimeter developed on the base of silicon strip detectors technique[2].
We describe the first step of this program called RIM1 NINA, small size charged particle telescope. This experiment is dedicated to the investigation of cosmic ray nuclei in the energy range of 12 - 100 MeV/amu.

2 The experimental tasks

This experiment will be carried out on board of the VNIIEM satellite Resource 01. The satellite has a polar circular orbit with an inclination of 98° an altitude of 690 km and a rotation period of 98 min. The telescope is oriented towards the zenith.

The instrument will allow to fulfil different physical tasks; the orbit in which the experiment flies allow to study two basically different regimes. Around the poles the observation will not be influenced by the particles captured in the magnetosphere and will be able to collect events from GCR (Galactic Cosmic Rays) and SEP (Solar Energetic Particles) fluxes [3] and non trapped ACR (Anomalous Component of Cosmic Rays) [4]. While in the remaining orbit the instrument will fly in the magnetosphere and will have access to the observation of the ACR component which is captured and accumulated in the magnetosphere self. In this second part of the orbit the instrument is also sensitive to phenomena induced by geophysical effects [5].

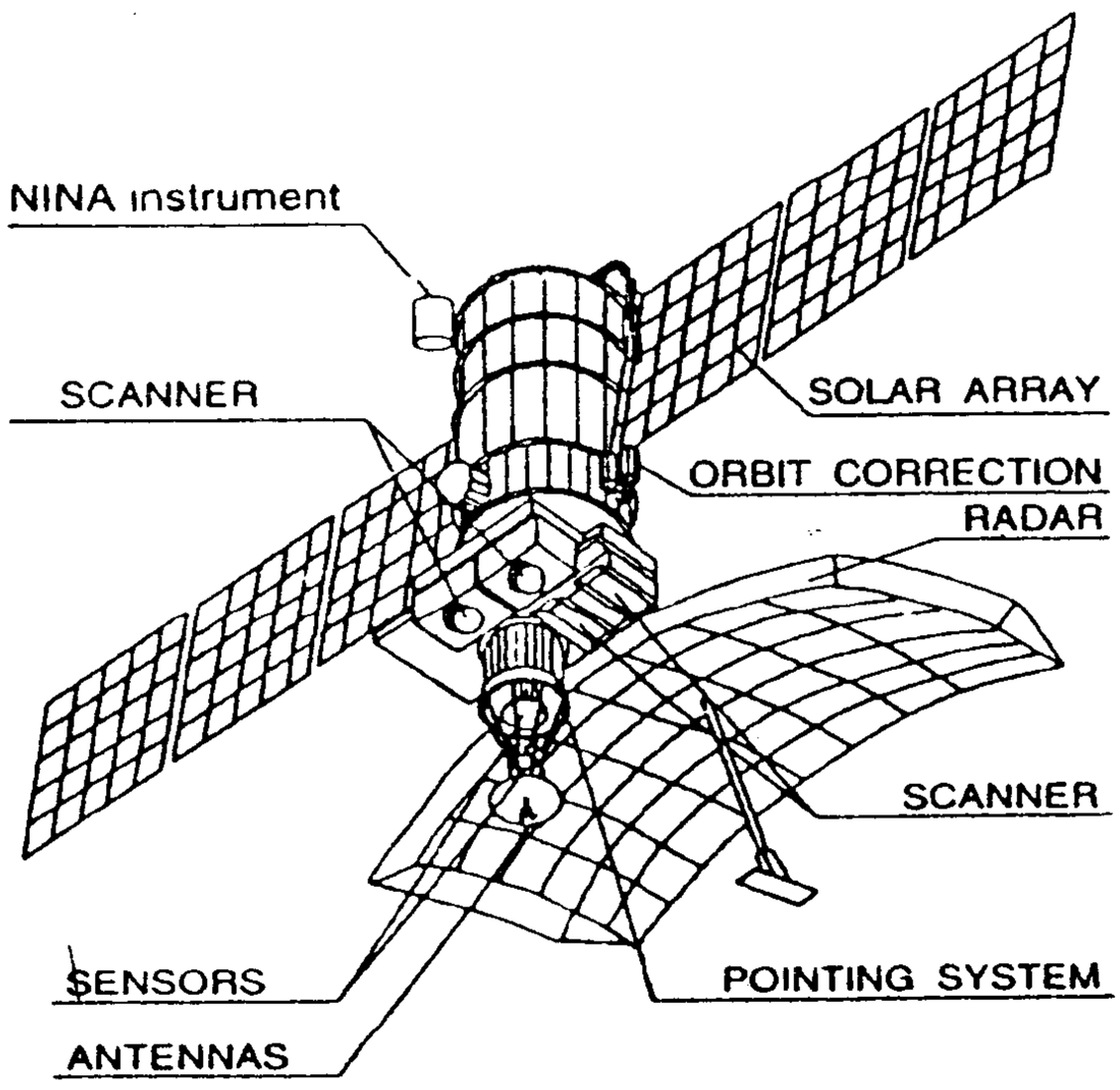

Figure 1

3 Description of the instrument

The NINA telescope will be located in the uppermost part of the spacecraft in a special vessel at atmospheric pressure as shown on Figure 1. The wall of the aluminium vessel has a thickness of 2 mm, a thin window of 300 μm Al has been provided in the field of view of the telescope.

The instrument consist of 16 layers of silicon strip detectors D_1-D_{16} having a total area of 60×60 mm^2. Each layer includes two detectors (each 380 μ thick) having perpendicular strips X and Y, the support of this detector assembly does not introduce passive material in the path of the particles. The detailed construction of the silicon detector is reported elsewhere [2]. The strips allow the determination of the deposited energy and of both coordinates X and Y of the detected particle.The scheme of the telescope is shown on Figure 2. The distance between the first two detectors D_1 and D_2 is 85 mm. The detectors D_2+D_{16} are situated one under the other and are equally spaced. The total height of the telescope's tower is 28.1 cm. A measure of the incident angle of the particle is allowed by the X and Y coordinates of the first two detectors D_1 and D_2. The angular resolution is about 2.4°. The particle energy is determined by measuring both range and energy deposit

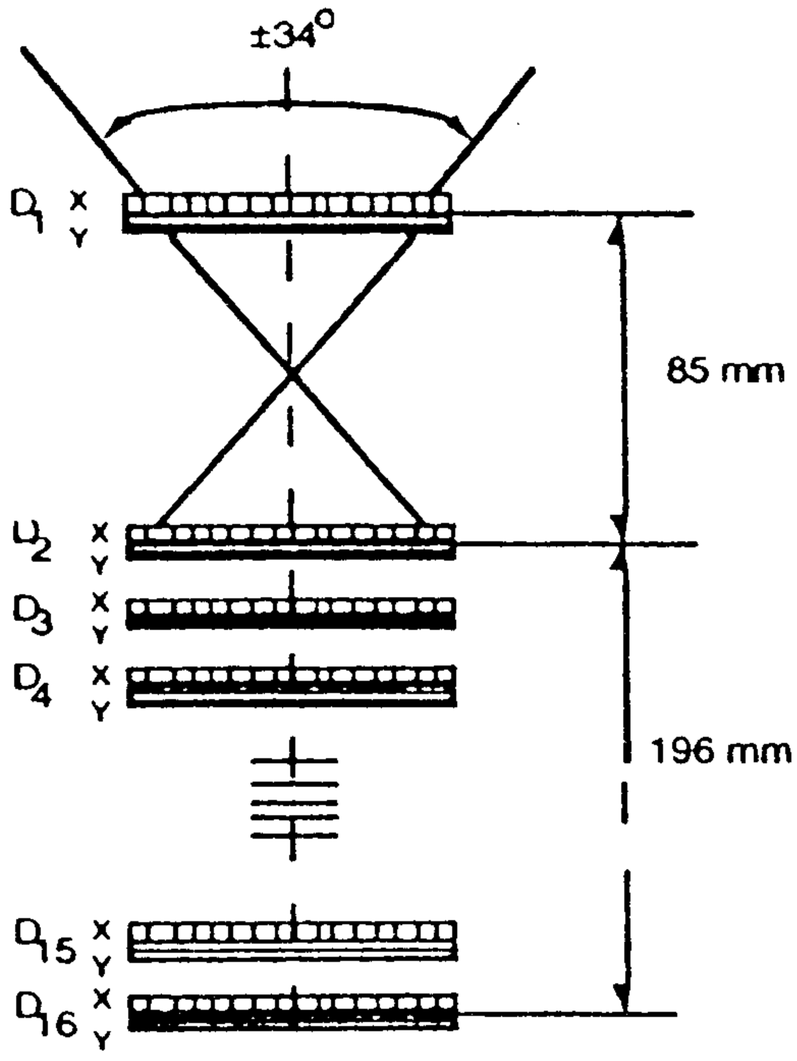

Figure 2

in each detector.A coincidence pulse coming from D_{1x} D_{1y} and D_2 triggers the read-out of the detectors.The D_{16} detector and all edge strips of the remaining detectors are in anti coincidence with this pulse so that only particles stopping within the spectrometer are accepted. This provides a geomfactor for 12-50 MeV protons 10.8-1.2 cm^2·sr. The performances of "NINA" instrument are presented in Table 1. The instrument is able to measure the energy of nuclei up to and above Oxygen. The read out logic has two energy thresholds corresponding to an energy deposit in one strip of 2.5 mip (minimum ionising particle, 1 mip ≈ 100KeV) and 25 mip. In this way the instrument can remain active to look for heavy nuclei also in presence of high proton fluxes. The dynamic range of the front end electronics is 1000. This value determines the acceptance energy windows for different kinds of particles. On the Figure 3 the plot ΔE-E for different particles is shown. ΔE is the energy deposited in D_{1x} detector, and E is total energy released in D_2-D_{15} detectors. It was obtained by Monte Carlo calculation using Vavilov-Landau distribution for fluctuations of ionization losses of charged particles. One can see the performance of the instrument to separate different groups of nuclei and to identify isotopes.

TABLE 1

Energy range protons ^4He ^{16}O	 12 +50 MeV/amu 12 +50 MeV/amu 26+105 MeV/amu
Geomfactor (protons E=12 MeV) (protons E=50 MeV)	10 cm^2·sr 1 cm^2·sr
Aperture (proton E=20 MeV) (proton E=50 MeV)	34° 20°
Angular resolution	2.4°
Dead time	4 ms
Resolution time	600 ns
Anticoincidence efficiency	99.99 %
Energy resolution	< 10 %

4 Data handling

If the event is accepted by the trigger the information is read by a data acquisition system driven by two microprocessors and stored in a FIFO memory. The microprocessor unit executes fast analysis of data, chooses good events and rejects wrong ones . The data are

then compacted and delivered to the spacecraft interface based on a powerful microprocessor block which organises the output information formats, stores it in a MASS MEMORY (15 MB) and control the transmission of data to the ground stations. The data will be transmitted to ground at the maximal rate of 5 Mbytes/day.

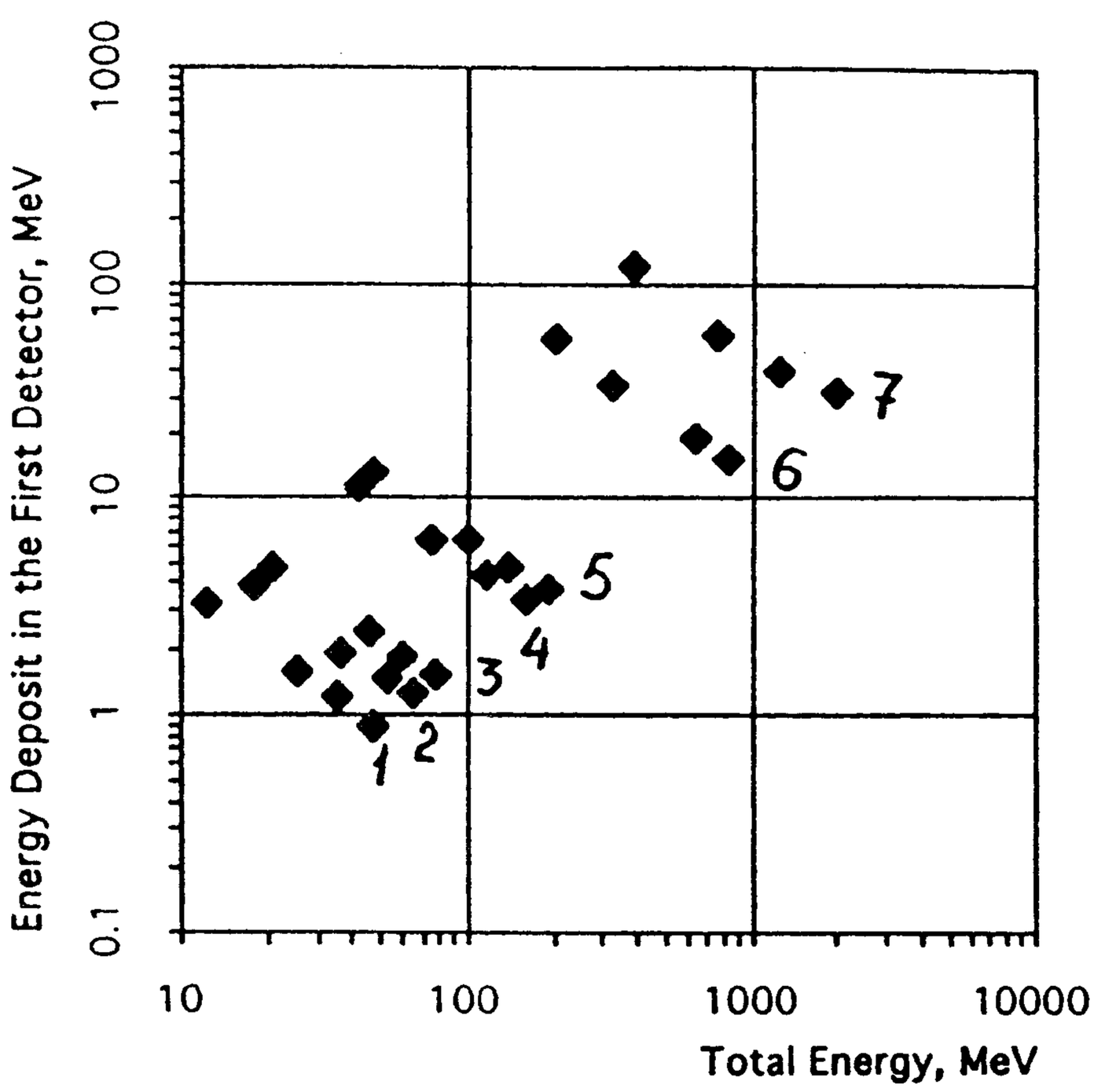

Figure 3

ΔE-E plot for diferent nuclei: 1 - Proton, 2 - Deuterium, 3 - Tritium, 4 - ^{3}He, 5 - ^{4}He, 6 - ^{9}B, 7 - ^{16}O.

5 Conclusion

The NINA instrument will be put in orbit in 1996. This will allow to carry out the measurements of the various components of cosmic rays accessible to the instrument in the period of solar minimum. This will give new contemporary information complementary to other instruments flying in different orbits and positions within the solar system.
The magnetosphere phenomena such as particle precipitation from radiation belt caused by different reasons, pulsation of intensities, creations of quasi belts of high energy particles will also be investigated.

References

[1] Russian-Italian Mission, RIM project, INFN-MEPI-VNIIEM, October 1993.
[2] M. Bocciolini et al., NIM A333 (1993) 77
[3] Galper A.M. et al. Proc. 14 Europeen Cos. Ray Symp. Budapest 1-SH-32P (1994)
[4] Cummings J. R. et al.Proc.23d ICRC 3 (1993)428.
[5] Galper A.M., Koldashov S.V., Voronov S.A. Adv. Space Res. 15 (1995) 131.

Rome 1995 XXIV ICRC OG 10.3.20, Vol. 3

Application of the image calorimeter in the high energy gamma astronomy

P.Carlson[1], M.Casolino[3], C.Fuglesang[4], A.M.Galper[2], A.Morselli[3], Yu.V.Ozerov[2], P.Picozza[3], R.Sparvoli[3], V.M.Zemskov[2], V.G.Zverev[2]

[1] *Royal Institute of Technology, Stockholm, Sweden*
[2] *Moscow Engineering Physics Institute, Moscow, Russia*
[3] *Dipartimento di Fisica e Sezione INFN dell'Universita' di "Tor Vergata", Roma, Italy*
[4] *ESA-EAC, Cologne, Germany*

Abstract

The capability of registration of the primary high energy cosmic ray gamma emission by a gamma-telescope made of an image calorimeter is shown in this paper. The problem of triggering and off-line identification of primary particles by the analysis of the electromagnetic showers induced in the calorimeter is under consideration. The estimations of the background flux of delayed secondaries induced by nuclear interactions are presented too.

1. Introduction

Last years several proposals for new gamma astronomy experiments onboard space vehicles were published [1,2,3,4]. The increased solid angle coverage is the main common achievement for new generation telescopes. Thereby these telescopes do not include the convenient facilities for background rejection such as Cherencov counters or Time-of-Flight devices. Despite the very attractive parameters of the proposed instruments, Their triggering performances are not satisfactory, so a brief analysis of possible methods of particle identification is presented below. The tasks of the identification of straight flux particles (from upper hemisphere) and estimation of the background from proton interactions are taken into account.

For this study the layout of GILDA telescope shown in fig 1 has been considered. A more detailed description of this telescope is presented in [4]. The telescope model used for simulation includes a tracker made of 10 layers of silicon strip detectors; each layer consists of two plates with mutually orthogonal strips. Tungsten plates of 0.15 radiation unit thickness are inserted between the Si-layers. The absorbing part below consists of 10 similar Si layers, but with thicker absorbing tungsten plates (1 Xo each). The total thickness of the telescope is about 11 Xo. The tracker is covered with an anticoincidence counters AC of 3 cm thickness. Scintillation counters C1,C2,C3 are included into the telescope for triggering.

The presented layout, in its basic features is similar the ones proposed in the above mentioned new projects, so it could be considered as a basis for studying the problem of triggering and estimations of the background; in this way, the results presented below will

concern not only GILDA but all wide aperture gamma-telescopes with selection of particles by the analysis of electromagnetic showers production.

For this device two levels of triggering are proposed. The first level trigger (fast) is produced by the condition of having the coincidence of pulses from C1, C2 and C3 counters (each with its own threshold) and the absence of a pulse from anticoincidence system. The fast trigger task is to select events corresponding to a given energy deposit distribution along the shower track. It will be possible to tune the counter thresholds in order to change the trigger rate and the energy range.

The second level trigger (slow) allows the formation of the output data set for separate detected good event and recording it into the satellite memory. It is produced after the readout and analysis of the data from all strips on condition of the accordance to some requirements of the energy deposited in all active layers and the spatial distribution of electromagnetic shower particles on the primary particle track depth in the plane, which is perpendicular to the direction of the primary particle. An analysis of the accordance to these requirements is executed by the board microprocessor. Because the data readout from Si-strip detectors and especially the data processing by the onboard CPU are relatively slow processes, the preliminary suppression of background is necessary.

Simulation study was performed by GEANT 3.14 software. Energy cutoffs for electrons and gammas was 100 keV, for hadronic particles was 10 MeV.

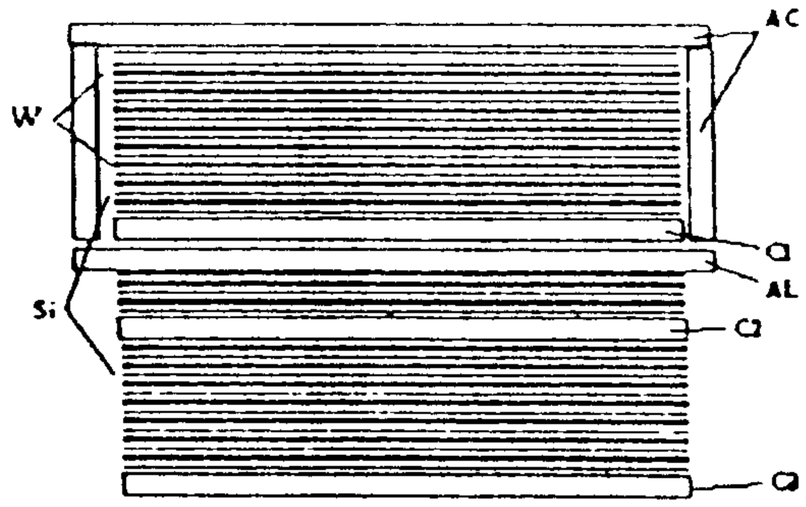

Fig. 1 Telescope layout

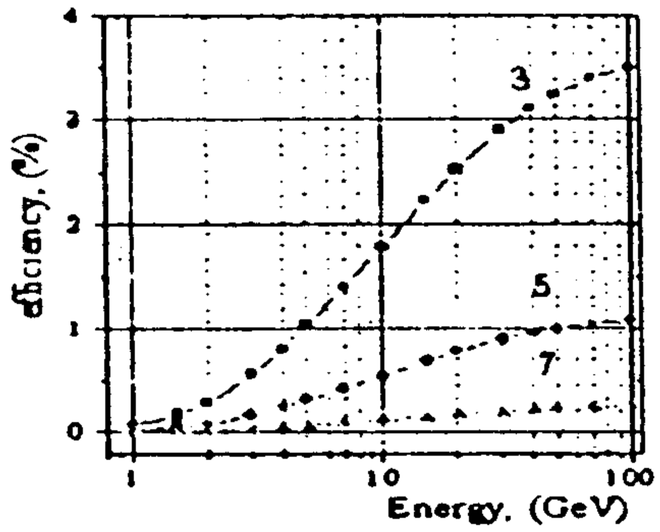

Fig 2 Soft trigger efficiency for inverse proton flux. Curves 3, 5, 7 are plotted on condition of hits 3, 5, 7 neighbor Si layers

2. Iidentification of particles direction.

The problem of rejection of inverse (from lower hemisphere) flux of gamma emission is very important in gamma astronomy experiments. Earth albedo gammas and secondary gamma quanta produced in cosmic ray interactions with satellite matter produce a huge background flux, which as a rule exceeds the primary cosmic gamma emission one.

For the separation of direct flux particles the criteria of certain distribution of energy deposit and spatial distribution of secondary particles along the depth of electromagnetic shower trace are suggested in this concept at the fast and slow trigger level.

Only the worse case from the viewpoint of the triggering was taken into account for the simulation of the inverse flux: an average electromagnetic shower, which has the maximum of its development at the C3 counter level. The simulation results show, that

the rejection of inverse γ by using certain energy thresholds in the trigger counters in a fast trigger can not be better than a factor of 20.

The additional rejection is provided at the slow trigger level by the analysis of the shower particles dispersion in the plane, perpendicular to the shower trace, and by the variation of this dispersion along the shower depth. For example, in our analysis the primary particles track in calorimeter is approximated by the straight line with the usage of strip coordinates in each separated strip detectors section. The results of the comparison of χ^2 values for such analysis of direct and inverse flux particles of energy 1 GeV show that the difference of χ^2 value is remarkable large. For direct flux χ^2 :corresponds to the degree of freedom, but for inverse flux all events have χ^2 more than 100 (difference reaches two orders of magnitude.) It was found that event selection by χ^2 value gives the possibility to achieve for slow trigger the high rejection coefficient (up to 10^3) for inverse flux particles without any influence on the telescope efficiency in the straight direction.

3. Background from π–μ–e decay.

The π–μ–e decay process is the strongest mechanism for background production for gamma-telescopes for low energy range. Anticoincidence counters do not suppress most of background electrons because they appear in telescope volume with delay corresponded to muon life time.

Two triggers for γ-quanta detection were under consideration:

1) hard trigger - includes the requirement of simultaneous signals from scintillation detectors C1-C3 with high energy thresholds (0.3, 5 and 0.3 MIP respectively). Such trigger provides the registration of γ-quanta of energy more than 500 MeV;

2) soft trigger, which provides a registration of γ-quanta of energy more than 50 MeV. For example, a trigger including condition of the simultaneous hits of 3 or more neighbor strip plates in the telescope top over C1 can be taken.

Two cases of proton incidence on telescope surface were taken into account:

- proton incidence at 0° at the center of top anticoincidence detector in up-down direction;
- proton incidence at the center of C3 counter in inverse direction.

For study of a background caused by π–μ–e decay, first, the coordinates and charge of stopping meson were calculated, then the path of each particle in telescope volume was analyzed. The average amount of stopping muons per one proton interaction increases strongly with the proton energy and reaches 1.0 at 50 GeV.

In Fig.2 the efficiency of proton registration as a function of energy is plotted for different soft triggers. The presented data correspond to the case of proton movement in inverse direction (down-up). For protons of direct flux, moving in straight direction, this value is smaller of a factor 3.5 . This difference can be explained by increasing of the stopping muon amount along the depth of electromagnetic shower.

In "hard" trigger case for $3.\ 10^5$ incidence protons no one false event was registered.

Note that π--μ–e decay background in soft trigger case could be suppressed by an order of magnitude at the slow trigger level by selection of two track events.

4. Neutral secondaries background producing in vehicle walls.

For a study of false events caused by proton interactions with production of neutral secondaries in the payload walls the proton incidence at the edge of the aluminum plate of 1.5 mm thick placed above the top scintillation detector AC was simulated.

First, a strong rise of background efficiency as a function of proton incidence angle was found. For the worst conditions of soft trigger and 85° angle the efficiency as a function of proton energy is plotted in Fig. 3. This is the worst case from the point of view of background estimations because the largest path of incident proton in payload wall. This curve provides a very high count rate for false events in real experiment due to corresponding cosmic ray proton fluxes in space. An attempt to lower background by image analysis in tracker (requirement of two tracks) was not successful - only a half of false events was rejected.

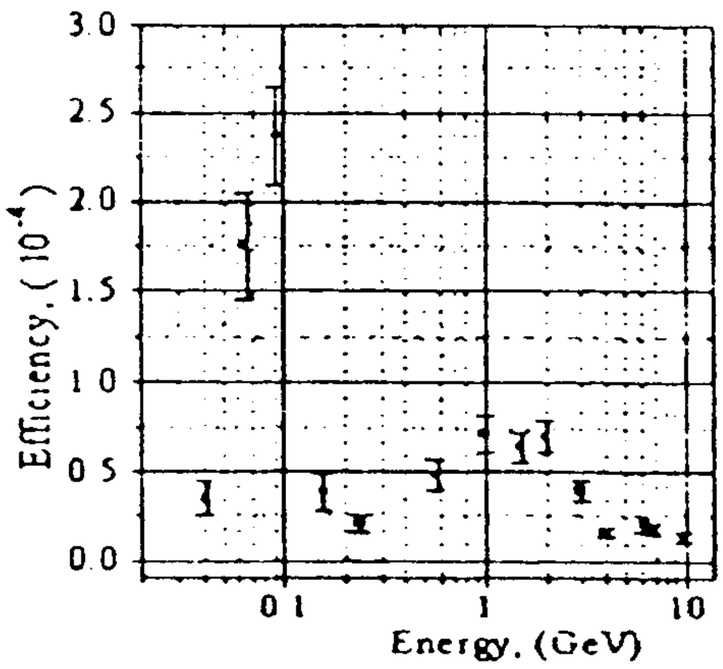

Fig.3 *Soft trigger efficiency at 85° proton incidence angle*

For hard trigger the same efficiency is much more suitable and not exceed 5. 10^{-6} for any proton energy.

For telescope EGRET the similar phenomenon was found in the experiment with a proton beam of energy 1.8 GeV[5]. The corresponding probability of false events was defined as 2.5 10^{-6}.

4. Conclusion.

Presented brief survey of simulation results has shown that the proposed telescope concept is capable for the detection of high energy gamma rays (more 500 MeV) from the viewpoint of the background conditions. The triggering problem in a low energy range seems very difficult and requires additional studies.

References.

1. W.B. Atwood et al. A proposal for high energy gamma-ray telescope.(1994).
2. A.Alpar, D.Bhattacharya et al. In AIP Conf. Proc., II Compton Symp., College park, MD(1993)304.
3. P.Carlson and C.Fuglesang. A proposal for a high energy gamma - ray experiment(1993).
4. G.Barbiellini et al. "Wide aperture telescope for high energy gamma astronomy". To be published in Proc. of Conf. "Trends in Astroparticle Physics", Stockholm, (1994).
5. D.J.Thompson et al. Calibration of the energetic gamma ray experiment telescope (EGRET) for the Compton gamma ray observatory. To be published in AJ (Suppl.)

Rome 1995 XXIV ICRC OG 10.3.23, Vol. 3

The CAPRICE RICH Detector

G. Barbiellini[10], G. Basini[7], R. Bellotti[11], M. Bocciolini[8], M. Boezio[10], F. Massimo Brancaccio[8], U. Bravar[10], F. Cafagna[11], M. Candusso[9], P. Carlson[4], M. Casolino[9], M. Castellano[11], G. De Cataldo[11], M. Circella[11], A. Codino[6], N. Finetti[6], T. Francke[4], N. Giglietto[11], R.L. Golden[1], C. Grimani[6], M. Hof[12], B. Marangelli[11], C.N. De Marzo[11], J.W. Mitchell[3], A. Morselli[9], M.P. De Pascale[9], P. Papini[8], A. Perego[8], S. Piccardi[8], P. Picozza[9], M. Ricci[7], P. Schiavon[10], M. Simon[12], R. Sparvoli[9], P. Spillantini[8], P. Spinelli[11], S.A. Stephens[2], S.J. Stochaj[1], R.E. Streitmatter[3], M. Suffert[5], A. Vacchi[10], N. Weber[4], N. Zampa[10]

[1] Particle Astrophysics Lab, New Mexico State Univ., Las Cruces, New Mexico, USA
[2] Tata Institute of Fundamental Research, Bombay, India
[3] Goddard Space Flight center/NASA, Greenbelt, Maryland, USA
[4] Royal Institute of Technology, Stockholm, Sweden
[5] Centre de Recherches Nucléaires, Strasbourg, France
[6] Dipartimento di Fisica dellÚniv. di Perugia and INFN-Sezione di Perugia, Perugia, Italy
[7] INFN Laboratori Nazionali di Frascati, Frascati, Italy
[8] Dipartimento di Fisica dell'Univ. di Firenze and INFN-Sezione di Firenze, Florence, Italy
[9] Dipartimento di Fisica dell'Universita` di Roma II "Tor Vergata" and INFN-Sezione di Roma II "Tor Vergata", Roma, Italy
[10] Dipartimento di Fisica dell'Univ. di Trieste and INFN-Sezione di Trieste, Trieste, Italy
[11] Dipartimento di Fisica dell'Universita` di Bari and INFN-Sezione di Bari, Bari, Italy
[12] University of Siegen , Siegen, Germany

Abstract

A compact RICH detector has been developed and used for particle identification in a balloon-borne spectrometer to measure the flux of antimatter in the cosmic radiation. This is the first RICH detector ever used in space experiments that is capable of detecting unit charged particles, such as antiprotons. The RICH and all other detectors performed well during the 27 hour long flight.

1 Introduction

The goal of the Cosmic AntiParticle Ring Imaging Cherenkov Experiment (CAPRICE) is to accurately measure the flux of antimatter (antiprotons and positrons) and light isotopes in the cosmic radiation and to continue the search for antinuclei. The NMSU/WiZard CAPRICE balloon-borne magnet spectrometer [1] includes a superconducting magnet, a

time-of-flight system of scintillators, a tracking system of drift chambers [2] and multiwire proportional chambers, an electromagnetic calorimeter [3-4] and a RICH detector [5]. The spectrometer flew 8-9 August 1994 from Lynn Lake, Manitoba, Canada, for 27 hours and collected data for more than 6 million cosmic ray particles. This paper describes the principle of the solid radiator RICH detector and its performance during the flight.

2 The RICH Detector

The principle of the RICH detector is shown in figure 1 [5]. When a charged particle traverses the detector from above Cherenkov light is emitted in a solid radiator of NaF. The cone of Cherenkov light refracts out of the crystal and is expanded in a nitrogen volume before entering into the photosensitive part of the detector through a thin quartz window.

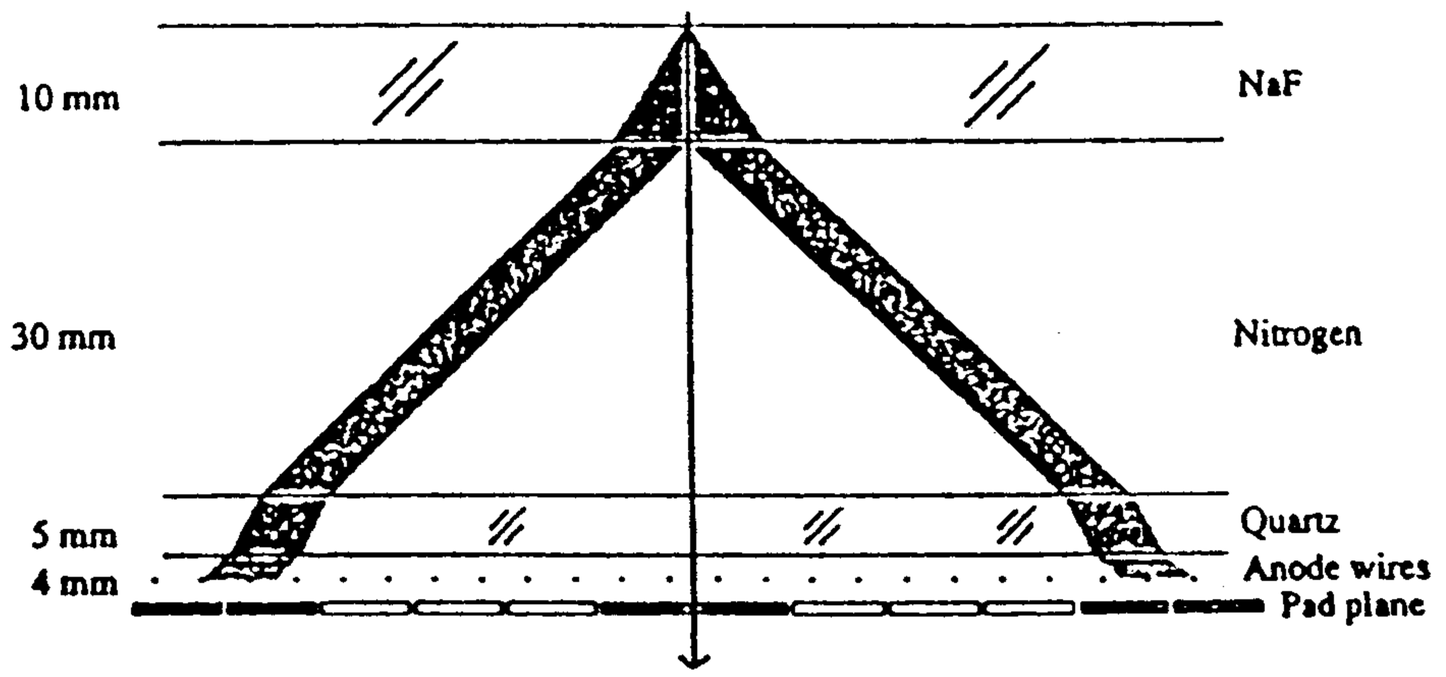

Figure 1. A schematic view of the NaF RICH detector. A β=0.88 event is indicated. The Cherenkov light emitted in the NaF crystal is detected in a photosensitive MWPC with pad readout.

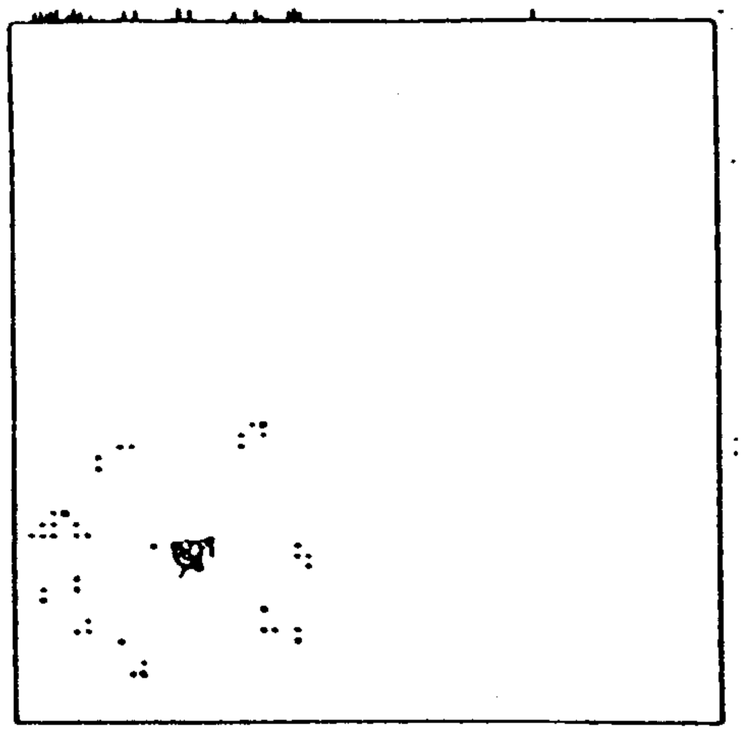

Figure 2. A single 4 GeV kinetic energy proton event at nearly perpendicular inc.

The Cherenkov photons produce photoelectrons through photoeffect with the photosensitive gas tetrakis-(dimethylamino)-ethylene (TMAE) [6]. The photoelectrons are amplified in a multiwire proportional chamber and the induced pulse in the cathode pad plane gives an image of the Cherenkov light.

A single 4 GeV kinetic energy proton event at nearly perpendicular incidence is shown in figure 2. The hits in the centre are due to ionization of the chamber gas by the proton and it is surrounded by a ring of Cherenkov light. The Cherenkov angle can be calculated

from the image and is used for particle identification as it is an accurate measure of the particle velocity. For β=1, charge one particles 10-20 photoelectrons are detected per event, depending on the incidence angle [5]. This is the first RICH detector used in space experiments that is sensitive to unit charged particles, e.g. antiprotons.

3 Experimental Results

The spectrometer flew 8-9 August 1994 for 23 hours at a float altitude between 36-38 km. All detectors performed well and data were collected for more than 6 million cosmic rays. Figure 3 shows the reconstructed Cherenkov angle as a function of rigidity for accumulated events at 36-38 km altitude. Figure a) shows 120000 charge one particles and b) 8000 charge two particles, where the charge is selected by the two scintillators. The good particle identification capability of the RICH is clearly visible.

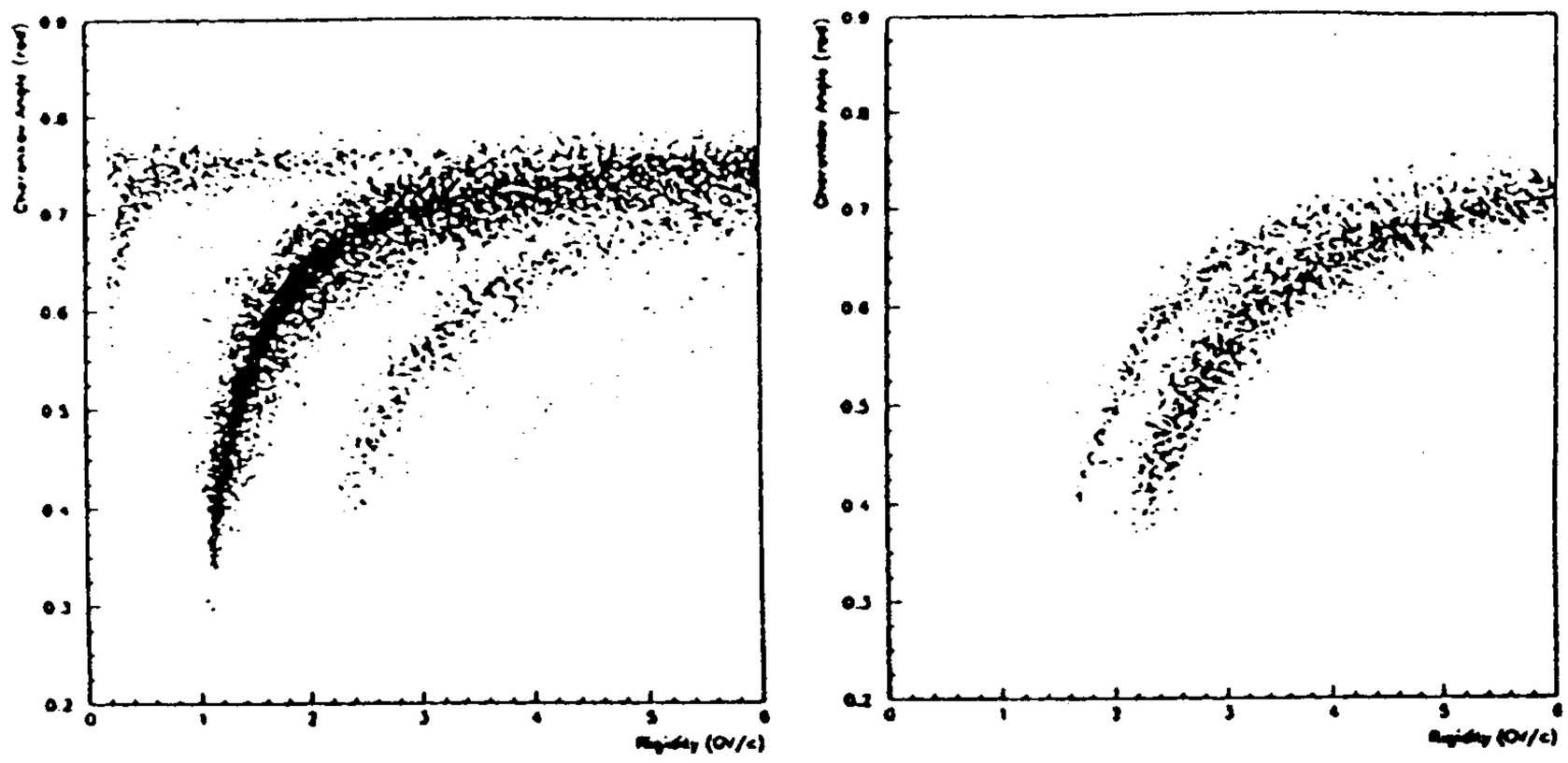

Figure 3. Reconstructed Cherenkov angle as a function of rigidity for a) Z=1 particles and b) Z=2 particles.

The threshold for emission of Cherenkov light in NaF is β=0.75. However, the particles need to have β>0.85 to have the image of the Cherenkov light well separated from the ionization with the geometry used in the CAPRICE RICH detector. Figure 4 shows the resolution (r.m.s.) of the reconstructed Cherenkov angle as a function of β for protons at an incidence angle of 9°±3° (the most probable incidence angle). As can be seen in the figure, the Cherenkov angle resolution is nearly constant 12 mrad for particles with a beta larger than 0.9. Figure 5 shows the resolution (r.m.s.) for protons with a rigidity of 3±0.5 GV/c (β=0.94-0.97) as a function of incidence angle towards the RICH. Zero means perpendicular incidence. The resolution increases with the incidence angle from 9 mrad at perpendicular incidence to 18 mrad at 20° incidence. All results presented in this paper have their origin in data collected during the flight.

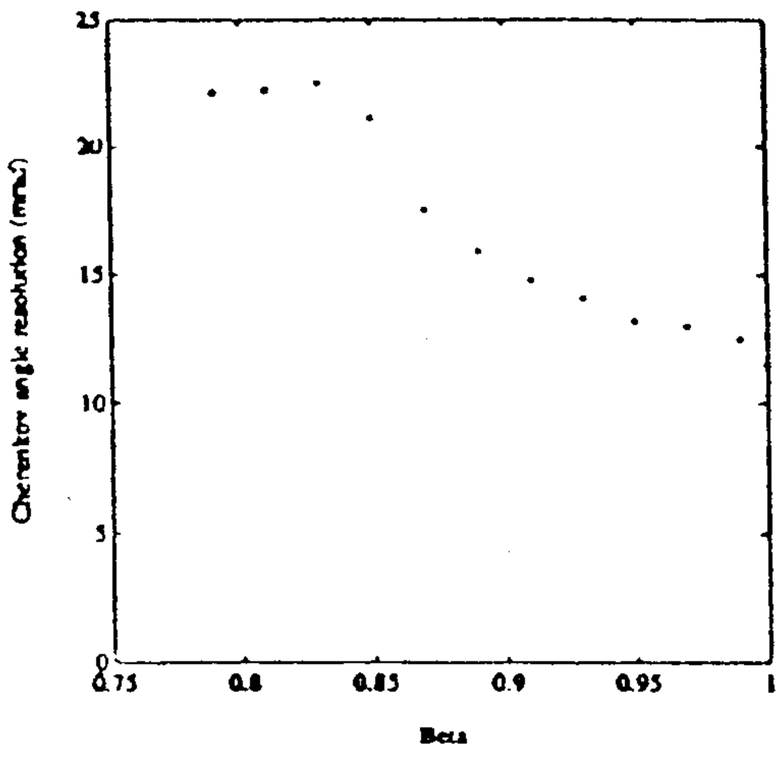

Figure 4. Reconstructed Cherenkov angle resolution as a function of beta for Z=1 particles.

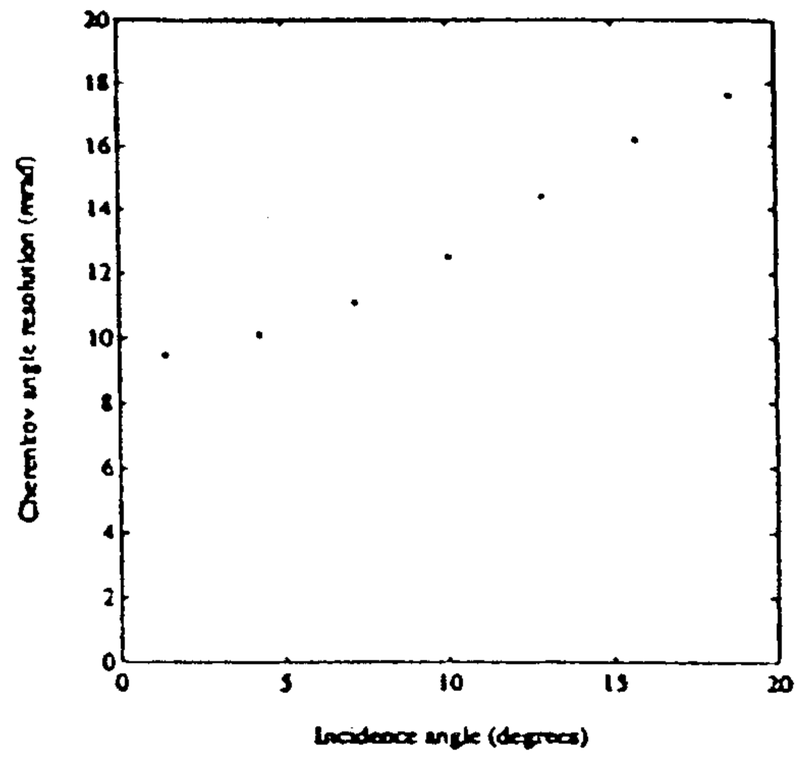

Figure 5. Reconstructed Cherenkov angle resolutioon as a function of incidence angle for Z=1 particles.

4 Conclusion

A compact RICH detector has been developed and used for particle identification in a balloon-borne spectrometer to measure the flux of antimatter in the cosmic radiation. This is the first RICH detector ever used in space experiments that is capable of detecting unit charged particles, such as antiprotons. The RICH and all other instruments performed well during the flight. The analysis is still in an early phase and we hope to improve the resolution of the RICH even further.

References

[1] Golden R.L., et al., Nucl. Instr. and Meth. A306 (1991) 366.
[2] Hof M., et al., Nucl. Instr. and Meth. A345 (1994) 561.
[3] Barbiellini G., et al., Nucl. Instr. and Meth. A333 (1993) 560.
[4] Barbiellini G., et al., Nucl. Phys. C 32 (1993) 77.
[5] Carlson P., et al., Nucl Instr. and Meth. A349 (1994) 577.
[6] Anderson, D. F., Phys. Lett., B118 (1980) 230.

Rome 1995 XXIV ICRC OG 10.3.24, Vol. 3

The WiZard/CAPRICE Silicon-Tungsten Calorimeter

G.Barbiellini[10], G.Basini[7], R.Bellotti[11], V.Bidoli[9], M.Bocciolini[8], M.Boezio[10], U.Bravar[10], F.Bronzini[13], F.Cafagna[11], M.Candusso[9], P.Carlson[4], M.Casolino[9], M.Castellano[11], F.Celletti[8], M.Circella[11], A.Codino[6], G.De Cataldo[11], C.N.De Marzo[11], M.P.De Pascale[9], N.Finetti[6], T.Francke[4], F.Fratnik[10], N.Giglietto[11], R.L.Golden[1], M.Grandi[8], C.Grimani[6], M.Hof[12], B.Marangelli[11], F.Massimo Brancaccio[8], G.Mazzenga[7], J.W.Mitchell[3], A.Morselli[9], P.Papini[8], A.Perego[8], S.Piccardi[8], P.Picozza[9], M.Ricci[7], P.Schiavon[10], M.Simon[12], R.Sparvoli[9], P.Spillantini[8], P.Spinelli[11], S.A.Stephens[2], S.J.Stochaj[1], R.E.Streitmatter[3], M.Suffert[5], A.Vacchi[10], N.Weber[4], N.Zampa[10]

[1] Particle Astrophysics Lab, New Mexico State University, Las Cruces, New Mexico, USA
[2] Tata Institute of Fundamental Research, Bombay, India
[3] NASA Goddard Space Flight Center, Greenbelt, Maryland, USA
[4] Royal Institute of Technology, Stockholm, Sweden
[5] Centre de Recherches Nucléaires, Strasbourg, France
[6] Dipartimento di Fisica dell'Università and INFN-Sezione di Perugia, Perugia, Italy
[7] INFN, Laboratori Nazionali di Frascati, Frascati, Italy
[8] Dipartimento di Fisica dell'Università and INFN-Sezione di Firenze, Firenze, Italy
[9] Dipartimento di Fisica dell'Università di Roma II "Tor Vergata" and INFN-Sezione di Roma II "Tor Vergata", Roma, Italy
[10] Dipartimento di Fisica dell'Università and INFN-Sezione di Trieste, Trieste, Italy
[11] Dipartimento di Fisica dell'Università and INFN-Sezione di Bari, Bari, Italy
[12] University of Siegen, Siegen, Germany
[13] Dipartimento di Fisica dell'Università di Roma "La Sapienza" and INFN-Sezione di Roma, Roma, Italy

Abstract

A silicon-tungsten calorimeter has been developed and flown in a balloon borne experiment in conjunction with a Ring Imaging Cherenkov Detector and a superconducting magnet spectrometer. This instrument is referred to as the WiZard/CAPRICE experiment. The objectives of this experiment were to measure the flux of low energy antiprotons, positrons and light nuclei in the cosmic radiation. The calorimeter is made of 8 x, y silicon sampling planes interleaved with 7 tungsten absorbers (7 radiation lengths); it provides the topology of the interacting events together with the measurement of the energy released by crossing particles. Results of its performance during the flight are given.

1. Introduction.

The calorimeter here described is an upgraded version carried out for the Cosmic AntiParticle Ring Imaging Cherenkov Experiment (CAPRICE) on balloon, to measure the flux of low-energy antiprotons and positrons and of light isotopes in the cosmic radiation. This is part of the WiZard Collaboration program of balloon flights dedicated to the study of cosmic rays. A first, smaller version of the calorimeter with a different read-out system was flown in 1993 from Fort Sumner, New Mexico, to measure the flux of electrons and positrons in the cosmic rays (flight TS93 [1]).

The 1994 experimental set-up for the balloon flight payload consists of a superconducting magnet, a tracking system (made of Multiwire Proportional and Drift Chambers [2,3]), a time of flight system of scintillators and a Ring Imaging Cherenkov (RICH) detector [4,5]. The Silicon Tungsten imaging calorimeter is located at the bottom, below the tracking system; it operates in conjuction with the RICH to recognize and separate particles and nuclei by distinguishing between hadronic and electromagnetic showers and by measuring the energy released in each sampling layer.

2. The Detector

The calorimeter is composed of 8 sensitive silicon planes, with an active area of (48x48) cm^2, interleaved with 7 layers of tungsten absorbers, each layer one radiation length (X_0) thick, for a total of 7 X_0. A single plane is a matrix of 8x8 silicon modules mounted on a G10 motherboard. Each module is composed of two 380 μm thick silicon detectors having an active area of (6 x 6) cm^2, divided in 16 conductive strips, 3.6 mm wide, and mounted back to back with perpendicular strips to provide double coordinate (x-y) read-out. The strips of each detector are connected to the neighbouring ones to form single strips 48 cm long. This arrangement defines one single read-out channel: one plane has, therefore, 256 channels, fed into two sets of eight front-end modules, 16 channels each, for x and y coordinates. The whole calorimeter has 2048 channels. Details about the characteristics of the silicon detectors, are published, together with the results of beam tests, in Refs. [6,7,8].

The flight configuration has been designed in order to place in the same mechanical structure all the required servicing devices. Figure 1 shows the complete arrangement which includes a cooling box and a dedicated CAMAC crate containing all the read-out and silicon power supply modules.

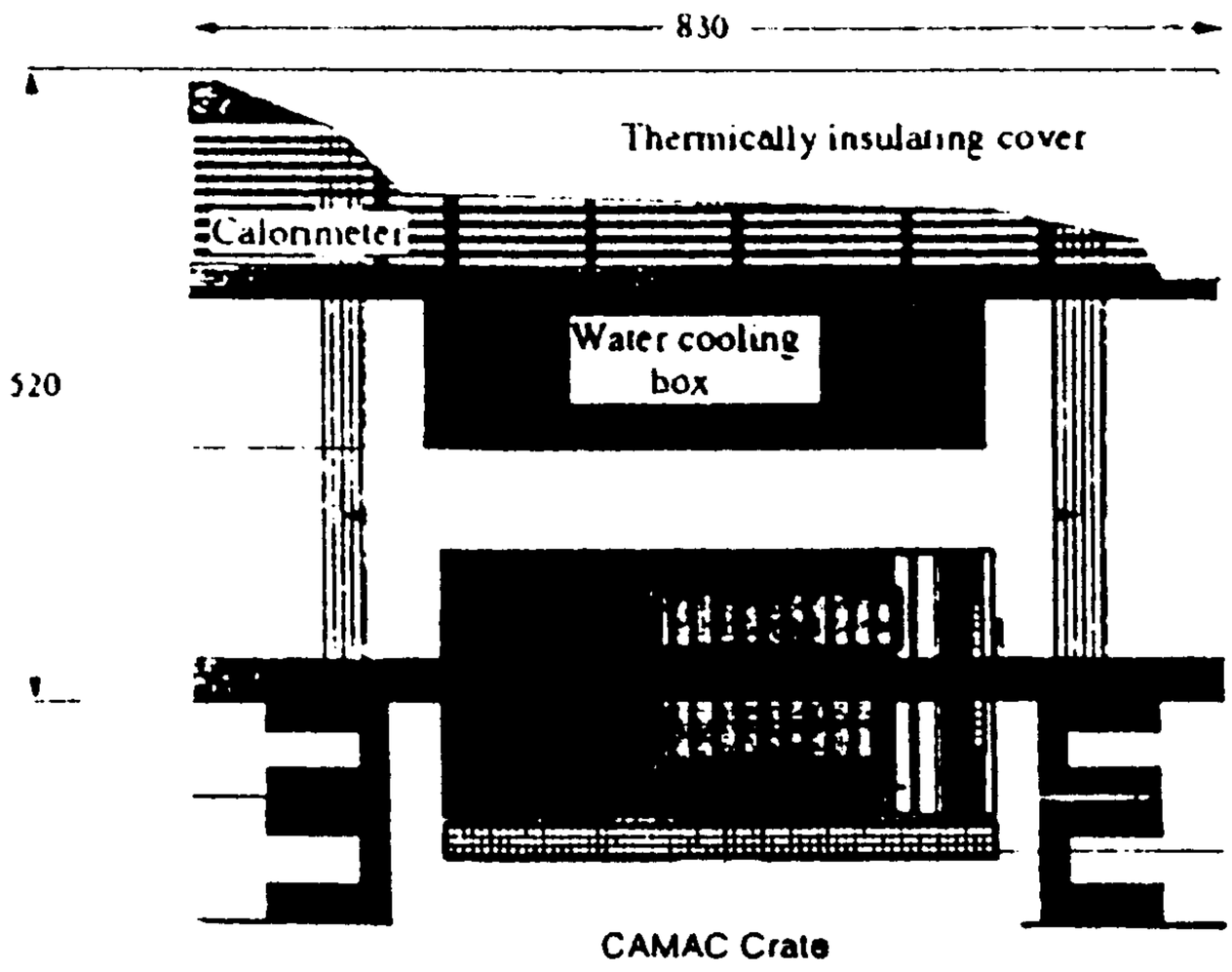

Figure 1. The complete arrangement of the calorimeter with its cooling box and the dedicated CAMAC Crate (dimensions are in mm).

The front-end of the calorimeter consists of a 16-channel module, providing the analog circuitry for the charge amplification and the sample-hold of each channel, as well as the logic to drive the sample-hold and the multiplexed output. Sixteen front-end modules are needed to handle the signals from the detectors of each plane for both coordinates. Each channel features a charge preamplifier, with a JFET in the input stage, a semi-gaussian shaping network with a peaking time of 7 μs and a conventional sample-hold circuitry.

A single CAMAC read-out driver provides the signals needed to perform the multiplexed read-out of all the front-end modules upon receipt of a trigger signal. A gate pulse is sent to the conversion units to start their operation causing the analog input to be sampled by an 8-bit ADC. The address of the actual channel is simultaneously put on a bus that connects all the conversion units. All the 256 channels of a plane are scanned at 1 MHz rate, in two subsequent cycles for the two amplifications. Thus, a complete read-out sequence takes 512 μs.

The conversion and buffering units, standard CAMAC modules, one for each calorimeter plane, also perform an optional zero-skip of the data and store them into buffer memories that are accessed by the controlling computer in the final stage of read-out.

3. Ground tests and flight performance

The expected performance of the calorimeter has been investigated through a Monte Carlo simulation program based on the GEANT code [9]. The simulation has been carried out in order to minimize the electron contamination over antiprotons and to maximize the selection efficiency of the latter particles. Simulated data have been analysed using a stochastic discrimination technique, also combined with a neural network. The actual response of the whole calorimeter and its efficiency have been measured with cosmic rays during ground tests triggering with an independent scintillator telescope.

The CAPRICE balloon flight took place in August 1994 from the base of Lynn Lake, Manitoba, Canada; about 6 million events have been recorded at a floating altitude above 36 km. Preliminary results are presented at this same Conference [10]. The calorimeter performed well over the entire flight and no re-calibration procedures from ground were needed, thus showing its good stability over time. The capability of this detector to provide the "image" of the events and of the energy deposited by crossing particles and nuclei is clearly shown in the following figures related to flight events: Figure 2 shows a non-interacting proton of 0.5 GeV kinetic energy; Figure 3 shows a stopping He nucleus of 133 MeV/n kinetic energy; Figure 4 illustrates an electromagnetic shower produced by a 1 GeV electron. From the ground it was possible to monitor the behaviour of each silicon strip. This was done by plotting the average deposited energy for each strip. Figure 5 shows, as an example, the plot of the deposited energy in four adjacent strips.

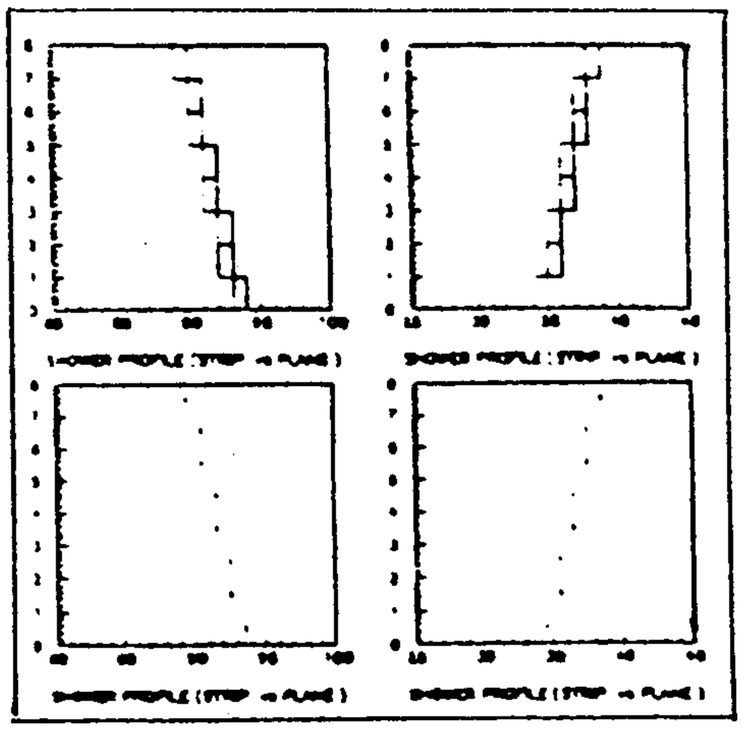

Figure 2. A non interacting proton of 0.5 GeV kinetic energy as seen in view x (left) and y (right): top and bottom: the size of the squares and the numbers represent the energy released in each strip; in particular, numbers refer to n. of mip's.

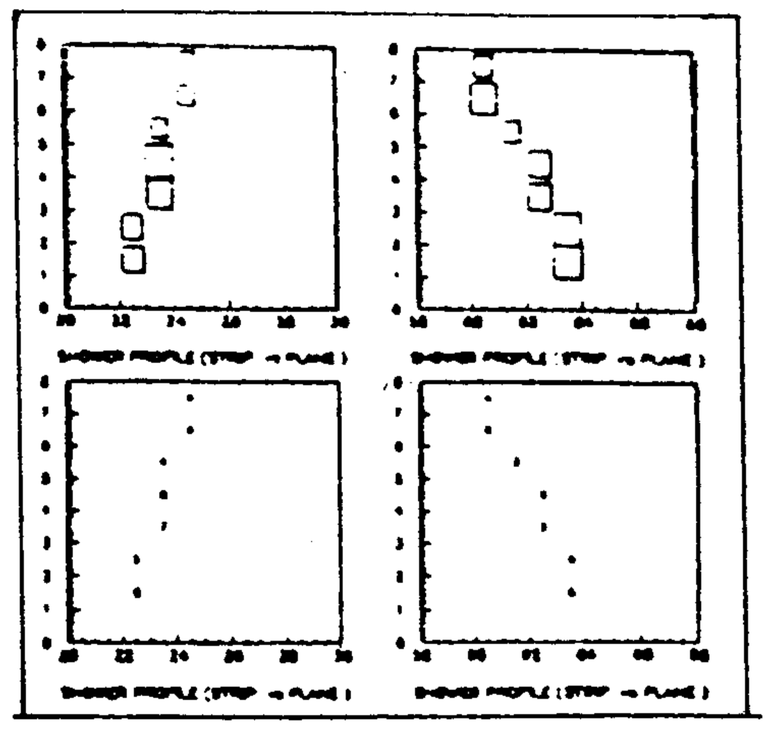

Figure 3. A ^4He nucleus, 133 MeV/n kinetic energy, stopping in the calorimeter ; same representation as in of fig. 2

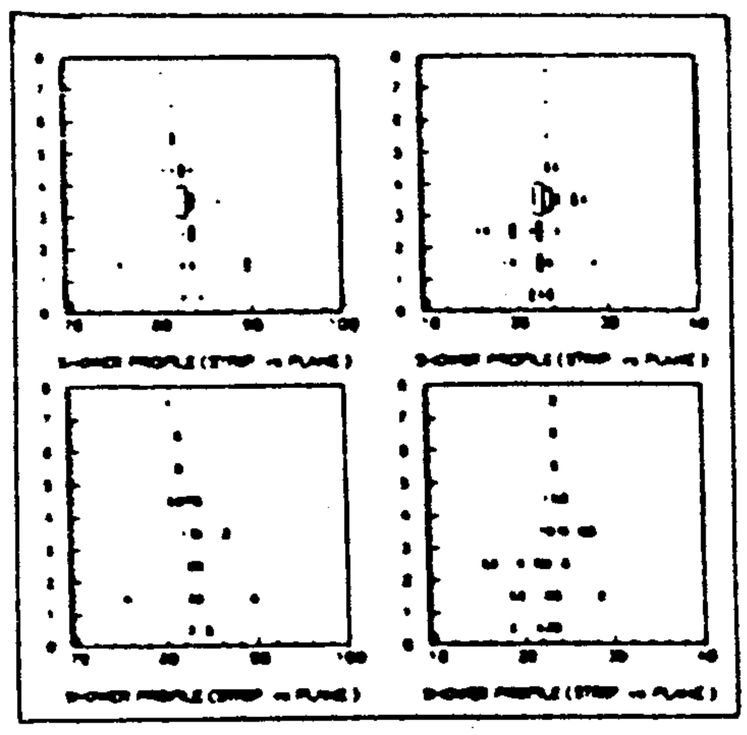

Figure 4. An e.m shower produced by a 1 GeV electron; same representation as in of fig. 2.

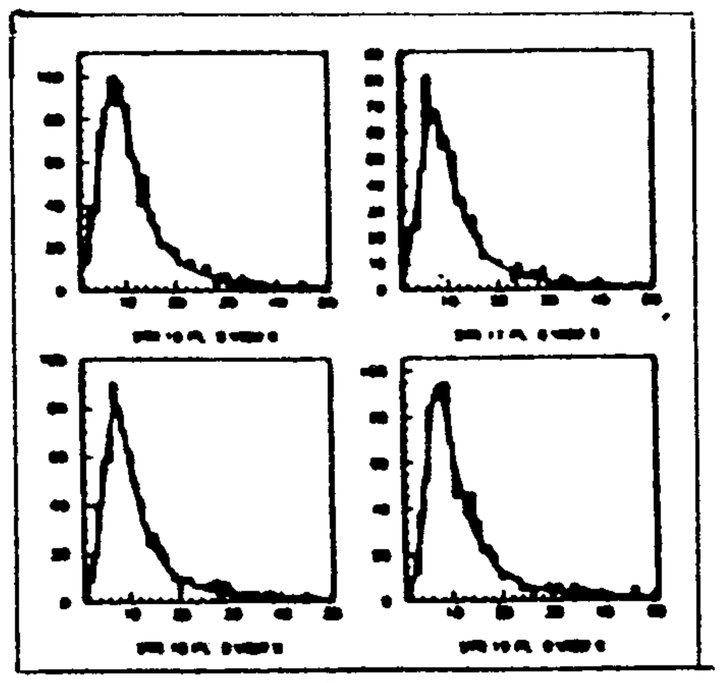

Figure 5 Deposited energy in four adjacent strips (in ADC channel units) integrated over about 1000 events. A 5-parameter fit is superimposed for energy calibration purposes to transform ADC channels to MIP units

Acknowledgments. This work was supported by NASA Grant NAG-110, the National Scientific Balloon Facility, the Istituto Nazionale di Fisica Nucleare and the Agenzia Spaziale Italiana.

References.

[1] F.Aversa et al., Proc. 6th Pisa Meeting on Advanced Detectors, La Biodola, Isola d'Elba, Italy 22-28 May 1994 , Nucl. Instr. Meth. **A360** (1995) 17
[2] R.L.Golden et al., Nucl. Instr. Meth. **A306** (1991) 366
[3] M.Hof et al., Nucl. Instr. Meth. **A345** (1994) 561
[4] P.Carlson et al., Nucl. Instr. Meth. **A343** (1994) 198
[5] P.Carlson et al., Nucl. Instr. Meth. **A349** (1994) 577
[6] M.Bocciolini et al., Proc. 3rd Int. Conf. on Calorimetry in High Energy Physics, Corpus Christ, Texas, (1992) p.285.
[7] M.Bocciolini et al., Nucl. Instr. Meth. **A333** (1993) 560.
[8] M.Bocciolini et al., Nucl. Phys. **B32** (1993) 77.
[9] GEANT, Detector Description and Simulation Tool. CERN, Geneva, Oct 1994
[10] G. Barbiellini et al. , "$\bar{p}$ *and* e^+ *identification capabilities of CAPRICE*" These Conf.Proceedings

Rome 1995 XXIV ICRC OG 10.3.26, Vol. 3

Status of the GILDA project for the 30 MeV- 100 GeV high energy gamma ray astrophysics

A.Morselli[1], G.Barbiellini[2], Y.V.Ozerov[3], M.Boezio[2], M.Candusso[1], M.Casolino[1], M.P.De Pascale[1], C.Fuglesang[4,5], A.M.Galper[3], A.Moiseev[3], P.Picozza[1], A.V.Popov[3], M.Ricci[6], R.Sparvoli[1], P.Spillantini[7], A.Vacchi[2], S.A.Voronov[3], V.M.Zemskov[3], V.G.Zverev[3]

1 Dept. of Physics, Univ. of Roma "Tor Vergata" and INFN, Italy
2 Dept. of Physics, Univ. of Trieste and INFN, Italy
3 Moscow Engineering Physics Institute, Moscow, Russia
4 Royal Institute of Technology, Stockholm, Sweden
5 European Space Agency, EAC, Cologne, Germany
6 INFN Laboratori Nazionali di Frascati, Italy
7 Dept. of Physics, Univ. of Firenze and INFN, Italy

Abstract

High energy gamma-ray astrophysics has greatly developed in the last few years because of the results of EGRET[1], on the Compton Gamma Ray Observatory. The satellite observations have shown the importance of continuing the investigation of high energy gamma radiation but the emerging of new astrophysical and cosmological problems require for future experiments the realization of telescopes with parameters significatively improved with respect to the previous missions. In a traditional point of view, this is achieved with the increase of the lenght L of the device and, consequently, the mass of the telescope and satellite (growing as L^3). Such kinds of experiments are becoming rather expensive and are approaching the maximum value in cost, satellite mass and consuming resources. The telescope project GILDA presented in this paper is based on the use of silicon strip detectors. The silicon technique consents to obtain a much wider solid angle aperture; in this way we can have more sensitivity without a growing in the size of the instrument. Here we show that also the calorimeter part alone of GILDA can be used for the detection of high gamma rays.

1 Introduction

The GILDA telescope, carrying out a gamma astronomy experiment, will be placed on a "Resource-0" class space satellite. Limitations in size, conditioned by the satellite hermetic module volume (a cylinder 110 cm in diameter and 75 cm in height), and in mass for the telescope ($\sim$ 400 kg) have set the principal constraints considered in designing the experiment project. The planned duration of the experiment is not less than 5 years.

The primary goal of the GILDA mission is the research and identification of new astrophysical sources, but also known objects as well as transient phenom-

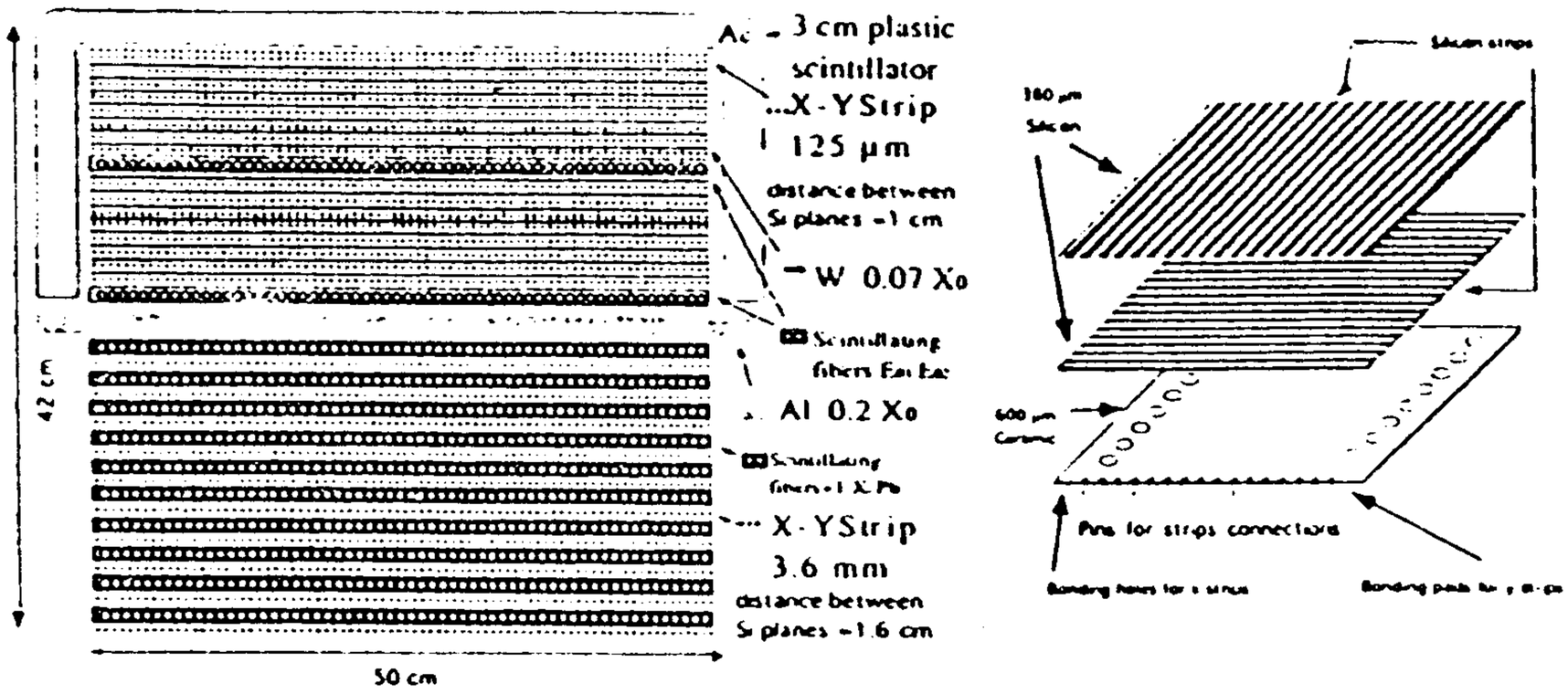

Figure 1: *The stratigraphy of the GILDA detector (left) and the structure of the basic 6× cm^2 module (right).*

ena will be studied. The energy range between 30 and 100 GeV is completely unexplored up to now and it is very interesting also in the view of the possible existence of the sources fluxes attenuation due to the infrared background[5]. With GILDA many goals within this range can be pursued. Here we only cite some of the scientific objectives, such as the study of compact gamma-ray sources, Active Galactic Nuclei, galactic diffuse emission, gamma ray bursts, solar gamma flares, and the research of Dark Matter and new exotic particles. More detailed descriptions can be found in[2].

2 The GILDA telescope

The GILDA design is derived from a refined study of the Wizard [4] silicon calorimeter that has already successfully flown in balloon experiments. The configuration of GILDA has a height of 42 cm, an area of 50 × 50 cm^2 and a total showering length of 11 X_0.

The stratigraphy of the instrument is shown in figure 1 (left), while a more complete description can be found in [2]. The first twenty planes form the converter zone, in which the silicon layers, made of 125 μm strips, are separated by tungsten plates of thickness 0.07 X_0. The last ten planes E_1...E_{10}, constituting the absorber, are composed of 3.6 mm silicon strips and separated by 1 X_0 thick layers of active scintillating lead fibers[2].

The configuration is encased in a plastic anticoincidence scintillator A_c (3 cm thick) around the converter zone. In addition there are two fiber scintillators (without lead), one, E_{01}, after the first seven planes (after 0.49 X_0) and

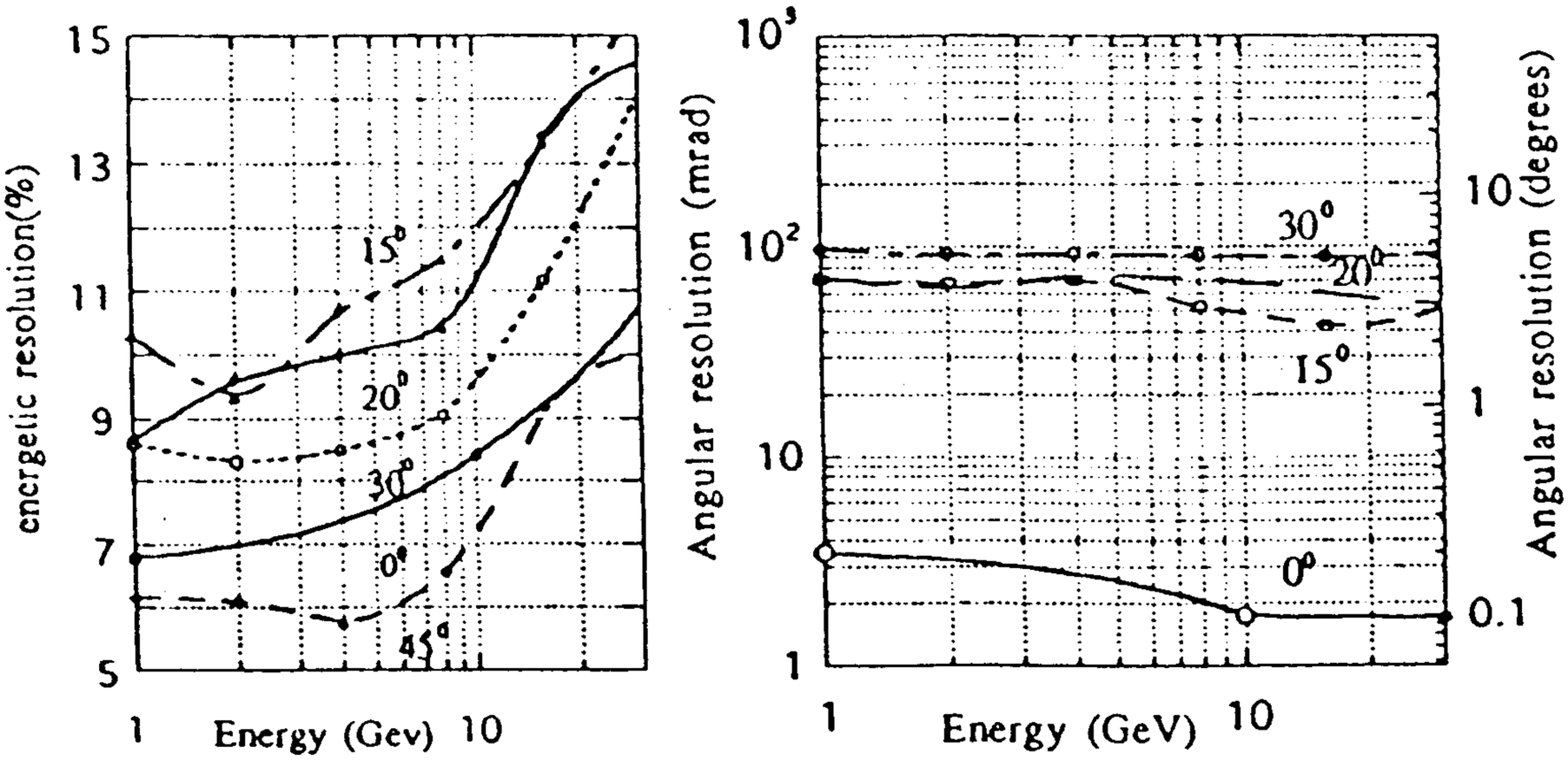

Figure 2: *Simulated GILDA absorber energy (left) and angular resolution (right) at different gamma incident angles, compared with the whole detector (at incident angle=0°).*

the other, E_{02}, after fourteen planes from the top of the detector.

The results concerning the energetic and angular resolutions of the total apparatus are reported elsewhere [2],[3]; here we want to remark the fact that the calorimeter alone (the absorber part of GILDA) can have a good energetic resolution and a quite good angular resolution at high energies. This means that for high energies, where the source flux is lower, we can use a much greater solid angle.

To trigger one event, the following conditions for the energy deposited in the first planes of the absorber must be verified:

$$E_1 > 0.1\ MIP, \quad E_2 > 1\ MIP, \quad E_3 > E_1$$

In figure 2 we present the results for the energy (left) and angular resolution (right) at different gamma incident angles obtained only with the absorber part of GILDA. For comparison the complete GILDA results are shown.

In figure 3 we have plotted the efficiency of the adopted trigger for the energy resolution (left) and of the angle reconstruction algorithm (right). The track reconstruction algorithm is based on an iteractive process, that stops when a direction converges within an error of 10 mrad. To be significative, a trajectory must be determined by at least four points.

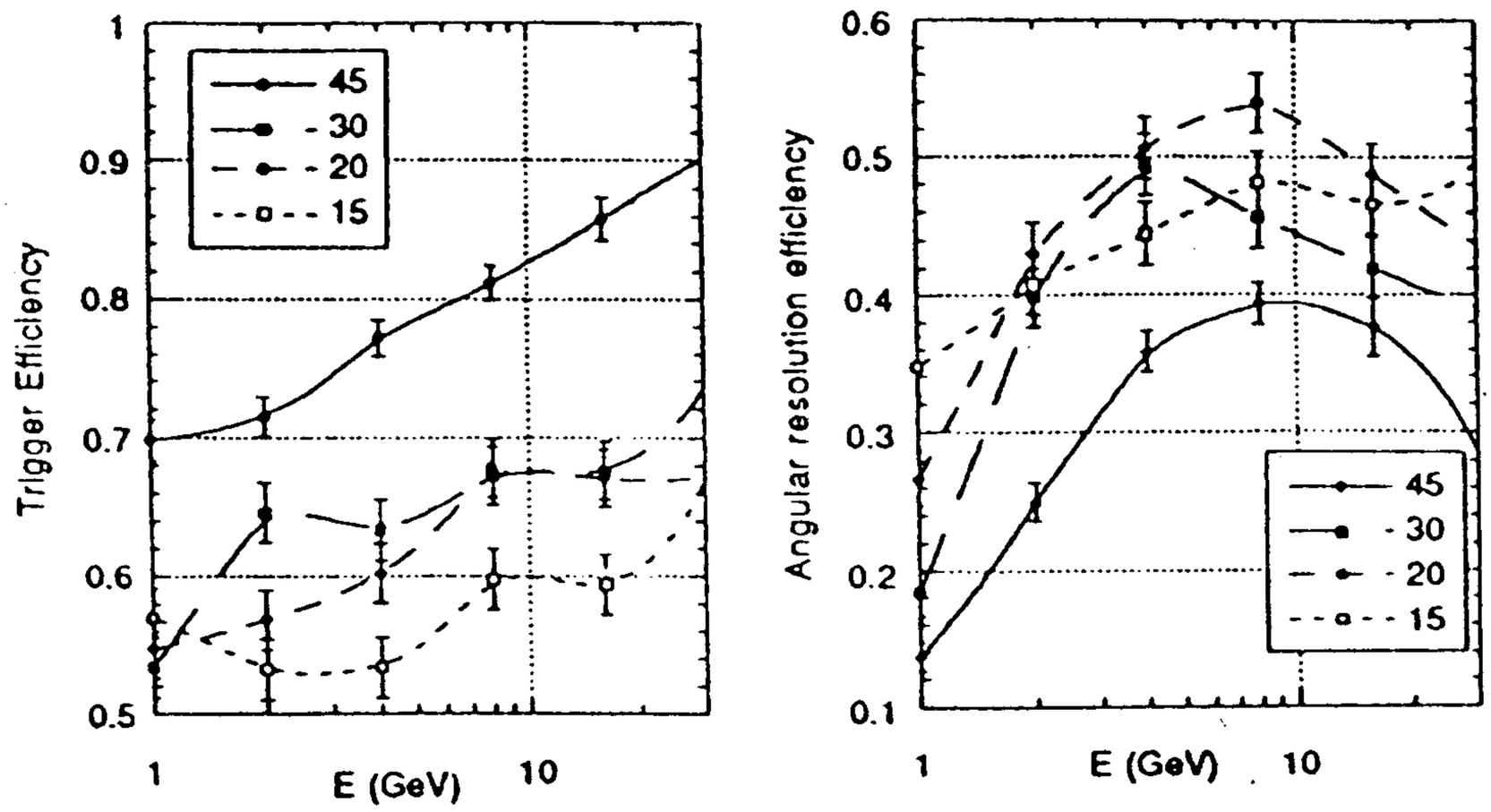

Figure 3: *Efficiency of the adopted trigger at different incident angles for the energy resolution (left) and for the angular resolution algorithm (right).*

3 Conclusion

The study resumed in this paper have shown that, though with angular and energetic resolutions than those obtained with the whole GILDA apparatus, it is possible to measure in a satisfactory way gamma rays between 1 GeV and 50 GeV using only the absorber part of the instrument. Since the Geometric Factor of the absorber part is a factor two greater than that of the complete GILDA, these results consent us to collect a double gamma rays flux from high energy sources than that previously evaluated [2].

References

[1] G. Kanbach et al., *Space Science Review*, **49**, 69, (1988).

[2] G. Barbiellini et al., Proc. of: *"Trends in Astroparticle Physics"*, 22-25/12/1994, Stockholm, Sweden, to be published on Nuclear Physics B.

[3] G. Barbiellini et al., Nuclear Instrument and Methods, **A354**,547,(1995)

[4] R.L. Golden et al., *Il Nuovo Cimento*, **105 B**, 2, 191, (1990).
G. Barbiellini et al., *Il Nuovo Cimento*, **102 B**, 661, (1988).

[5] F.W. Steker, O. C. De Jager & M. H. Salamon, *Ap.J*, **L49**, 390, (1992).
A. Morselli, Proceedings of the *"International Symposium on cosmic ray physics in Tibet"*, August 12-17, Lhasa, China, 1994.

Rome 1995 XXIV ICRC OG 10.4.8, Vol. 3

Performance of the Transition Radiation Detector Flown on the NMSU/WIZARD TS93 Balloon-Borne Instrument

F. Aversa[10], G. Barbiellini[10], G. Basini[6], R. Bellotti[4], V. Bidoli[9], M. Bocciolini[5], M. Boezio[10], F.M. Brancaccio[6], U. Bravar[10], F. Bronzini[8], M.T. Brunetti[7], A. F. Cafagna[4], M. Candusso[9], M. Casolino[9], M. Castellano[4], F. Celletti[5], M. Circella[4], A. Codino[7], Colavita[10], G. De Cataldo[4], C. De Marzo[4], M.P. De Pascale[9], N. Finetti[5], F. Fratnik[10], N. Giglietto[4], R.L. Golden[1], M. Grandi[5], C. Grimani[7], M. Hof[11], B. Marangelli[4], G. Mazzenga[6], M. Menichelli[7], W. Menn[11], M. Miozza[7], J.W. Mitchell[3], A. Morselli[9]. J.F. Ormes[3], P. Papini[5]. A. Perego[5]. S. Piccardi[5], P. Picozza[9]. A. Rainò[4]. M. Ricci[6]. P. Schiavon[10], M. Simon[11], R. Sparvoli[9]. P. Spillantini[5]. P. Spinelli[4]. S.A. Stephens[2]. S.J. Stochaj[1]. R.E. Streitmatter[3]. A. Vacchi[10]. N. Zampa[10]

[1] *New Mexico State University, Las Cruces, USA*

[2] *Tata Institute of Fundamental Research, Bombay, India*

[3] *N.A.S.A. Goddard Space Flight Center, Greenbelt, USA*

[4] *Dipartimento di Fisica and Sezione I.N.F.N. dell'Università di Bari, Italy*

[5] *Dipartimento di Fisica and Sezione I.N.F.N. dell'Università di Firenze*

[6] *I.N.F.N. Laboratori Nazionali, Frascati, Italy*

[7] *Dipartimento di Fisica and Sezione I.N.F.N.*

[8] *Dipartimento di Fisica and Sezione I.N.F.N. dell'Università "La Sapienza", Roma, Italy*

[9] *Dipartimento di Fisica and Sezione I.N.F.N. dell'Università di "Tor Vergata", Roma, Italy*

[10] *Dipartimento di Fisica and Sezione I.N.F.N. dell'Università di Trieste*

[11] *Siegen University, Siegen, Germany*

Abstract

We have built and tested a transition radiation detector (TRD) to discriminate positrons from protons in the balloon flight TS 93 experiment. We present the TRD performance using flight data obtaining a proton-positron rejection factor of the order of 10^{-3}. During the 24 hour flight, we have collected data in the momentum range 4 – 50 GeV/c. Using the TRD together with the Silicon calorimeter, we achieve an overall rejection factor of about 10^{-5} of positron against the proton background over the entire momentum range.

1 Introduction

Transition radiation detectors (TRDs) are frequently used to identify electrons in a high hadron background in particle physics experiments, mainly in the hundred GeV/c momentum range when other particle identification methods may prove inefficient [1]. Recently they have been employed also in particle astrophysics experiments for the same purpose [2].

We have built a TRD for a cosmic ray space experiment performed on the NMSU-Wizard balloon-borne instrument [3, 4]. This facility has already carried out detailed measurements of both antiprotons in the 1-20 GeV energy range and positrons in the 3-60 GeV energy range. The main objective of this experiment is to investigate whether the e^+/e^- ratio really increases above 15 GeV and, in addition, whether the e^+/p ratio indicates evidence of energy losses for positrons. All the observations produced to date are affected by the uncertainties connected to the subtraction of a significant background due to the high flux of protons with respect to the positrons. Since the e^+/p ratio is expected to be about 10^{-3}, we need to rely on an apparatus which has a probability to identify erroneously a proton as a positron of the order of 10^{-5}. For this purpose we have employed an imaging silicon calorimeter in conjunction to the TRD; taking into account the performance of the calorimeter we require for the TRD a rejection factor against protons of the order of 10^{-3}.

2 TRD general description

The transition radiation detector is placed above the magnet spectrometer inside of the pressure vessel, usually referred to as the "gondola". The TRD has an active area of 76×80 cm^2 chosen to match the acceptance of the rest of the apparatus. As with all detectors designed for balloon flight, the weight (237 Kg) and the power (100 Watts for 2560 channels) had to be kept to a minimum. Nevertheless the performance is close to analogous devices working in accelerator experiments. The TRD is based on ten modules each consisting of a carbon fiber radiator followed by a multiwire proportional chamber. These ten modules are housed inside an aluminum box. Each radiator consists of a light (1.8 kg) and stiff aluminum frame containing four polyethylene bags, 20 mm thick, filled with carbon fiber segments (6 mm long, 7 mm thick,1.76 g/cm^3 density), and has overall dimensions of 80×80×5 cm^3. The bags are kept inside the frames by two Mylar foil windows, 25 μm thick, stretched to 40 kg/m and glued to the frame external edges. The radiator density has been fixed to the optimal value of 0.060 g/cm^3 . The first (top) TRD module, as with the prototype tested on beam [5], has an additional identical radiator to get nearly the same transition radiation yield as the following modules.

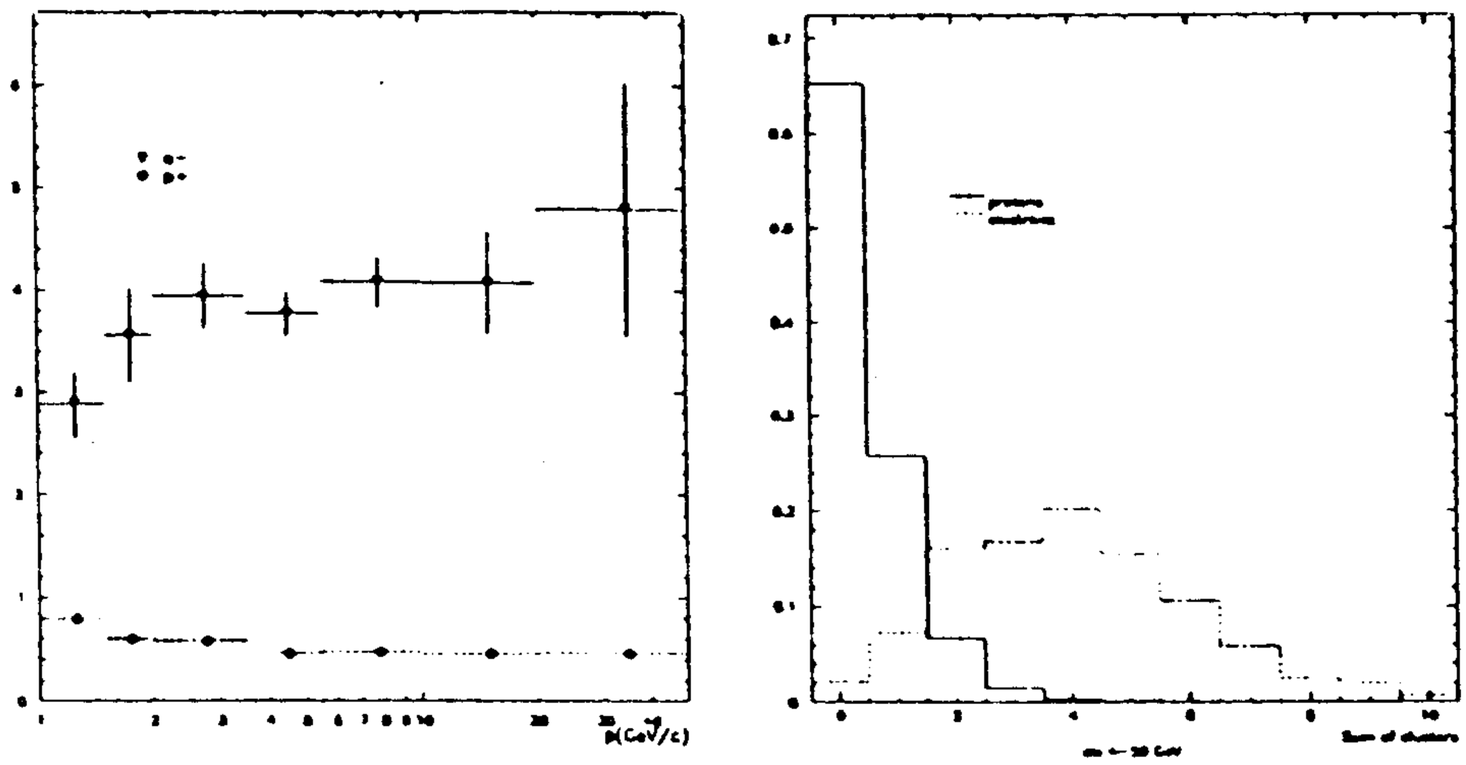

Figure 1: a) Mean number of clusters in the TRD versus the momentum for e- and protons. The statistical error is shown. Fig.1b: The sum of cluster distribution for protons and electrons

This solution has generally been used by many other experiments. The total radiation length for this TRD, taking into account all the material inside the alluminum box, is 0.13 X_0.

The proportional chambers have an active surface of 76×80 cm^2 and the anode-cathode gap has been fixed to 8 mm in our design. The anode plane is equipped with 256 gold plated tungsten wires. The wires are 25 μm thick, have 3 mm spacing and are stretched to a tension of 70 g ; in these conditions at the typical operation high voltage (2.95 KV) no intermediate anode to cathode spacer is needed to prevent wire instabilities. No windows external to the cathode planes have been used in this chamber design. The chambers are filled with a xenon (80%) - methane (20%) mixture chosen to give optimal TR photon conversion with low δ-ray background production. With such a mixture the electron drift velocity is found to be about 300 ns/cm at the supply high voltage.

3 TRD performances during the flight

The long flight duration and the good particle identification performed by the other detectors in the apparatus [6] (TOF, spectrometer and the calorimeter), allow us to use flight data to verify the TRD performances, already tested on beam [7]. We have therefore selected a subsample of electrons and protons,

using the information coming from the rest of the apparatus, in order to verify the previous calibration. The results in Figure 1a show, as we expected, that the TRD saturation occurs for electron/positron energies larger than 3 GeV, while protons are not radiating in the whole momentum range (3-50 GeV/c). This property ensures an electron/positron identification practically independent of the particles momentum.

4 Analysis procedures

In order to classify events, we analyze the particle hit pattern in the ten chambers. As reported in [7] the indicators more efficient to an event classification in the TRD are the sum of hits along the track N_{cl}, the number of planes fired N_{pl} and the geometric mean between this two quantities: $\sqrt{N_{cl} \cdot N_{pl}}$. The geometric mean has been found to be the best indicator having pratically the same power of a likelihood procedure [7]. To evaluate the proton contamination versus the electron acceptance, we apply a variable cut on the distributions shown in Figure1b for protons and electrons and calculate the proton contamination and relative electron acceptance. After this operation we found a proton contamination of $2.3 \cdot 10^{-3}$ at about 50% electron efficiency and $1.2 \cdot 10^{-2}$ at 70% electron efficiency.

References

[1] C. W. Fabjan et al., Nucl. Instr. and Meth. **181** (1981) 119.

[2] K.K. Tang,The Astroph.Journ. **278** (1984),881.

[3] Golden R. L et al., Nucl. Inst. Meth., **A306** (1991),366.

[4] Golden R. L et al., "WiZard-Related Balloon Program" , proposal submitted in response to NRA-92-OSSA-10, 1992.

[5] R. Bellotti et al.,1993, Proc.23rd Int. Cosmic Ray Conf. (Calgary)

[6] Bellotti, R. et al., these Proceedings.

[7] E. Barbarito et al.,"A transition radiation detector for positron identification in a ballon-borne particle astrophysics experiment",accepted by Nucl. Instr. and Meth.

Rome 1995 XXIV ICRC OG 10.4.10, Vol. 3

STUDY OF COSMIC RAY NUCLEI DETECTION BY AN IMAGE CALORIMETER

P.Carlson[1], M.Casolino[3], C.Fuglesang[4], A.M.Galper[2], A.Morselli[3], Yu.V.Ozerov[2], P.Picozza[3], R.Sparvoli[3], ,V.M.Zemskov[2], V.G.Zverev[2]

[1] *Royal Institute of Technology, Stockholm, Sweden*
[2] *Moscow Engineering Physics Institute, Moscow , Russia*
[3] *Dipartimento di Fisica e Sezione I.N.F.N dell'Universita' di "Tor Vergata", Roma, Italy*
[4] *ESA-EAC, Cologne, Germany*

Abstract

It is shown that a cosmic gamma-ray telescope made of a multilayer silicon tracker and an imaging CsI calorimeter, is capable of identifying cosmic ray nuclei. The telescope charge resolution is estimated around 4 % independently of charge. Simulation methods are used to determine the telescope properties for nuclei detection.

1. Introduction

The success of EGRET, the high energy γ-ray detector of CGRO, capable of detecting γ-rays in the energy range 50 MeV - 30 GeV, has triggered several proposals for new generation experiments with improved energy and angular resolution as well as an increased solid angle coverage : GILDA[1], HUGIN [2], GLAST[3] and TIGER [4]. A common feature among these new ideas is the use of silicon tracking detectors and CsI crystal calorimeters.

During the work with the GILDA concept, we realized that the silicon tracker system could also be used to identify different nuclei and thereby make it possible to measure a flux of some of them in an energy range that has not been accesible previously. In this paper we give the results of a detailed simulation study of the detection method.

2 Telescope.

For the study of the nuclides detection capability the earl GILDA telescope layout was used (see Fig.1). See [1] for details of GILDA experiment The top part, hereafter called "converter", consists of 14 tungsten- silicon layers with a scintillator in the middle. Each layer has two 48 x 48 cm^2 silicon plates made of 6 x 6 cm^2 elements [6] arranged to give coordinates in perpendicular directions. The silicon elements are 380 mkm thick. The tungsten plates are 0.25 mm thick, corresponding to 7% of a radiation length.Plastic scintillation anticoincidence counters with 3 cm thickness cover the converter.The bottom part below the converter consists of 20 layers of CsI crystals. Each layer is made up of 32 1.5x1.5x48 cm^3 rods, arranged alternatively in perpendicular directions. Each CsI rod is

read out with a photodiode. The total CsI thickness is 30 cm, corresponding to 17 radiation lengths.

The plastic scintillation counters C_1 and C_2 are used for triggering. Nine layers of silicon strip detectors with 3.75 mm strip width are placed between the CsI layers in order to measure the spatial distribution of the electromagnetic shower particles. This is made to reject particles entering from below and also to discriminate against hadronic showers.

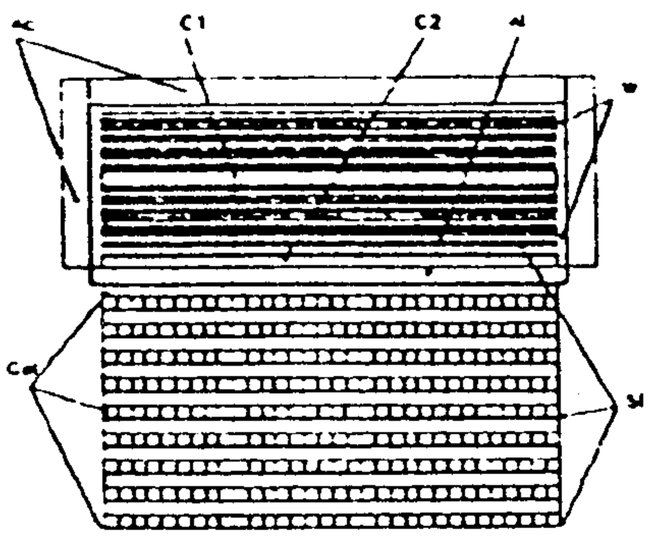

Fig. 1 Telescope layout

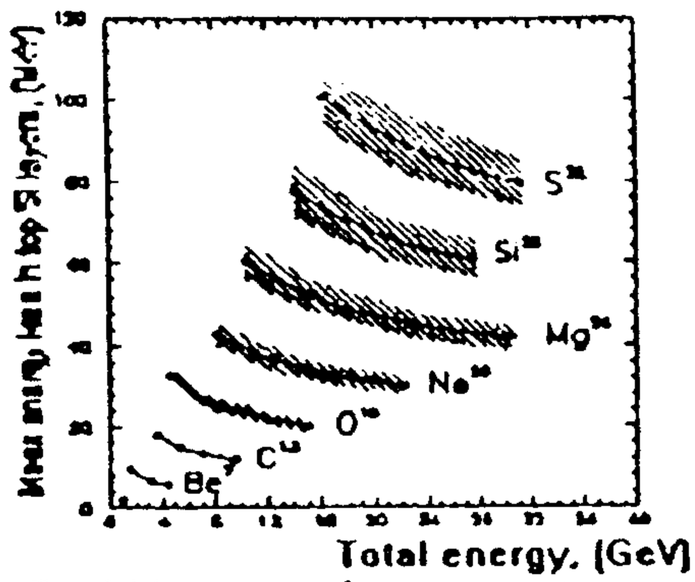

Fig 2 Mean energy loss in converter vs total energy

3. Stopping nuclei

The basic principle for detecting nuclei in telescope is to measure the total energy in the CsI calorimeter, requiring that the nucleus enters the calorimeter but does not leave it. For each nucleus there is a corresponding minimum energy, maximum energy and energy interval δE available. 14 silicon strip detector layers in the converter are used to measure dE/dx. The simulation program GEANT 3.15 [5] is used to study in detail the response of device for different nuclei.

The possible energy range for stopping nuclei detection varies from 0.2-0.4 Gev/n for α-particles to 1.0-3.0 Gev/n for Ge^{72} For each nucleus the energy loss in the silicon layers in the converter was studied for several values of the incident nucleus energy.

In the simulation process for each event the energy deposited in all active elements of the telescope was stored. For each event the total energy deposit in active layers and the mean value of the energy deposits in the top 18 layers of the silicon detectors were calculated. The hadronic interactions were first neglected (see below). The results are shown in Fig. 2 where the mean energy loss in the top silicon layers is plotted as a function of the total energy.

The simulated data shows the expected variation of the mean energy loss with total energy. The powerful nucleus - nucleus discrimination, due to the sampling of the energy loss in 18 silicone layers, is clearly visible from the hatched area corresponding to 68% of the events around each mean value.

In the results presented so far we assumed for simplification no hadronic interactions. Due to the imaging facilities of our device events without hadronc showers could be selected easy.

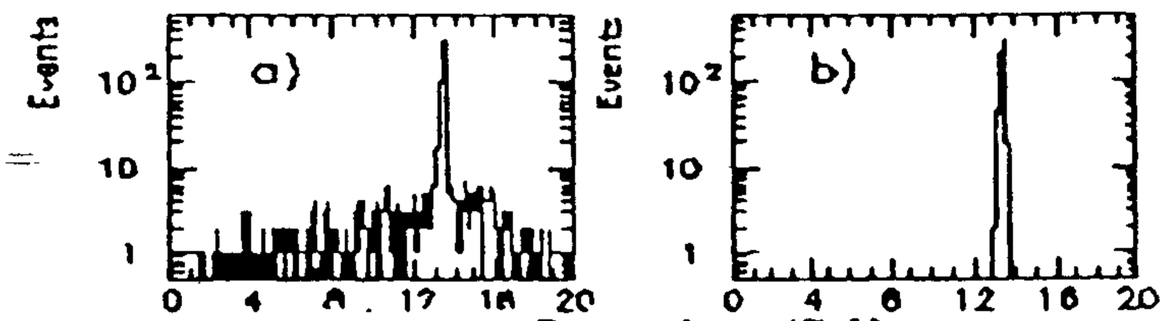

Fig. 3 Total energy loss distribution for O nuclei (E=0.9 GeV/n) including hadronic interactions: a)-all events; b)-events without showers

This is illustrated in Fig. 3 a) where the total energy deposited in the CsI layers is shown in the case of 0.9 GeV/n oxygen nuclei. It is possible to exclude events with the hadronic interactions using the information from the silicon strip and CsI detectors.(see Fig 3 b)) In fact it is sufficient to require a maximum number of 2 hits in any CsI layer and 2 hits in any silicon layer. The energy resolution for selected events is almost the same as that obtained for the case with neglected hadronic processes.

4. Non-stopping nuclei

The energy range available for stopping nuclei will allow many interesting astrophysical measurements. However, the particular feature of telescope with a large number of CsI layers where the energy loss is sampled makes it possible to extend this range by a novel approach. The basic idea is that for each nucleus a limited energy range above the maximum as given by the requirement of total containment, the variations of the energy loss as a function of layer number will make possible an energy estimation. The idea is illustrated in Fig. 4 for S^{32} and Si^{28} of a 1.9 GeV/n and 2.3 GeV/n kinetic energy.The energy loss is almost constant in the first 10 layers at 2.4 GeV/n. When the nucleus has slowed down the energy loss increases. It is this change in energy loss that is used to determine the energy..

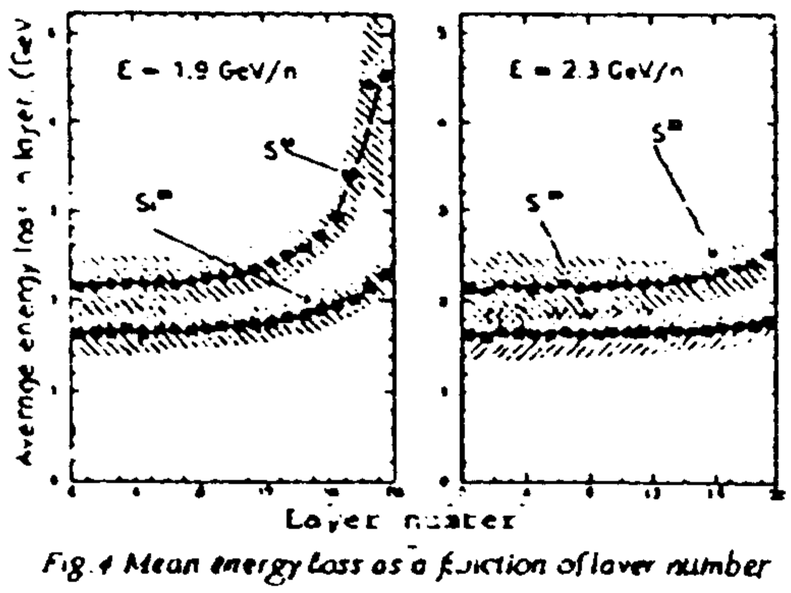

Fig.4 Mean energy loss as a function of layer number

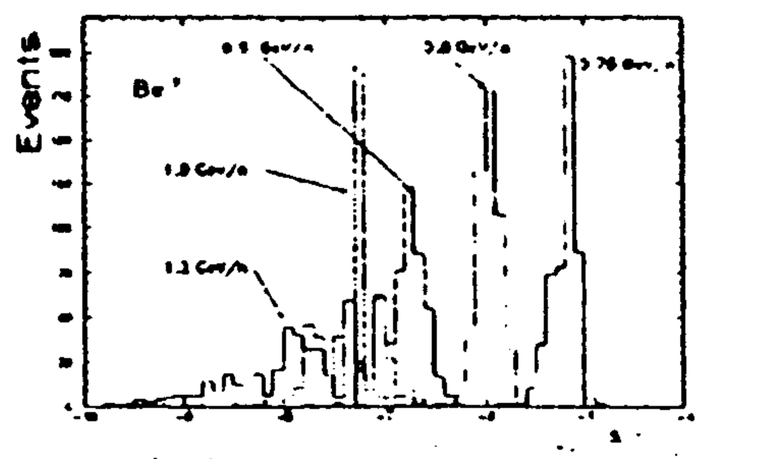

Fig.5 A3 distribution for several energies of Be⁹ nuclei

For each event the energy loss per layer CsI ΔE is parametrized as $\Delta E=A_1+e^{A2x+A3}$ where x is the layer number.

Clearly A_1 represents minimum ionization energy loss in separate CsI layer for the relativistic case. A_2 and A_3 characterizes the rise of ΔE . .It was found that A_2 was very sensitive to fluctuations in energy loss and was therefore fixed at 0.2, the most probable

value for several different nuclei and energies. Fig. 5 shows the results for the parameter A_3 for Be^7 with kinetic energy in the range of 0.75 - 1.2 GeV/n keeping A_2 fixed at 0.2. The maximum energy for stopping Be^7 is 0.72 GeV/n. Clearly the parameter A_3 allows an energy determination up to about 1 GeV/n, thus extending substantially the stopping niclei range (0.3 - 0.7 GeV/n). The method could be improved and optimized by also using the information from the silicon layers in the converter.

An interesting feature of the energy loss study is the possibility to identify the nuclei for energies above the extended range discussed above. Our study shows that different nuclei are clearly separated for any energy. The relativistic rise effect is also present as expected. Thus telescope will allow a detailed study of also the higher energy cosmic rays.

5. Conclusion

The properties of tlescope allow us to make the following remarks concerning the scientific importance of the proposed experiment from the point of view of cosmic ray nuclide detection. First, this experiment will make it possible to reach a collecting power of an order of hundreds of m^2 sr day . The triggering problem for nuclides detection could be solved easy enough. The possible range of Z value measurement depends on the dynamic range of the Si - detector preamplifiers. But it is now evident enough, that, for example, B/C discrimination could be provided in a wide energy range. Besides the obvious tasks of a measurements of abundance ratios of different nuclei, important for the development of different existing models of cosmic ray propagation in Galaxy, some very attractive scientific goals can be underlined. For example only very limited statistics is available from the previous experiments on the flux of very heavy nuclides, and this telescope could significantly improve on that. Also, telescope can provide measurements of certain very high energy nuclei (more than tens of GeV/n). The charge resolution is good enough for at least B-C discrimination. The relativistic rise effect can be used to estimate the energy. Because such nuclides are almost all primary, these measurements could give very valid information about processes in the cosmic ray sources. Additionally the long term detection of cosmic ray nuclides in very high energy range allows us to examine possible anisotropy of the cosmic rays and also their probable time variations [6]

References.

1.G. Barbiellini et al. "Wide aperture telescope for high energy gamma astronomy". To be published in Proc. of Conf. "Trends in Astroparticle Physics", Stockholm,(1994).
2. P. Carlson and C. Fuglesang. A proposal for a high energy γ - ray experiment (1993).
3. W.B. Atwood et al. A proposal for high energy gamma-ray telescope.(1994).
4. A. Alpar, D. Bhattacharya et al.In AIP Conference Proceeding, The second Compton Symposium,College park,MD (1993)304.
5. GEANT User's Guide, CERN program Library.
6 V.S. Berezinsky et al. Astrophysics of Cosmic Rays. (ed. by V.L. Ginzburg) North Holland (1990).

Rome 1995 XXIV ICRC OG 10.5.1, Vol. 3

Use of neural network techniques to identify cosmic ray electrons and positrons during the 1993 balloon flight of the NMSU/Wizard-TS93 instrument

R. Bellotti[1], M. Candusso[2], M. Casolino[2], M. Castellano[1],
F. Aversa[3], G. Barbiellini[3], G. Basini [5], M. Bocciolini[4], M. Boezio[3],
F.M. Brancaccio[4], U. Bravar[3], F. Cafagna[1], M. Circella[1], A. Colavita[3],
G. De Cataldo[1], C. De Marzo[1], M.P. De Pascale[2], N. Finetti[4], N. Giglietto[1],
R.L. Golden[7], C. Grimani[6], M. Hof[10], B. Marangelli[1], W. Menn[10],
J.W. Mitchell[9], A. Morselli[2], J.F. Ormes[9], P. Papini[4], A. Perego[4],
S. Piccardi[4], P. Picozza[2], A. Rainò[1], M. Ricci[5], P. Schiavon[3],
M. Simon[10], R. Sparvoli[2], P. Spillantini[4], P. Spinelli[1], S.A. Stephens[8],
S.J. Stochaj[7], R.E. Streitmatter[9], A. Vacchi[3], and N. Zampa[3]

[1] *Università di Bari and INFN, Bari, Italy.* [2] *Università di Roma Tor Vergata and INFN, Rome, Italy.* [3] *Università di Trieste and INFN, Trieste, Italy.* [4] *Università di Firenze and INFN, Firenze, Italy.* [5] *INFN Laboratori Nazionali di Frascati, Italy.* [6] *Università di Perugia and INFN, Perugia, Italy.* [7] *New Mexico State University, Las Cruces, USA.* [8] *Tata institute of Fundamental Research, Bombay, India.* [9] *NASA Goddard Space Flight Center, Greenbelt, MD, USA.* [10] *Siegen University, Siegen, Germany.*

Abstract

The detectors used in the TS93 balloon flight produced a large volume of information for each cosmic ray trigger. Some of the data was visual in nature, other portions contained energy deposition and timing information. The data sets are amenable to conventional analysis techniques but there is no assurance that conventional techniques make full use of subtle correlations and relations amongst the detector responses. With the advent of neural network technologies, particularly adept at classification of complex phenomena, it would seem appropriate to explore the utility of neural network techniques to classify particles observed with our instrument. In this paper neural network based methodology for signal/background discrimination in a cosmic ray space experiment is discussed. Results are presented for electron and positron classification in the TS93 flight data set and will be compared to conventional analyses.

1 Introduction

The electrons and positrons identification in primary cosmic radiation is a very difficult task because of the low signal/background ratio, the short duration of the data taking and the limited geometrical factor available on board balloon-borne facilities. As a consequence the measurement of these particles requires detector performances as high as possible, in particular the

capability to identify signals at high acceptance region with a very low degree of background contamination.

In order to improve the discrimination capabilities of particle detectors, classifiers based on a multi-dimensional with non-linear boundaries feature space, such as feed-forward neural networks [1], were explored with success in various previous works [2, 3, 4, 5, 6]. Moreover the systems based on NNs are very noise- and damage-resistant, therefore they are useful for signal/background discrimination in cosmic ray space measurement that are characterized by critical experimental conditions.

This paper studies the identification capabilities of a transition radiation detector and a silicon-tungsten calorimetr using neural network computational architectures. Both detectors have been employed in the cosmic ray space experiment NMSU/Wizard-TS93, performed on the NASA balloon-borne magnet facility, for electron and positron identification in the momentum range from 4 to 50 GeV/c.

2 Data selection and analysis

Data set was collected during the balloon flight of the NMSU/Wizard-TS93 instrument at 4 GeV/c momentum cutoff. The flight took place on September 8, 1993 from Fort Sumner, New Mexico (USA). The TS93 experimental set-up consists of: (1) a superconducting magnet, equipped with multi wire proportional chambers and drift chambers, used as spectrometer; (2) a set of plastic scintillator that provides both the trigger and the time-of-flight information; (3) a transition radition detector, for identification of particles with γ Lorentz factor $\geq$ 1000 and (4) a silicon-tungsten imaging calorimeter to identify particles according to the different topological and energetic pattern released in the the detector (i.e. straight tracks for muons and non-interacting protons; hadronic showers for protons; electromagnetic showers for electrons and positrons). Details on the apparatus characteristics can be found in ref.[7, 8, 9].

The validation of the detector performances on flight data has been obtained using a tagged high-purity real data sample selected by means of severe one-dimensional cuts. In particular the TRD (calorimeter) results have been carried out using NNs with application data tagged by the time-of-flight, the spectrometer and the calorimeter (TRD).

2.1 Classifying the TRD data

The pattern space used [6, 10] for the classification of the TRD data consists of the total number of hits detected by each TRD planes in a spatial

window (10 planes · 5 wires) around the physical track, as reconstructed using the spectrometer information. A three-layer feed-forward neural network trained by the back-propagation in incremental learning mode is used. The input layer consists of ten neurons, one associated with each of the input variables. Several NN configurations employing different numbers of hidden neurons have been investigated and a hidden layer with ten neurons has been selected. The feature space is formed by the last-layer neuron output. Three different kinds of input data has been used: (i) *training data*, for the synaptic weights formation; (ii) *test data*, for the performances evaluation of the trained NN; (iii) *application data*, for validation of the NN procedure in the specific experimental context. Training and test data has been obtained by a simulation, whereas application data are real events tagged in according to the procedure previously described.

As a comparison, the discrimination capability evaluations of the detector has also been done by means of a one-dimensional cut on the *geometrical mean* indicator $GM = (n_{planes} \cdot n_{hits})^{1/2}$ where n_{planes} is the number of fired planes in the spatial window defined before and n_{hits} is the total number of hits in the same window. Table 1 shows the background contamination at various signal acceptance obtained on the application data *(real data)* by the NN techniques and the traditional method. The results obtained by the NN classifier on the application data set are in excellent agreement with the predicted ones from the analysis of the test data set. It can be seen that in the high signal acceptance region the NN techniques overcomes the classical analysis.

Table 1: *Background contamination* $(\cdot 10^{-2})$ *evaluated for different signal acceptance (%) by the neural network and the geometrical mean indicator on the tagged real data sample (TRD application data).*

Acceptance:	46.0	50.0	56.0	63.0	66.0	78.0	88.0	94.0
NN indic.	0.38	0.61	0.63	0.95	1.22	3.80	6.12	19.16
GM indic.	0.13	0.17	0.49	0.57	1.25	5.03	7.75	34.88

2.2 Classifying the Calorimeter data

Calorimeter data have been preprocessed to extract some discriminating parameters to give in input to the NN. The four-layer feed-forward network [11, 12] is able to perform a multidimensional analysis among the two different classes. As in the TRD case, training and test samples used Montecarlo data while application data are selected from the TS93 data. Several architectures of the feed-forward NN are currently under test in order to achieve

the best performance. Results obtained and a comparison with a conventional analysis will be available at the Conference.

3 Conclusions

In this paper two different classification systems, for TRD and calorimetr respectively, are proposed to identify electrons and positrons gathered by the NMSU/Wizard-TS93 cosmic ray space experiment. The validation of the systems has been done using a sample of high purity real data. The classifiers are based on a neural network computational architectures in order to carry out a careful multidimensional analysis. This distribuited parallel processing model of the systems is able to take into account important instrumental effects and allows selection of signals with high performance in the high acceptance region.

References

[1] J. Hertz, A. Krogh and R.G. Palmer, Introduction to the Theory of the Neural Computation - Addison-Wesley (1991).

[2] Delphi Collab., Phys. Lett. B 295(1992)383.

[3] L3 Collab., Phys. Lett. B 303(1993)237.

[4] Aleph Collab., Phys. Lett. B 313(1993)549.

[5] W.S. Babbage and L.F. Thompson, Nucl. Instr. Meth. A 330(1993)482.

[6] R. Bellotti et al., Comp. Phys. Comm. 78(1993)17.

[7] R.L. Golden et al., Proposal to NASA NRA-92-OSSA-10.

[8] E. Barbarito et al., to appear in Nucl. Instr. Meth. A (1995).

[9] F. Aversa et al., Nucl. Instr. Meth. A 360(1995)17.

[10] R. Bellotti et al., Nucl. Instr. Meth. A 350(1994)556.

[11] M. Casolino et al., Nucl. Instr. Meth. A 360 (1995).

[12] M. Casolino et al., *Proc. of Physics Computing 94*, Lugano, CH, R. Gruber and M. Tomassini eds. 719, Geneva, CH (1994).

Rome 1995 XXIV ICRC SH 6.4.19, Vol. 4

Solar Modulation Of Hydrogen And Helium Cosmic Ray Nuclei Spectra Above 400 Mev/Nucleon, From 1976 To 1993

R.L. Golden[1], P.J. Paradis[1], S.J. Stochaj[1], B.G. Mauger[2], S. Horan[2], G.D. Badwhar[3], R.R. Daniel[3], J.L. Lacy[3], S.A. Stephens[1,3,4], J.E. Zipse[3], B.L. Kimbell[1], W.R. Webber[1], G. Basini[7], F. Bongiorno[7,8], F.M. Brancaccio[7], M. Ricci[7], J.F. Ormes[11], E.S. Seo[11], R.E. Streitmatter[11], P. Papini[5], S. Spillanitini[5], M.T. Brunetti[9], A. Codino[9], C. Grimani[9], M. Menichelli[9], I. Salvatori[9], M.P. de Pascale[10], A. Morselli[10], P. Picozza[10], M. Circella[6], F. Cafagna[6], R. Belotti[6], C.N. DeMarzo[6], P. Spinelli[6], M. Hof[12], M. Simon[12], J.W. Mitchell[11], L.M. Barbier[11], F. Aversa[14], G. Barbiellini[14], A. Vacchi[14], F. Fratnik[14], U. Bravar[14], P. Schiavon[14], Colavita[14] and N. Zampa[14]

[1] Particle Astrophysics Laboratory, New Mexico State University, USA

[2] Physical Science Laboratory, Las Cruces, New Mexico 88003, USA

[3] NASA Johnson Space Center, Houston, Texas 77058, USA. [4] Tata Institute of Fundamental Research, Bombay, India. [5] Universita di Firenze and INFN, Firenze, Italy. [6] Universita di Bari and INFN, Bari, Italy. [7] INFN, Laboratori Nazionali di Frascati, Italy. [8] Universita di Roma "La Sapienza," Rome, Italy. [9] Universita di Perugia and INFN, Perugia, Italy. [10] Universita di Roma "Tor Vergata" and INFN, Rome, Italy. [11] NASA Goddard Space Flight Center, Maryland, USA. [12] University of Siegen, Siegen, Germany. [14] Dipartimento di Fisica and Sezione INFN dell'Universita di Trieste, Trieste, Italy

Abstract

Hydrogen and helium cosmic ray nuclei spectra gathered from 1976 to 1993 have been corrected to the top of the atmosphere and normalized at high rigidities. The variation of these primary cosmic ray fluxes above 400 Mev/nucleon has been examined as a function of the phase of the solar cycle with the force-field approximation model. The intensity of the normalized fluxes between solar maximum and minimum conditions varies by a factor of 6 for hydrogen and a factor of 4.3 for helium at the lowest rigidities considered.

1 Introduction

Hydrogen and helium nuclei constitute more than 95 % of the total cosmic ray component observed at the top of the earth's atmosphere. A study of their spectral shapes and how these are affected by solar modulation is essential for understanding particle propagation and acceleration mechanisms. In this paper, observations of hydrogen and helium spectra are reported above 400 Mev/nucleon, for 7 balloon flights covering nearly two solar cycles. A summary of the experiments reported here is given in Table 1.

2 The Apparatus

The 1991 spectrometer configuration is described in Paradis (1995). A detailed description of the original spectrometer, flown from 1976 to 1989, and an analysis of its performance can be found in Golden et al., 1991.

TABLE 1. The PAL Observing Program.

FLIGHT	DATE	LOCATION	GEOMAGNETIC CUTOFF R_c (Gv/c)	ATMOSPHERIC DEPTH (g/cm^2)	MDR (Gv/c)
CRL3	5/20/76	PALESTINE, TX, USA	4.5	5.8	110
CRL7	6/21/79	PALESTINE, TX, USA	4.5-5.5	5.4	125
CRL8	9/26/86	AINSWORTH, NE, USA	1.7	5.0	110
LEAP	8/21/87	PRINCE ALBERT, CANADA	0.7-1.1	4.7	50
MASS 89	9/5/89	PRINCE ALBERT, CANADA	0.7	5.0	120
MASS 91	9/23/91	Ft SUMNER, NM, USA	4.3	5.8	200
TS93	9/8/93	Ft SUMNER, NM, USA	4.3-4.5	4.5	200

3 Data Analysis

Positive particles were selected in the deflection range corresponding to kinetic energies greater than 400 Mev/nucleon. Only particles with rigidities above local geomagnetic cutoff were considered. The data at lower energies was omitted to avoid large energy-dependent corrections. Typical selection criteria for the tracking system can be found in Paradis (1995). These ensure that a particle's rigidity has been determined reliably. Various combinations of scintillator pulse heights from the time-of-flight detectors were used to determine the charge of the particles. Timing information was also used to eliminate multi-particle events and the small albedo component. Background and charge cut efficiencies were determined by using independent scintillator measurements.

4 Solar Modulation : Force-Field Approximation

The force-field approximation to the steady-state, spherically symmetric model of Gleeson and Axford (1968) has been used to fit the observed spectra. This model describes the solar modulation in terms of convection, diffusion and adiabatic energy losses in the heliosphere. At high energies, Gleeson and Axford relate the differential intensity j(r,E) at radial position r and total energy E to the undisturbed intensity at infinity (the interstellar differential intensity) $j_-(E+\Phi)$. In this formulation, the parameter Φ can be interpreted as the average energy loss experienced by the particles in propagating from infinity. The parameter Φ is a function of the particle's charge and energy, and in general, it is different for each species. It also depends strongly on the form of the diffusion coefficient .

Assuming interstellar rigidity power-law spectra, corresponding deflection spectra were computed at the top of the atmosphere. These spectra were then propagated down to the spectrometer. Energy-dependent efficiency factors were used to take into account energy dependences in the selection criteria, in the geometric factor of the experiments, and in the nuclear interaction cross sections in the material above the spectrometer. The spectra thus computed were convolved with the resolution function of their respective experiment and compared with the observed data. The deflection range for each individual fit was selectively restricted in order to minimize instrumental and geomagnetic cutoff effects. The results of the fits to the force-field approximation model are summarized in Figure 1.

Figure 1 shows a plot of the fitted modulation parameters against scaled neutron monitor count rates observed on the day(s) of each flight. The relation between the fitted modulation parameters and the corresponding Climax neutron

monitor count rates can be described by $\Phi = \Phi_0 + e^{P_1 + P_2 X}$. The parameter Φ_0 can be interpreted as the residual modulation, X is the (scaled) neutron monitor count rate, and P_2 is a small negative parameter. Although the fits are quite good (low overall χ^2's), the fitted hydrogen data predicts a residual modulation $\Phi_0 \sim 420$ Mev while the helium data predicts $\Phi_0 \sim 540$ Mev.

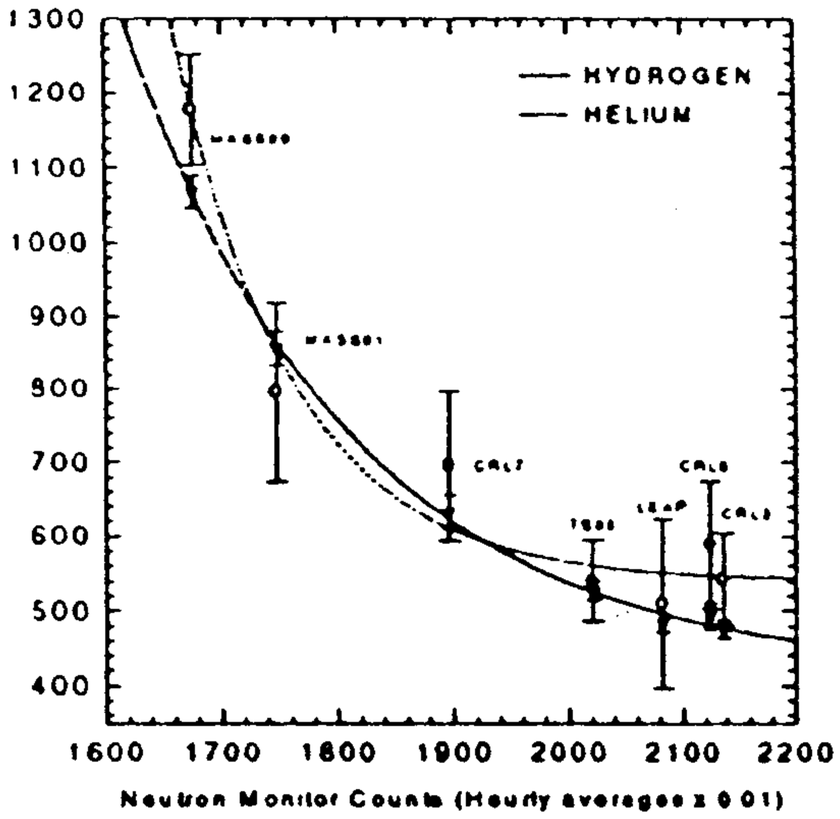

Figure 1. Fitted Modulation Parameters

This is inconsistent with the interpretation of the modulation parameter $\Phi = |Ze|\phi$ in the model chosen, which should, in principle, give twice as much residual modulation for helium as for hydrogen. The values for P_1 and P_2 were (15 ± 1) and (-0.0052 ± 0.0008) for hydrogen, and (23 ± 13) and (-0.0100 ± 0.0077) for helium. Details of the fitting procedure and the complete results can be found in Paradis (1995).

5 Normalized Fluxes At The Top Of The Atmosphere (TOA)

The hydrogen and helium absolute fluxes were first obtained at the spectrometer by deconvolving the observed spectra and dividing the deflection bin counts by the collecting power of the MASS 91 experiment. Deconvolution of the observed data was necessary due to bin spillover near zero deflection as a result of the finite resolution function of the spectrometer.

The correction procedure to the top of the atmosphere has been explained in Paradis (1995). Briefly, corrections were made for nuclear interactions in the payload, attenuation in the atmosphere, and continuous ionization energy losses in the material above the spectrometer. For the protons, the work of Papini et al (1993) was also used to correct for secondary production in the atmosphere.

All the fluxes were normalized to the MASS 91 integral fluxes below 0.06 c/Gv (i.e. above rigidity = 16.67 Gv/c), and multiplied by a correction factor to account for the differences in solar modulation (Webber, 1995).

The absolute proton and helium fluxes, corrected to the TOA, are summarized in Figures 2 and 3. Also shown in the figures are power-law spectra $\propto (d)^{0.7}$, corresponding to unmodulated spectra.

6 Conclusions

As can be seen in Figures 2 and 3, the magnitude of the normalized fluxes varies considerably with the amount of solar modulation. At the lowest rigidities considered, we observe a difference of a factor of 6 in the proton fluxes, and of a factor of 4.3 in the helium fluxes between minimum and maximum solar modulation conditions.

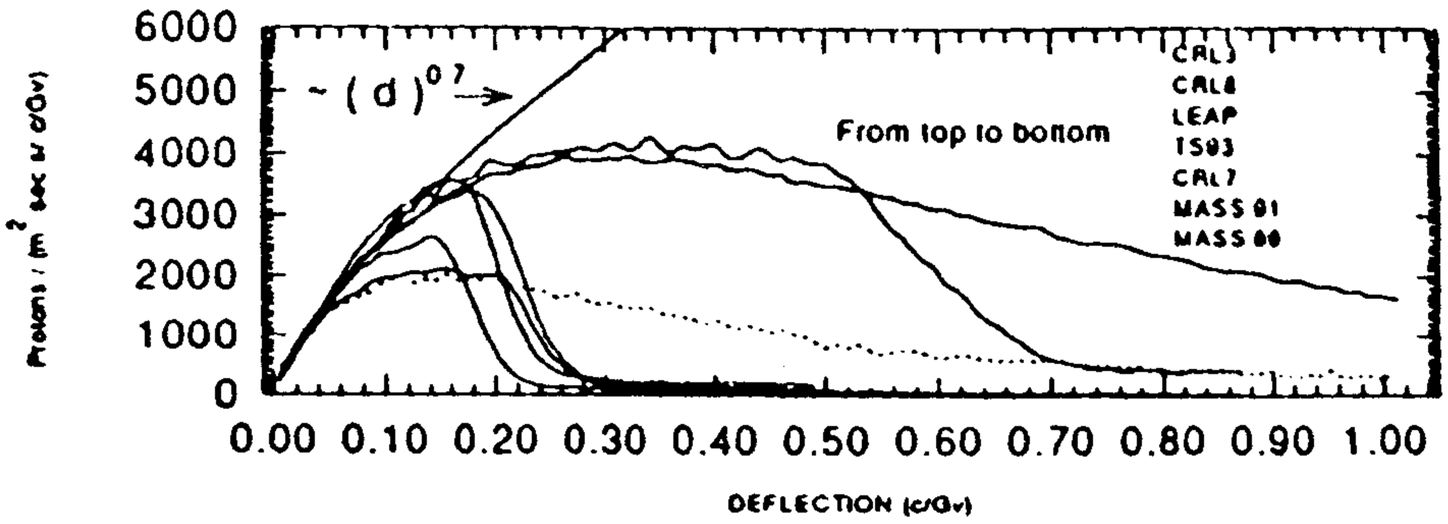

Figure 2. Normalized Hydrogen Fluxes.

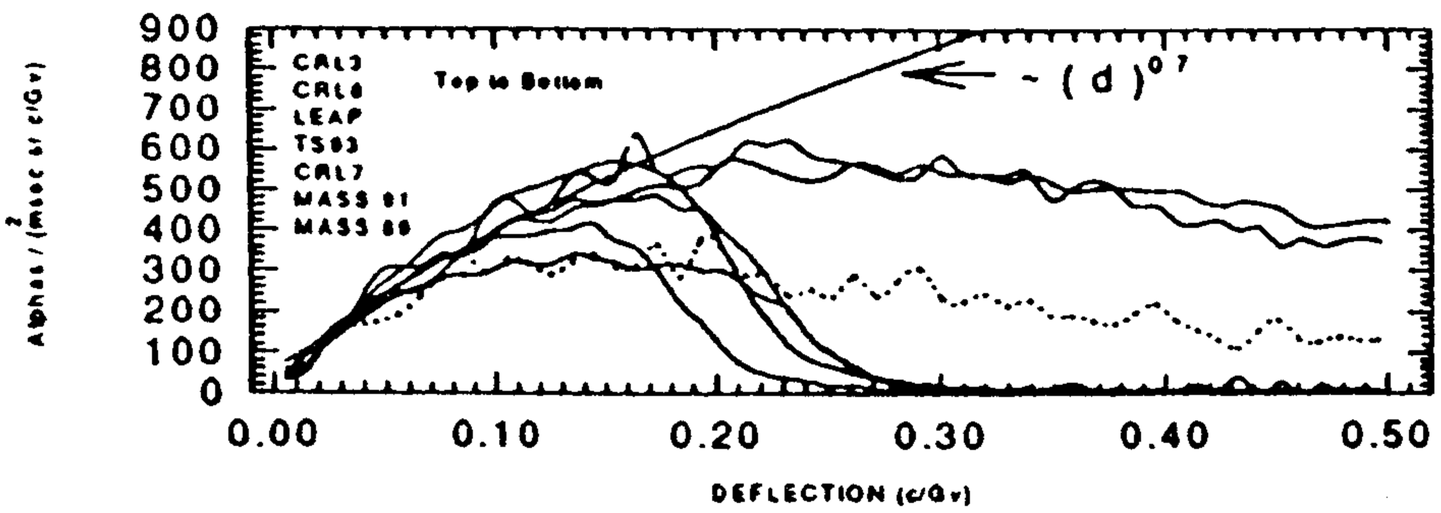

Figure 3. Normalized Helium Fluxes.

In analyzing the modulation effects with the force-field approximation, we see a strong correlation between solar activity as measured by the neutron monitor count rates and the fitted modulation parameters. However, the prediction from this model that $\Phi = |Z\,e|\phi$ is not verified. This is attributed to some structure in the observed spectra which gives rise to high uncertainties in the fitted parameters. We conclude that the force-field modulation model can only predict the general shape of the spectra, and that more sophisticated models may be required to explain the detailed structure of the observations. The irregularities in the observed spectra might be instrumental, but the mechanisms for such effects are unknown.

Detailed tables of the proton and helium spectra observed at the spectrometer, and of the same spectra corrected to the top of the atmosphere can be found in Paradis (1995). It is hoped that these extensive and detailed observations will provide a valuable tool for testing models of solar modulation and geomagnetic effects.

7 Acknowledgments

This work was supported under NASA grant NAG -110.

References

Axford, W. I. & Gleeson, L. J. 1968, Ap. J., 154, 1011
Golden, R.L. et al.:1991, Nucl. Instr. Meth., A396, 366
Papini, P., et al., 1993d, Proc. 23rd ICRC, Calgary, 3, 761
Paradis, P.J., 1995, Ph.D. Dissertation, New Mexico State University
Webber, W. R., 1995, Personal Communications

Rome 1995 XXIV ICRC SH 8.1.13, Vol. 4

Differential Flux Measurement of Atmospheric Pion, Muon, Electron and Positron Energy Spectra at Balloon Altitudes

C. Grimani[1], P. Papini[2], S.A. Stephens[3], G. Basini[4], F. Bongiorno[4], F. Massimo Brancaccio[2], M.T. Brunetti[1], A. Codino[1], N. Finetti [2 1], R.L. Golden[5], M. Hof[6], M. Menichelli[1], J.W. Mitchell[7], A. Morselli[8], J.F. Ormes[7], M.P. De Pascale[8], C. Pfeifer[6], S. Piccardi[2], P. Picozza[8], M. Ricci[4], I. Salvatori[1], M. Simon[6], P. Spillantini[2], S.J. Stochaj[5], R.E. Streitmatter[7]

[1] *Università di Perugia and INFN, Perugia, Italy.* [2] *Università di Firenze and INFN, Firenze, Italy.* [3] *Tata Institute of Fundamental Research, Bombay, India.* [4] *I.N.F.N.-Laboratori Nazionali di Frascati, Frascati, Italy.* [5] *Particle Astrophysics Lab, New Mexico State University, Las Cruces, USA.* [6] *Universität Siegen, Fachbereich Physik, Siegen, Germany.* [7] *NASA Goddard Space Flight Center, Maryland, USA.* [8] *Università di Roma "Tor Vergata" and INFN, Rome, Italy.*

Abstract

The fluxes of atmospheric electrons, positrons, positive and negative muons and negative pions have been determined using the NMSU WiZard-MASS2 balloon-borne instrument. The instrument was launched from Fort Sumner, New Mexico, (geomagnetic cut-off of about 4.5 GV/c) on September 23, 1991. The flight lasted 9.8 hours and remained above 100,000 ft. Muons and negative pions were observed and their momenta were determined. Since these particles are not a part of the primary component, the measurement of their fluxes provides information regarding production and propagation of secondary particles in the atmosphere. Similarly, observations of electrons and positrons well below the geomagnetic cut-off provides insight into electromagnetic cascade processes in the upper atmosphere. In addition, the determination of the energy spectra of rare particles such as positrons can be used for background subtraction for cosmic ray experiments gathering data below a few g/cm^2 of overlying atmosphere.

1 Introduction

Galactic cosmic rays diffusing towards the Earth are deflected by the geomagnetic field. No primary cosmic rays reach the top of the atmosphere below a typical value of the cut-off rigidity characteristic of each site on the Earth. Cosmic rays observed at balloon altitudes below the cut-off are generated by higher energy particle interactions in atmosphere. The measurement of particle fluxes at a few g/cm^2 of atmospheric depth permits cascade calculations to be checked. Moreover, the knowledge of the atmospheric component is needed for background subtraction in the measurements of rare particles, such as positrons, made with balloon-borne experiments.

2 Apparatus and Data Analysis

The MASS2 experiment consisted of the following devices: a time-of-flight scintillator system (TOF), a gas Cherenkov detector (G), a superconducting magnet spectrometer and a streamer tube imaging calorimeter (C). The TOF consisted of 3 planes of plastic scintillator paddles located at the top of the instrument and below the chamber stack. The TOS is used to determine the particle's velocity. A TOF resolution of few hundreds ps assures an up-down rejection at more than 30 standard deviations. The G detector was filled with Freon 12 giving a threshold Lorentz factor of 23.5. The spectrometer consisted of a superconducting magnet and a hybrid system of 8 MWPCs and two modules of drift chambers. The magnet generated a maximum magnetic field of 2.2 T in the chamber region. The spectrometer MDR was 210 GV/c. The imaging calorimeter consisted of 40 planes of 64 brass streamer tubes each, for a total of 7.3 radiation lengths and 0.75 nuclear interaction lengths. The calorimeter permitted the topological reconstruction of the particle interactions. The secondary electron and positron differential fluxes were determined between 300 MeV/c and 4 GeV/c while pions and muons between 5 and 15 GeV/c and 250 MeV/c and 20 GeV/c respectively. The particle selection criteria are shown in Table 1. Test 1, Test 2, Test 3 and Test 4 give a reliable deflection determination in the magnetic spectrometer. Test 5 permits the selection of minimum ionizing particles from the total sample of events, Io being the expected pulse-height corresponding to a minimum ionizing particle and T1 and T2 the average of the top and bottom scintillator charge measurements. Test 6 and Test 6a verify whether or not that a Cherenkov signal has been generated. The average number of photoelectrons generated by a fully relativistic particle was about 18. Test 7 is an energy dependent criterion for particle selection in the calorimeter, see [?] for shower-cluster (s-c) definition. A high number of shower-clusters is characteristic of a high multiplicity, collimated electromagnetic shower. On the other hand, a small number of shower-clusters is related to a low multiplicity, high opening angle hadronic shower. Non-interacting particles should not generate shower-clusters. Tests 7 were used above 1 GeV since no reliable shower identification can be made in the calorimeter for low energy particles generating a small number of secondaries. Since pions have to be separated from the bulk of the other negative particles, mainly electrons and muons, we selected interacting pions only; the number of shower-clusters generated by hadronic interactions and the shower opening angle were found to be very powerful tools. Below 2 GeV, good particle separation was obtained by using the particle square masses as a function of beta (see Papini et al., presented at this conference).

Table 1: *Electron, Positron, Pion and Muon Selection Criteria*

Test1. At least 11 chambers in the direction of the maximum bending of the magnet (x-view) and 6 in the orthogonal direction (y-view) give a good signal. **Test2.** The least-square fit ot the reconstructed track must have $\chi^2_x \leq 8$ and $\chi^2_y \leq 8$. **Test3.** The number of drift chamber planes with hits at more than 4 cm from track has to be less than 3 in both views. **Test4.** The uncertainty in deflection has to be less or equal to 0.03.
Test5. $Z_{T1} \leq 1.8 Io$ and $Z_{T2} \leq 1.8 Io$
Test6. Cherenkov pulse-height $\geq$ 1. photoelectron.
Test6a. Cherenkov pulse-height $\leq$ 1. photoelectron
Test7a. Electrons and positrons 1 - 2 GeV/c: A minimum of 2 calorimeter planes show s-c in, at least, one calorimeter view. 2 - 4 GeV/c: A minimum of 4 calorimeter planes show s-c in, at least, one calorimeter view.
Test7b.Pions The maximum number of s-c shown by the calorimeter views is greater than 4 and smaller than 12. The shower opening angle in the calorimeter has to be at least 25 degrees.
Test7c.Muons No more than one plane, in both calorimeter views, shows s-c

3 Results and Discussion

The geometrical factor, the experiment live time and the efficiencies of the apparatus have been taken into account for particle absolute flux determination. The geometrical factor for low energy particles ranged from 232 cm^2 sr to 284 cm^2 sr while, when the calorimeter was included for selection, the geometrical factor was 167 cm^2 sr. The spectrometer and scintillator efficiencies were .93±0.03 and .85±0.06 respectively. The calorimeter efficiency was 1 for Test 7a between 1 and 2 GeV and .98 above 2 GeV, it was .64 for Test 7b and .93 for Test 7c. The flight lasted 35330 s with a dead time of 36%. Before flux determination the total number of pions was calculated from the observed interacting events and the contribution of non-interacting pions was subtracted from the muon flux. In Figures 1 and 2 we have reported the particle differential fluxes measured by this experiment for electrons, positrons, positive and negative muons and negative pions. Previous measurements made at different atmospheric depths [?, ?] have been reported also along with calculations [?]. A good agreement is observed with the theoretical expectations. It may be

noted that just below the geomagnetic cut-off energy, one needs to consider the ranging down of primary particles due to energy loss processes and hadronic interactions, which would make these particles appear as secondaries.

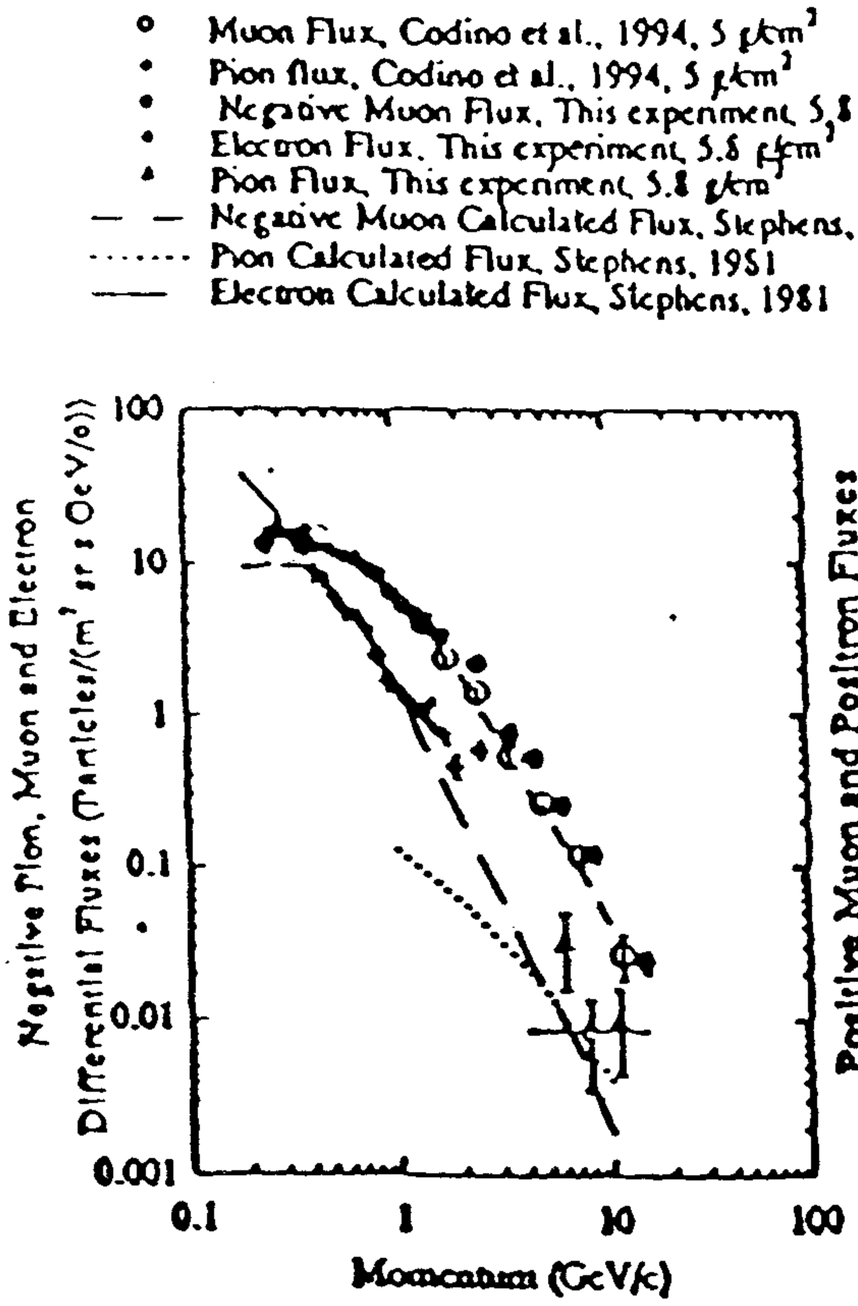

Figure 1: *Negative atmospheric particle fluxes*

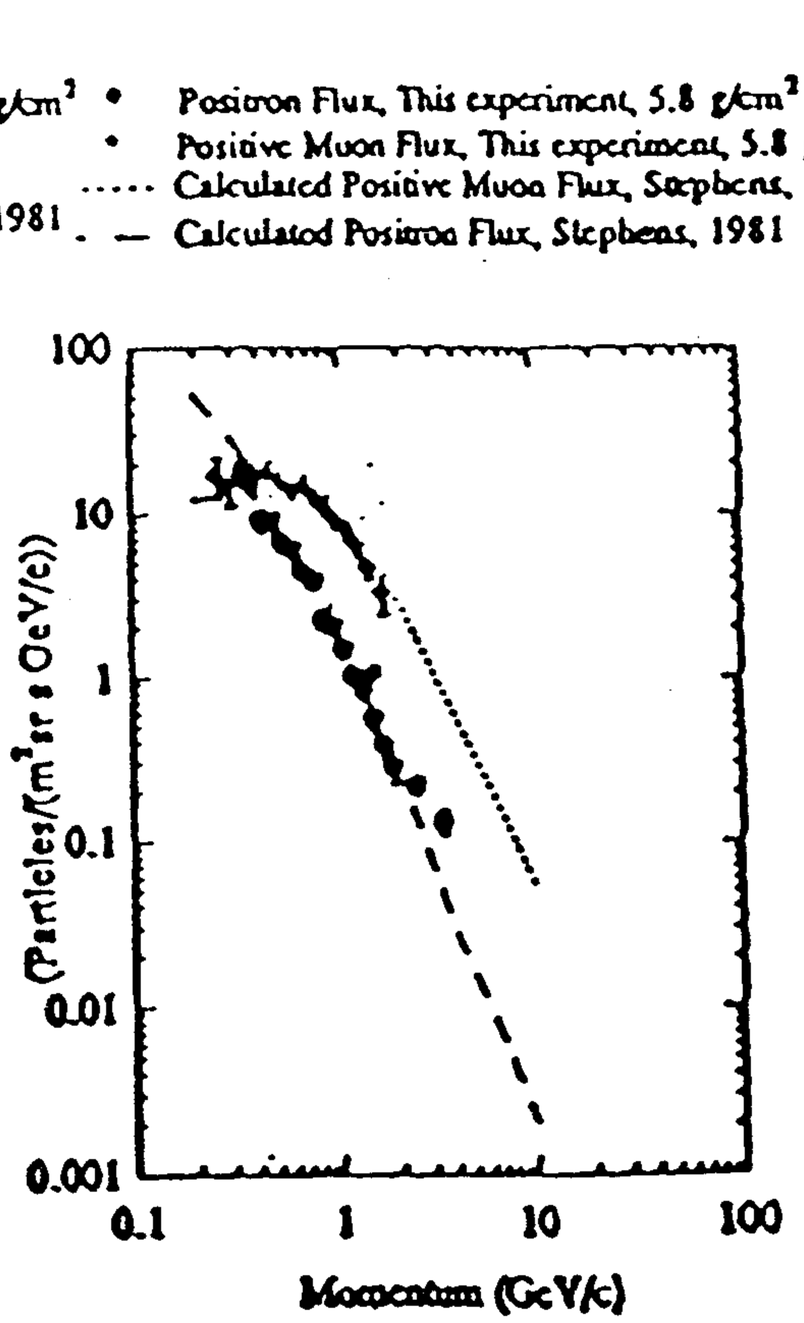

Figure 2: *Positive atmospheric particle fluxes*

Acknowledgements. This work was supported by NASA, Grant NAG-110, the National Scientific Balloon Facility, USA, the Istituto Nazionale di Fisica Nucleare and the Agenzia Spaziale Italiana, Italy and the German Space Agency DARA, Germany.

References

[1] Golden R. L. et al., Ap. J., 436 (1994) 769
[2] Grimani C. et al., 23rd ICRC, Calgary, 4 (1993) 507
[3] Codino A. et al., Conf. Pap. Vulcano Workshop, Nuovo Cimento, (1995)
[4] Stephens, S. A., , 17th ICRC, Paris, 4 (1981) 282

Rome 1995 XXIV ICRC SH 8.1.14, Vol. 4

Atmospheric proton and deuterium energy spectra determination with the MASS2 experiment

P. Papini[1], C. Grimani[2], G. Basini[3], F. Bongiorno[3], F. Massimo Brancaccio[1], M.T. Brunetti[2], A. Codino[2], N. Finetti[2], R.L. Golden[4], M. Hof[5], M. Menichelli[2], J.W. Mitchell[6], A. Morselli[7], J.F. Ormes[8], M.P. De Pascale[7], C. Pfeifer[5], S. Piccardi[1], P. Picozza[7], M. Ricci[3], I. Salvatori[2], M. Simon[5], P. Spillantini[1], S.A. Stephens[8], S.J. Stochaj[4], R.E. Streitmatter[6]

[1] *Università di Firenze and INFN, Firenze, Italy.* [2] *Università di Perugia and INFN, Perugia, Italy.* [3] *I.N.F.N.-Laboratori Nazionali di Frascati, Frascati, Italy.* [4] *Particle Astrophysics Lab. New Mexico State University, Las Cruces, USA.* [5] *Universität Siegen, Fachbereich Physik, Siegen, Germany.* [6] *NASA Goddard Space Flight Center, Maryland, USA.* [7] *Università di Roma "Tor Vergata" and INFN, Rome, Italy.* [8] *Tata Institute of Fundamental Research, Bombay, India.*

Abstract

The energy spectra of atmospheric-secondary protons and deuterium nuclei have been measured during the September 23, 1991, balloon flight of the NMSU/WiZard – MASS2 instrument. The apparatus was launched from Fort Sumner, New Mexico. The geomagnetic cutoff at the launch site is about 4.5 GV/c. The instrument was flown for 9.8 hours at an altitude of over 100,000 feet. Particles detected below the geomagnetic cutoff have been produced mainly by the interactions of the primary cosmic rays with the atmosphere. The measurement of cosmic ray energy spectra below the geomagnetic cutoff provide direct insights into the particle production mechanism and allows comparison to atmospheric cascade calculations.

1 Introduction

When proton and deuterium flux measurements are carried out with balloon-borne experiments floating at few g/cm^2 of atmospheric depth (typically 5 g/cm^2) the corrections for atmospheric production are of primary importance below 1 GeV. The characteristics of the nuclear processes involved in the atmospheric cascade are not yet completely known. Therefore, the theoretical calculation of the proton and deuterium atmospheric production during cosmic ray propagation is not a trivial matter [1, 2, 3, 4, 5, 6, 7]. The measurement of the secondary cosmic ray component using balloon-borne instrument below geomagnetic cutoff can provide information on nuclear production and cosmic ray propagation in the atmosphere.

In this paper we present the preliminary secondary proton and deuterium differential flux measurements made with the MASS2 apparatus in 1991 during a flight at an average atmospheric depth of 5.8 g/cm^2 .

2 Experiment, data analysis and results

The MASS2 apparatus is shown in Figure 1. It consists of a time of flight scintillator system (ToF), a gas Cherenkov detector, a superconducting magnet spectrometer and a streamer tube imaging calorimeter.

The ToF system comprises of twelve 1 cm thick plastic scintillator paddles. The paddles were arranged into 3 planes: two planes, with five paddles each, were located at the top of the payload and one plane, with two paddles, was located between the tracking system and the calorimeter. The signals from the top scintillator planes were read out from only one end of each paddle (T_1 and T_2), whereas the bottom ToF plane was read out at both ends of each paddle (T_3 and T_4). Therefore, three independent dE/dx measurement were recorded.

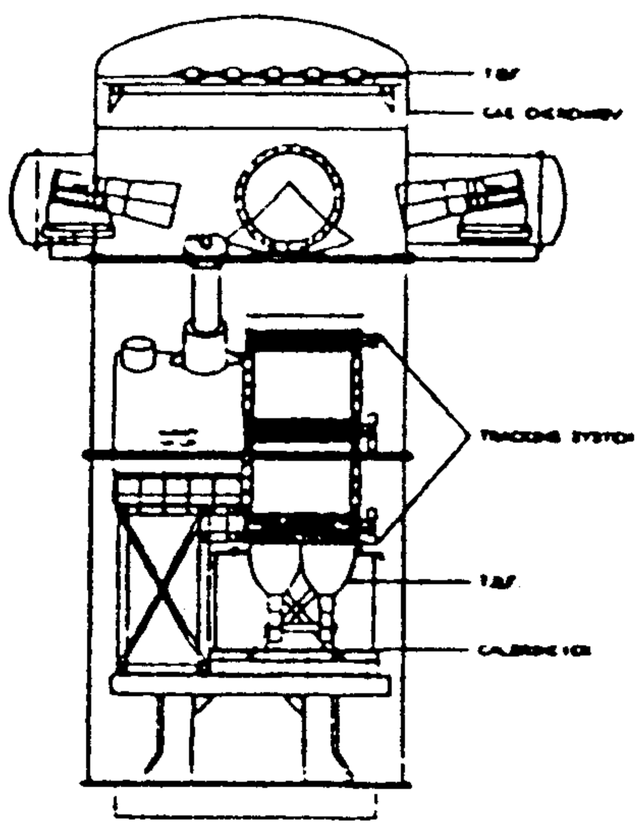

Figure 1: *A schematic diagram of the MASS2 apparatus*

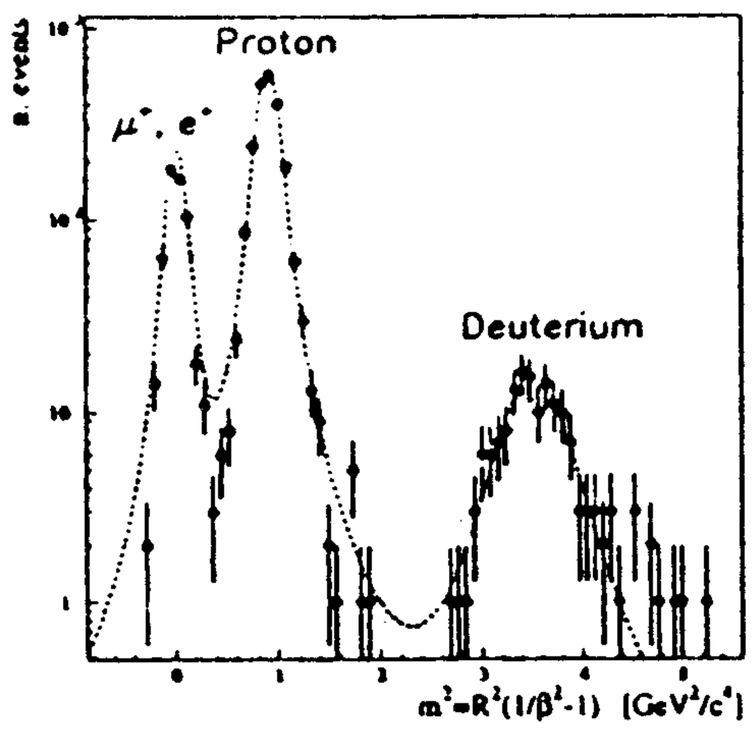

Figure 2: *Mass square distribution at 1 GV/c rigidity*

With a resolution of few hundreds ps the ToF system was used to determine the velocity of the particles as well as remove albedo particles. The pulse-height analysis of the scintillator signals measured the magnitude of the particle's charge.

The magnet spectrometer consisted of a superconducting magnet, 8 multiwire proportional chambers and 2 modules of drift chambers. The field generated by the magnet ranged from 1.5 to 22 kGauss in the chamber region. The tracking system offered twenty trajectory measurements in the view of the maximum bending of the magnet (x-view) and twelve in the orthogonal direction (y-view). The Maximum Detectable Rigidity (MDR) was found to be 210 GV/c for protons. The Cherenkov detector and the calorimeter were

not used to determine proton and deuterium fluxes.

Table 1 shows the single charge particle selection criteria for the tracking system and the scintillators.

Table 1: Tracking system selection and charge selection criteria

1	A minimum of 11 tracking detector planes in the x-view and 6 in the y-view should have good measurement
2	The least square fit to the reconstructed track must satisfy $\chi^2 \leq 8$ for each tracking view
3	Not more than 3 spurious hits in the drift chambers for each view
4	$\Delta d \leq 0.03$ c/GV, where d is the deflection
5	$\frac{\Delta T}{T} = \sqrt{2}\left\|\frac{T_1-T_2}{T_1+T_2}\right\| < 0.4$; $T_{1,2}$=1 means 1 m.i.p. signal
6	$T < 2.5 + 4.95d^2$, where $T = \frac{T_1+T_2}{2}$

Criteria 1–4 have been applied to the tracks from the spectrometer in order to have a reliable deflection measurement. We used the top scintillator pulse-height signals (criteria 5 and 6) to select particles having charge 1.

The sample of positive particles that passed the selection in Table 1 are protons, deuterium, muons and positrons. The time of flight system was used to select proton and deuterium events. The velocity (β), as determined by the ToF system, and the rigidity (R) measured by the spectrometer are used to calculate the particle mass:

$$m(GeV/c^2)^2 = R(GV/c)^2(1/\beta^2 - 1) \qquad (1)$$

Figure 2 shows the positive particle mass square distribution around 1 GV/c. It is possible to note the deuterium peak ($m^2 \sim 3.5$ GeV^2/c^4), the proton peak ($m^2 \sim 0.9$ GeV^2/c^4) and the muon and positron peaks ($m^2 \sim 0$ GeV^2/c^4). Using the mass square distribution we separated the proton and deuterium particles up to 2 GV/c. For each rigidity value we have evaluated the background contamination and the efficiency of the selection criteria used for the proton and deuterium selections.

To convert the observed number of counts at the spectrometer into absolute flux we took into account the geometry factor, the experiment exposure time and the selection efficiencies by including the rigidity dependence of these quantities. We extrapolated the measured proton and deuterium fluxes at the top of the payload correcting for the loss of particles interacting in the payload, above the spectrometer, and the ionization energy losses for non-interacting particles.

The proton and deuterium fluxes are shown in Figure 3. Note the geomagnetic cutoff effect on the primary proton flux at about 3.5 GeV and the

flux increase at low energies due to the proton atmospheric production. The deuterium flux is given in the energy range below the geomagnetic cutoff.

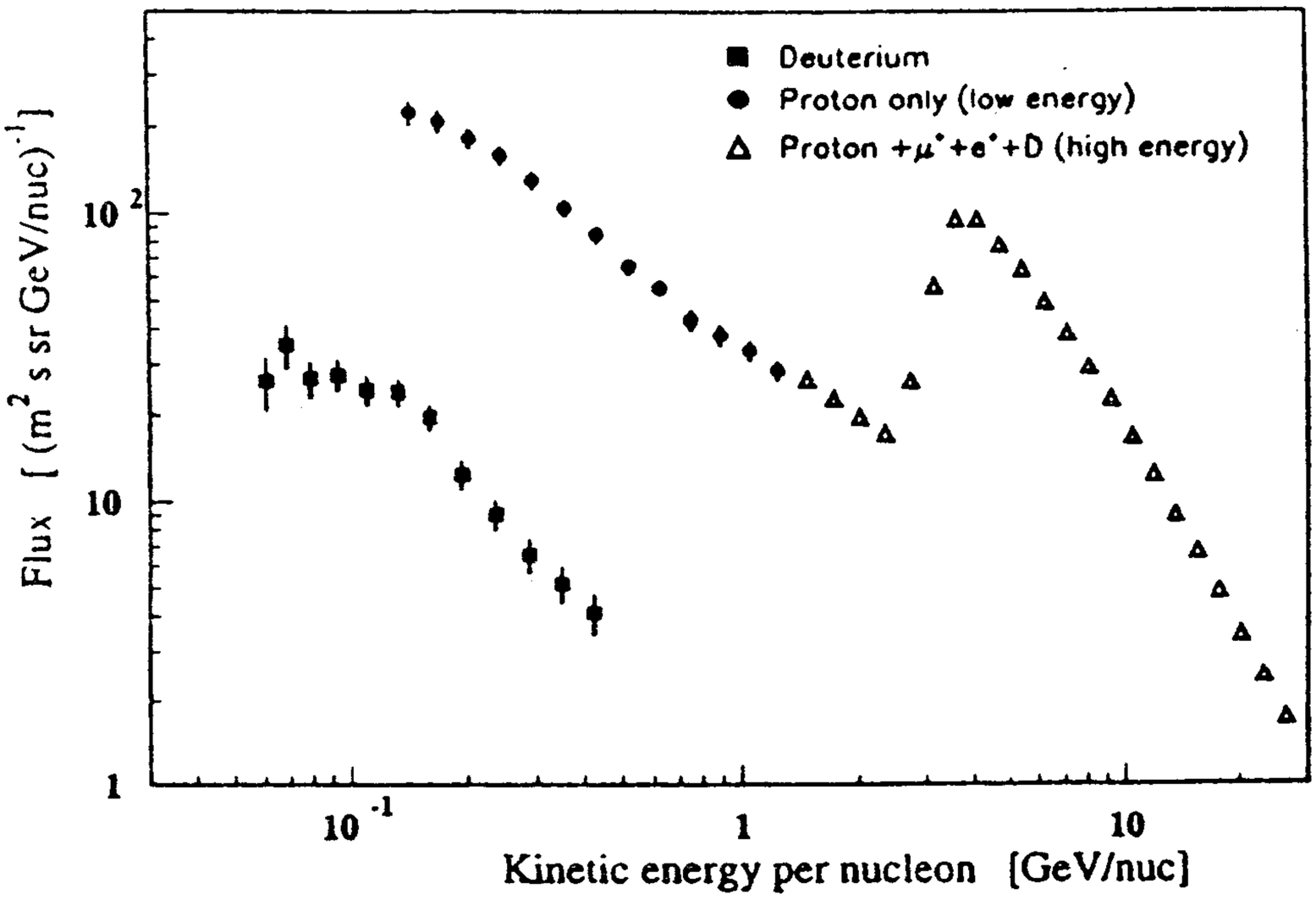

Figure 3: *Proton and deuterium fluxes at the top of the payload.*

Acknowledgment

This work was supported by NASA Grant NAG–110 and the National Scientific Balloon Facility, USA, the Istituto Nazionale di Fisica Nucleare and the Agenzia Spaziale Italiana, Italy, and the German Space Agency DARA, Germany.

References

[1] Ormes J.F., Webber W.R., J. Geophys. Res., 73 (1968) 4231
[2] Papini P., Grimani C., Stephens S.A., 23rd ICRC, Calgary, 3 (1993) 761
[3] Papini P., Grimani C., Stephens S.A., 23rd ICRC, Calgary, 1 (1993) 503
[4] Rygg T.A., et al., J. Geophys. Res., 76 (1971) 7445
[5] Teegarden B.J., J. Geophys. Res., 19 (1967) 4847
[6] Webber W.R., Yushak S.M., Ap. J., 275 (1983) 391
[7] Yushak S.M., Ph.D. Thesis, Clarkson University (1978)

Rome 1995 XXIV ICRC SH 8.1.15, Vol. 4

Ground Level Cosmic Ray Observations

S.A. Stephens[1], S. Piccardi[2], C. Grimani[3], P. Papini[2], G. Basini[4],
F. Bongiorno[4], F. Massimo Brancaccio[2], M.T. Brunetti[3], A. Codino[3],
R.L. Golden[5], M. Hof[6], N. Finetti[3], M. Menichelli[3], J.W. Mitchell[7],
A. Morselli[8], J.F. Ormes[7], M. P. De Pascale[8], C. Pfeifer[6],
P. Picozza[8], M. Ricci[4], I. Salvatori[3], M. Simon[6],
P. Spillantini[2], S.J. Stochaj[5], R.E. Streitmatter[7]

[1] *Tata Institute of Fundamental Research, Bombay, India.* [2] *Università di Firenze and INFN, Firenze, Italy.* [3] *Università di Perugia and INFN, Perugia, Italy.* [4] *I.N.F.N.-Laboratori Nazionali di Frascati, Frascati, Italy.* [5] *Particle Astrophysics Lab, New Mexico State University, Las Cruces, USA.* [6] *Universität Siegen, Fachbereich Physik, Siegen, Germany.* [7] *NASA Goddard Space Flight Center, Maryland, USA.* [8] *Università di Roma "Tor Vergata" and INFN, Rome, Italy.*

Abstract

Cosmic rays at ground level have been collected using the NMSU/Wi-Zard - MASS2 instrument. The 17-hr observation run was made on September 9th 1991 in Fort Sumner, New Mexico, USA. Fort Sumner is located at 1270 meters a.s.l., corresponding to an atmospheric depth of about 887 g/cm^2. The geomagnetic cutoff is 4.5 GV/c. The charge ratio of positive and negative muons and the proton to muon ratio have been determined. These observations will also be compared with data collected at a higher latitude using the same basic apparatus.

1 Introduction

The observed cosmic ray spectra at ground level result from the propagation of primary cosmic rays in the atmosphere. The ground cosmic ray radiation consists mainly of weakly interacting muons. In this paper we present a very preliminary analysis to determine the muon charge ratio and proton to muon ratio and we compare our present results to previous measurements [1, 2].

2 Experiment

The MASS2 apparatus consisted of a magnetic spectrometer, a TOF system, a gas Cherenkov counter and an imaging calorimeter to detect respectively the rigidity and the particle's charge sign; the particle's absolute charge and beta; an indication of the particle's Lorentz factor. The magnetic spectrometer was an improved version of the detector [3] used to discover antiprotons in cosmic

rays in 1979, it consists of a superconducting magnet that generates a field ranging from 2.2 to .15 tesla and a hybrid traking system comprised of 8 MWPCs and two modules of drift chambers. The TOF system consists of 3 layers of scintillator 1 cm thick. The scintillator signals from the two top planes were read out from only one end of each paddle (T_1 and T_2 signals) whereas the single bottom plane was read out at the two ends (T_3, T_4). The Cherenkov counter consisted of 4 mirror segments that focused Cherenkov light on 4 phototubes; its inner volume was filled, for the ground run, with Freon 22 with a threshold Lorentz factor of 32. The Cherenkov detector is described in [4]. The dimensions of the calorimeter are 50 cm × 50 cm × 40 cm (depth), this detector was positioned below the bottom scintillator and consisted of 40 layers of 64 brass streamer tubes arranged perpendicularly to each other. The walls of the streamer tubes served as the converter material for the calorimeter, yielding a total depth of 7.33 radiation lengths, equivalent to 0.75 nuclear interaction lengths. The imaging calorimeter is a powerful tool to separate different particle interactions in order to distinguish between non interacting particles (like muons or non interacting protons), hadronic interactions and electromagnetic showers.

3 Analysis and results

Selection criteria for muons are summarized in Table 1.

Table 1: Muons selection criteria

1	A minimum of 11 tracking detector planes in the X-view and 6 in the Y-view should have good measurements.
2	The least square fit of the spectrometer reconstructed track must have $\chi^2 \leq 8$ in both views.
3	3 spurious hits maximum in the drift chamber planes per view
4	$\sigma_\eta \leq .03$ (c/GV) where η is the deflection and σ_η its error.
5	$1 < T_1 + T_2 < 4$ ($T_{1,2} = 1$ means 1 m.i.p. signal).
6	$\left\lvert \frac{T_1 - T_2}{T_1 + T_2} \right\rvert < 0.4$; ($T_{1,2}$=1 means 1 m.i.p. signal).
7	Only a paddle for scintillator layer gives a signal. There is consistency between particle trajectory and scintillator hits.
8	Trajectory containement at bottom of the calorimeter.
9	At least one calorimeter view gives signal.
10	The ratio between trajectory single hits (2 Moliere radii) and the sum of multiple and single hits must be greather than 0.8 (by taking the maximum between the two views).

Our scintillator cut efficiency has been determined by selecting with the bottom scintillator only those events generating a signal corresponding to charge 1 particles. This sample was used to test the top scintillator cut (5–7). We have found an efficiency of 87.25% ±.65% in the whole rigidity range.

To test the calorimeter muon selection cuts we have used the Cherenkov detector in the rigidity range between −3 and 3 GV/c. In this interval only muons do not generate Cherenkov light (the proton contrubution can be neglected since no significant differences were found between positive and negative charge particles).

We selected a muon sample by requiring a signal lower than 0.5 photoelectrons. With this sample we tested the calorimeter cut (10). A calorimeter cut efficiency of 97.67% ± 1.23% was found. We also checked that this efficiency was constant versus rigidity, and equal for negative and positive deflection.

The cut (9) efficiency was 97.85% over the all ground data sample, constant in deflection and equal for negative and positive particles.

The ground data spectrometer efficiency has to be estimated. At this stage we present a very preliminary analysis. Absolute fluxes will be presented at this conference.

For proton analysis we mainly used the Cherenkov detector in the rigidity range between 3.7 and 20 GV, in this deflection range protons only don't produce Cherenkov light, therefore we could select a pure proton sample by requiring the absence of the Cherenkov signal. A high background, due to muons passing this cut because of the Cherenkov inefficiency, requires the addition of a calorimeter criterion to select interacting protons only.

Cuts (1–9) in Table 1 were applied for proton selection too.

Table 2: Proton selection criteria

1	Cherenkov signal corresponding to less than .5 photoelectrons.
2	Maximum shower width greather than .6 Moliere radii.
3	Minimum shower width greather than .5 Moliere radii. This condition was skipped when only one calorimeter view was working and the number of hits was greater than 20

A wide number of calorimeter hits and high shower opening angle, are characteristic of a hadronic interaction, therefore for each calorimeter view we calculated the total number of hits and the interaction width from the trajectory extrapolated from the spectrometer.

Proton selection criteria are summarized in Table 2.

A sample of 93 events passed the selection for protons. To estimate the possible muon or electron contamination on this sample we applied the same set of cuts to a sample of negative particles in the same rigidity interval. Two events only passed the cuts out of a total of 5357 particles. Since positive particles were 7030, we estimated a contamination of 2.6 events.

To estimate the proton calorimeter efficiency we made a visual scan of a pure proton sample selected with the Cherenkov detector: no interactions were rejected by our cuts, therefore we determined an efficiency better than 99%.

To compute the p/μ ratio we selected muons with all cuts in Table 1, adding the requirement of a Cherenkov signal higher than .5 photoelectrons. We computed the efficiency of this cut with a negative rigidity particle sample in the range between 5 and 100 GV. We have found an efficiency of 96%.

We calculated the p/μ ratio taking into account the different efficiencies for muon and proton selection and the total number of protons from the observed interacting events.

Figure 1 shows the charge ratio μ^+/μ^-, compared to previous measurements taken at a different atmospheric depth [1]. The present results are compatible within the errors. The solid curve is a theoretical prediction [5].

Figure 2 shows the proton to muon ratio.

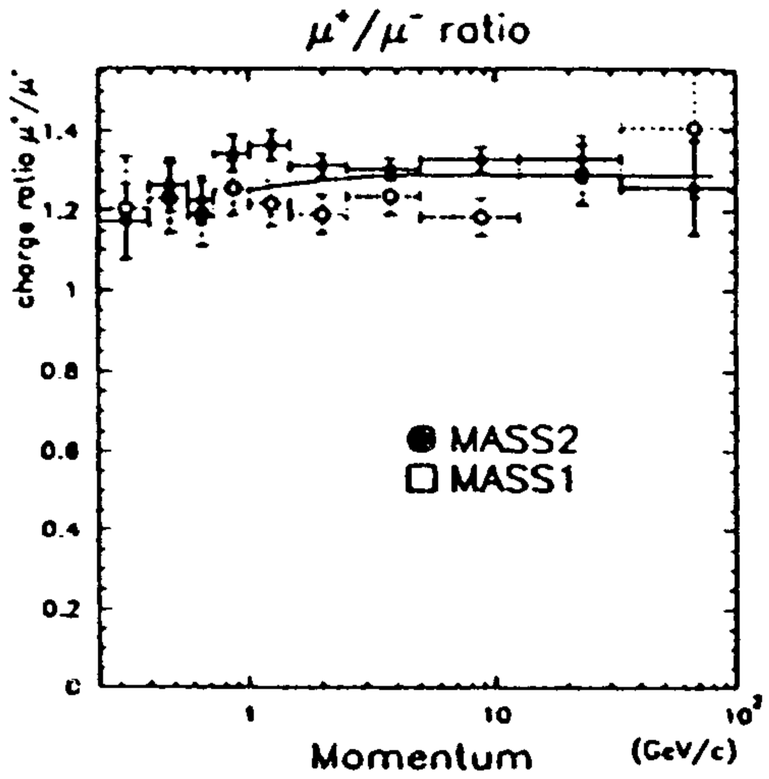

Figure 1: *Muon charge ratio.*

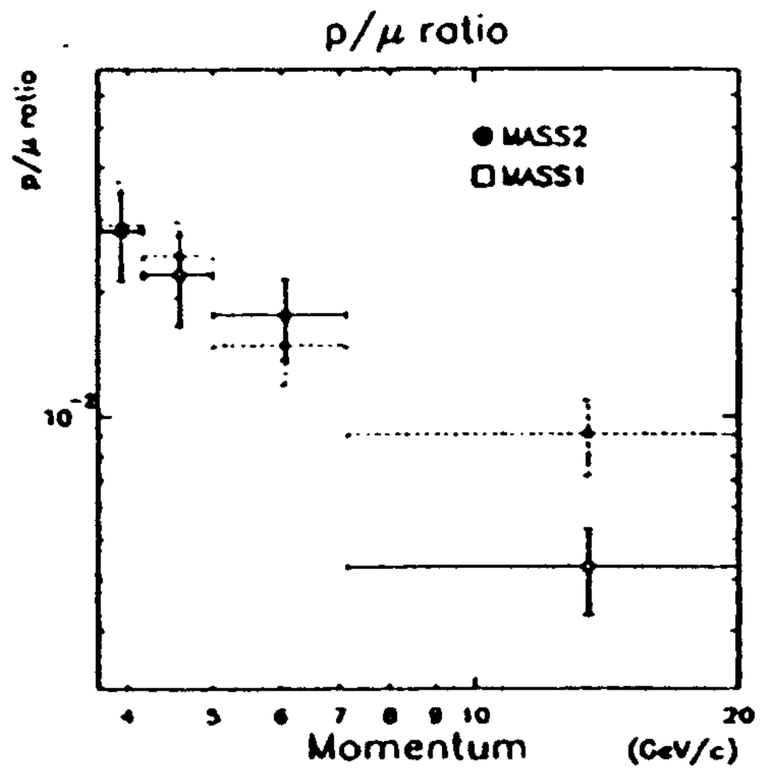

Figure 2: *Proton to muon ratio.*

Acknowledgment

This work was supported by NASA Grant NAG-110 and the National Scientific Balloon Facility, USA, the Istituto Nazionale di Fisica Nucleare and the Agenzia Spaziale Italiana, Italy, and the German Space Agency DARA, Germany.

References

[1] M. P. De Pascale et al., J. Geophyis. Res. 98 (1993) 3501

[2] G. Basini et al., Proc. 23rd ICRC, Calgary 3 (1993) 773

[3] R. L. Golden et al., Nucl. Instr. Meth., A306 (1991) 366

[4] R. L. Golden et al., to be submitted, (1995)

[5] S. A. Stephens, 16th ICRC, 10 (1979) 96

Rome 1995 XXIV ICRC SH 8.1.16, Vol. 4

^{3}He spectrum at small atmospheric depths for different geomagnetic cutoff values

P. Papini[1], C. Grimani[2], S.A. Stephens[3]

[1] *Università di Firenze and INFN, Firenze, Italy.*
[2] *Università di Perugia and INFN, Perugia, Italy.*
[3] *Tata Institute of Fundamental Research, Bombay, India.*

Abstract

We have carried-out a calculation to determine the energy spectra of secondary ^{3}He at small atmospheric depths. It is produced in the spallation reaction of primary helium and heavier nuclei in the overlying atmosphere. We examine the effect of the geomagnetic cut-off on the spectral shape of the secondary ^{3}He nuclei. The calculations are being carried out for both solar minimum and maximum periods. Results from these calculations will be presented at the Conference.

1 Introduction

^{3}He nuclei are secondary cosmic rays, which are produced in the interactions of primary cosmic rays with the interstellar medium during their propagation in the Galaxy. Most of the nuclei are produced by the interaction of ^{4}He and as their rigidities are different, the study of ^{3}He fraction gives important insights on the cosmic ray propagation as well as on the solar modulation. Most of the experiments to determine the ^{3}He spectrum are carried out with balloon-borne instruments. As a result, it is essential to correct for the ^{3}He background produced by spallation of ^{4}He and heavier cosmic ray nuclei in the overlying atmosphere.

Experimental determination of the geomagnetic threshold rigidity for cosmic rays can not be made using singly charged particles as they are also produced in the atmosphere by different processes. However, this can be best studied with helium nuclei and one can determine also the transmission function at locations, where there are panumbral bands. However, ^{3}He produced in the atmosphere would influence the shape of the rigidity spectrum measured in a magnet spectrometer. Therefore, one needs to correct accurately ^{3}He produced in the atmosphere to derive the shape of the transmitted spectrum of primary nuclei. ^{3}He production depends on the primary cosmic ray composition and energy spectra at the top of the atmosphere, which depends on the geographical location and the solar activity. We have calculated the secondary spectrum of ^{3}He at small atmospheric depths with zero cut-off and

preliminary results were earlier presented for both maximum and minimum periods of solar activity [1]. This calculation has been now modified to include the geomagnetic threshold effect.

In this paper we describe the procedure used for the calculation of ^{3}He production in the atmosphere and the final results will be presented at this conference.

2 Calculation procedure

In order to calculate the ^{3}He atmospheric production we use three transport equations: one for the ^{3}He ($J_{^3He}$), one for the ^{4}He ($J_{^4He}$) and one for the nuclei heavier than helium (J_N).

The equations are given below.

$$\frac{\partial J_{^3He}(E,x)}{\partial x} = \frac{\partial}{\partial E}\left[J_{^3He}(E,x)\frac{dE}{dx}\right] - \frac{J_{^3He}(E,x)}{\lambda_{^3He}(E)} + \int_E^\infty \frac{J_{^4He}(E',x)}{\lambda_{^4He\to{}^3He}(E')}\Phi(E',E)dE' + \int_E^\infty \frac{J_N(E',x)}{\lambda_{N\to{}^3He}(E')}\Phi(E',E)dE' \quad (1)$$

$$\frac{\partial J_{^4He}(E,x)}{\partial x} = \frac{\partial}{\partial E}\left[J_{^4He}(E,x)\frac{dE}{dx}\right] - \frac{J_{^4He}(E,x)}{\lambda_{^4He}(E)} + \int_E^\infty \frac{J_N(E',x)}{\lambda_{N\to{}^4He}(E')}\Phi(E',E)dE' \quad (2)$$

$$\frac{\partial J_N(E,x)}{\partial x} = \frac{\partial}{\partial E}\left[J_N(E,x)\frac{dE}{dx}\right] - \frac{J_N(E,x)}{\lambda_N(E)} \quad (3)$$

In the above equations the first term on the R.H.S. corresponds to continuous energy loss due to the ionization process. The second term represents the loss of particles due to interactions with air nuclei. The integral terms give the production of ^3He and ^4He where $\Phi(E',E)$ is the outgoing nucleus distribution function that is the probability that a nucleus with kinetic energy per nucleon E' produces a ^3He (or a ^4He) nucleus with kinetic energy per nucleon E. A best fit to observed data has been made to determine the ^4He flux at the top of the atmosphere for minimum and maximum solar modulation.

We have found suitable to use the C+O spectrum shape, which is measured accurately, to represent the heavy nucleus component for Z>2. In fact, the steeper spectra of secondary light nuclei is compensated by the relatively flatter spectra of heavy nuclei. From a comparison of the cosmic ray abundances as a function of energy [2, 3] we have found that the C+O spectrum needs to be

multiplied by a factor 2.25 in order to determine an equivalent C+O spectrum, which includes all nuclei with Z>2. This weighting factor appears to be nearly independent of energy within the uncertainty of the measured data.

In order to include the geomagnetic effect in the ^{3}He production, we have first made use of the observed shape of the rigidity spectrum of helium nuclei at a geographic location for the primary ^{4}He and heavier nuclei. We then correct this shape using the calculated ^{3}He spectrum to derive the true spectrum and thus perform this calculation.

The transport equations 1–3 are then solved simultaneously by numerical integration technique described earlier [1]. The results on the ^{3}He spectra as a function of the geomagnetic latitude will be presented at the conference.

References

[1] Papini P., Grimani C., Stephens S.A., 23rd ICRC, Calgary, 1 (1993) 499

[2] Engelmann J.J., et al., Astron. Astrophys., **233** (1990) 96

[3] Simpson J.A., Ann. Rev. Nucl. Part. Sci., bf 33 (1983) 323

Rome 1995 XXIV ICRC SH 8.1.17, Vol. 4

Production of secondary Deuterium in the atmosphere at various latitudes

P. Papini[1], C. Grimani[2], S.A. Stephens[3]

[1] *Università di Firenze and INFN, Firenze, Italy.*
[2] *Università di Perugia and INFN, Perugia, Italy.*
[3] *Tata Institute of Fundamental Research, Bombay, India.*

Abstract

Secondary deuteriums in the atmosphere are produced in interactions by primary cosmic rays. The shape of their energy spectrum depends on the primary cosmic ray spectrum incident at the top of the atmosphere. At high energies, the spectral shape depends on the primary spectrum of helium and heavy nuclei. However, at very low energies, especially below the geomagnetic cut-off, the spectral shape depends on the evaporation and recoil processes and hence almost indipendent of the spectral shape of the primary radiation. We have undertaken a calculation of the secondary deuterium spectrum at small atmospheric depths at various latitudes and the results will be presented.

1 Introduction

The cosmic ray deuterium is one of the most interesting secondary cosmic nuclei for the study of the cosmic ray propagation in the Galaxy. Its importance comes from the fact that its interaction mean free path is larger than the matter traversed by cosmic rays during their propagation in the Galaxy. Some a large fraction of the deuterium is produced by the spallation of helium nuclei, a direct comparison between the spectra of these two nuclei is very informative, as their mass to charge ratio is the same and hence their modulation in the solar system. There are only a few measurements of cosmic ray deuterium at energies greater than 100 MeV per nucleon and they were obtained using balloon-borne instruments flying at few g/cm^2 of atmospheric depth. Since deuterium is produced also in the interactions of cosmic protons and nuclei in the overlying atmosphere, atmospheric correctios are needed to derive the primary deuterium from the observations. Its production is dependent on the primary cosmic ray composition and spectra at the top of the atmosphere. As a result, the secondary deuterium spectrum in the atmosphere is very sensitive to the latitude, specially at small energies below the geomegnetic threshold. At high latitudes, it also depends upon the solar activity. It is very important to carry out calculations of atmospheric deuterium production

as a function of the latitude in order to compare with the observations. One can also examine the effect of solar modulation as a function of geomagnetic threshold. Preliminary results of atmospheric deuterium calculations by taking into account different solar modulation conditions were presented earlier for zero geomagnetic threshold [1]. In this paper we summarize the calculation procedure, whereas the final results relating to the geomagnetic cut-off effect on secondary deuterium production will be presented at this conference.

2 Calculation procedure

The transport equation describing the production and propagation processes in the atmosphere is:

$$\frac{\partial J_D(E,x)}{\partial x} = \frac{\partial}{\partial E}\left[J_D(E,x)\frac{dE}{dx}\right] - \frac{J_D(E,x)}{\lambda_D(E)} + P(E,x) \qquad (1)$$

The first term on the R.H.S. represents the continuous deuterium energy losses due to ionization. The second term gives the particle loss resulting from interactions and the term $P(E,x)$ represents the atmospheric production due to cosmic ray interactions with air nuclei. As described in [1] the main contributions to the deuterium production cames from three processes:

1. deuterium production from air nucleus spallation;
2. deuterium production from $p(n) + p(n) \longrightarrow D + \pi$ reaction;
3. spallation of cosmic helium and heavier nuclei.

At each atmospheric depth the deuterium production $P(E,x)$ results from the propagation of primary cosmic rays at that depth. The energy spectra of protons, neutrons and helium have been obtained by solving simultaneously the respective transport equations of these particles in atmosphere[2]. The contribution to deuterium production of nuclei heavier than helium has been included in the calculations assuming that each nucleon with atomic number A behaves like a sample of A/4 helium nuclei.

The three deuterium production processes mentioned above dominate in different energy ranges: production from cosmic helium and heavier nuclei is dominant at high energy, whereas the air nucleus spallation process prevails at low energy. The $p(n)+p(n) \longrightarrow D+\pi$ process gives an important contribution at about 100–200 MeV/nuc.

In order to determine the secondary deuterium spectrum at different latitudes, we have constructed the primary rigidity spectra with nearly a sharp threshold at low and very high latitudes. In the intermediate latitudes, where panumbral bands play an important role, we made use of the spectral shape of

the observed rigity spectrum of helium nuclei to construct the incident spectra of p, He and heavy nuclei. These spectra are then propagated in the atmosphere to determine the secondary deuterium spectra at small atmospheric depths by solving the equation (1).

The results will be presented at this conference.

References

[1] Papini P., Grimani C., Stephens S.A., 23rd ICRC, Calgary, **1** (1993) 503

[2] Papini P., Grimani C., Stephens S.A., 23rd ICRC, Calgary, **3** (1993) 761

Rome 1995 XXIV ICRC SH 8.1.18, Vol. 4

Secondary proton production at small atmospheric depths as a function of the geomagnetic cut-off

P. Papini[1], C. Grimani[2], S.A. Stephens[3]

[1] *Università di Firenze and INFN, Firenze, Italy.*
[2] *Università di Perugia and INFN, Perugia, Italy.*
[3] *Tata Institute of Fundamental Research, Bombay, India.*

Abstract

A detailed calculation of the energy spectrum of secondary protons in the atmosphere is being carried out in the energy range 20 MeV – 40 GeV. In this calculation, we have taken into account all processes leading to the production of secondary protons with the air target nuclei. The energy spectrum of secondary protons as a function of the atmospheric depth has been calculated using all relevant energy loss processes. In this paper, we examine the effect of the geomagnetic cut-off on the spectral shape of secondary protons especially at energies below the geomagnetic cut-off for small atmospheric depths.

1 Introduction

Secondary protons are produced in nuclear interactions of cosmic ray nuclei with air nuclei during cosmic ray propagation in the atmosphere. Although primary protons are not expected to reach the earth's atmosphere below the geomegnetic threshold rigidity at a given geographic location, one sees considerable amount of protons well below the threshold rigidity at balloon altitudes. These are either due to the fragmentation of heavier nuclei or due to the interaction of primary protons and the evaporation of target nuclei in the atmosphere. Therefore, the secondary proton spectrum observed below the geomagnetic threshold rigidity depends upon the latitude at which the observation is made. The intensity of this radiation depends also on the solar activity, specially at high latitudes. Most of the experiments to measure cosmic ray composition and energy spectra were carried out using balloon-borne instruments at different latitudes. An exact knowledge of the secondary spectrum provides a valuable check on the performance of the instrument at the float altitude. Preliminary results of the production of secondary protons at small atmospheric depths at very high latitude, where the geomegnetic cut-off is very low, were presented earlier [1]. In this paper we consider the variation of the secondary proton spectrum with latitude due to the effect of the geomagnetic field.

2 Calculation procedure

In order to determine the proton differential energy spectrum as a function of the atmospheric depth, we solve simultaneously the transport equation for the secondary protons along with those of primary protons, secondary neutrons and primary helium nuclei.

The transport equations are:

$$\frac{\partial J_P(E,x,\theta)}{\partial x} = \frac{\partial}{\partial E}\left[J_P(E,x,\theta)\frac{dE}{dx}\right] - \frac{J_P(E,x,\theta)}{\lambda'_P(E)} \tag{1}$$

$$\frac{\partial J_{He}(E,x,\theta)}{\partial x} = \frac{\partial}{\partial E}\left[J_{He}(E,x,\theta)\frac{dE}{dx}\right] - 0.5\frac{J_{He}(E,x,\theta)}{\lambda'_{He}(E)} \tag{2}$$

$$\begin{aligned}\frac{\partial J_N(E,x,\theta)}{\partial x} &= -\frac{J_N(E,x,\theta)}{\lambda_P(E)} + \\ &+ 1.25J_{He}(E,x,\theta)\left(\frac{1}{\lambda'_{He}(E)} - \frac{1}{\lambda_{He}(E)}\right) + \\ &+ \int_E^\infty dE'\Phi(E')\left[\frac{J_N(E',x,\theta)}{\lambda_P(E')}(1-\alpha)+\right. \\ &+ \left.\frac{J_P(E',x,\theta)+J_S(E',x,\theta)}{\lambda_P(E')}\alpha + 1.25\frac{J_{He}(E',x,\theta)}{\lambda_{He}(E')}\right] + \\ &+ P_{air}(E,x,\theta)\end{aligned} \tag{3}$$

$$\begin{aligned}\frac{\partial J_S(E,x,\theta)}{\partial x} &= \frac{\partial}{\partial E}\left[J_S(E,x,\theta)\frac{dE}{dx}\right] - \frac{J_S(E,x,\theta)}{\lambda'_P(E)} + \\ &+ 1.25J_{He}(E,x,\theta)\left(\frac{1}{\lambda'_{He}(E)} - \frac{1}{\lambda_{He}(E)}\right) \\ &+ \int_E^\infty dE'\Phi(E')\left[\frac{J_P(E',x,\theta)+J_S(E',x,\theta)}{\lambda_P(E')}(1-\alpha)+\right. \\ &+ \left.\frac{J_N(E',x,\theta)}{\lambda_N(E')}\alpha + 1.25\frac{J_{He}(E',x,\theta)}{\lambda_{He}(E')}\right] + P_{air}(E,x,\theta)\end{aligned} \tag{4}$$

where $J(E,x,\theta)$ are the differential fluxes as a function of the kinetic energy, of the atmospheric depth and the zenith angle. The subscript letter to the flux term corresponds to primary protons (P), neutrons (N), helium nuclei (He) and secondary protons (S).

In the above set of equations, equation (1) describes the change in the primary proton spectrum at any given depth in the atmosphere. The first term on the R.H.S. of this equation takes care of the ionization energy loss. The second term describes the loss of protons due to interactions, where λ' is the interaction length in air. In the same manner, equation (2) is for the

helium spectrum at a given depth. We have multiplied the interaction term in equation (2) by a factor 0.5 because in ^{4}He interactions there is, on average, 50% probability that either ^{3}He or ^{3}H are produced.

Equation (3) describes the neutron spectrum in the atmosphere. The second term on the R.H.S. of this equation gives the number of stripped neutrons from interacting helium nuclei, having the same energy per nucleon as the parent nuclei. In this term, the first part in the brackets is the total interaction probability, which includes pure spallation and those processes involving large momentum transfer due to pion production. The second part is the interaction probability which involves large momentum transfer. From the cross section available in literature as a function of energy, we estimated that, on average, 2.5 free nucleons are produced in each interaction. It is reasonable to assume that this number of produced nucleons is shared equally by protons and neutrons, and hence we have a factor 1.25 in this term. The next term takes care of the particle energy loss during inelastic interactions, where the lower integration term represents the threshold energy for pion production. The first part of this term in the square brackets is related to the surviving neutrons during inelastic interactions of protons; here the mean charge exchange probability α is assumed to be 0.333. The second part of this term represents the number of surviving protons which become neutrons due to the charge exchange process in proton interactions and the third part corresponds to interacting neutrons in helium interactions. In this term, Φ is the normalized energy distribution function of the outgoing particle and it is the probability that the incoming nucleon with kinetic energy per nucleon E' produces an outgoing nucleon with kinetic energy E. The last term in equation (3) is the production of neutrons from the target air nuclei during inelastic interactions either through evaporation or by recoil processes [1].

Equation (4) describes the change in the secondary proton spectrum in the atmosphere, it is similar to equation (3) except for the fact that it contains also the ionization energy loss term. It can be noted that both the equations (3) and (4) are coupled to all other equations and hence we need to solve the above set of equations simultaneously.

For the interaction mean free paths, $\lambda_{P,He}$, used in the above equations, we considered collisions where large momentum transfer takes place, such as those associated with pion production. For this purpose, we have modified the energy dependence of the P+P inelastic cross section [2] to take into account the effect of the Fermi momentum distribution of the target nucleons [3]. The parametrization of the cross-section thus obtained was normalized at high energies to the P–Air and He–Air interaction lengths.

The interaction length as a function of energy, λ'_P, for interactions including spallation and deep inelastic interactions is obtained using the measured P+C cross section [4]. This cross section is then normalized, at high energies,